AD-A174 146 FIBER MATRIX INTERFACE EFFECTS IN FAILURE OF CERAMIC 1/2
MATRIX FIBER COMPOSI (U) ROCKWELL INTERNATIONAL
THOUSAND OAKS CA SCIENCE CENTER D MARSHALL ET AL
UNCLASSIFIED OCT 86 SC5432 AR N00014-85-C-0416 F/G 11/4 NL

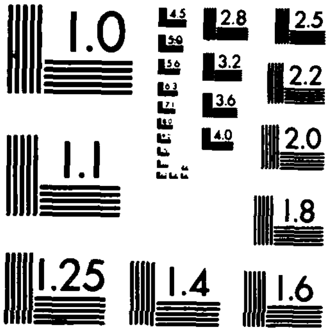

MICROCOPY RESOLUTION TEST CHART
NATIONAL BUREAU OF STANDARDS-1963-A

(12)

SC5432.AR

Copy No. 12

FIBER MATRIX INTERFACE EFFECTS IN FAILURE OF CERAMIC MATRIX FIBER COMPOSITES

ANNUAL REPORT FOR THE PERIOD
July 15, 1985 through July 14, 1986

CONTRACT NO. N00014-85-C-0416

Prepared for

Scientific Officer
Program Manager Non-Metallic Materials
Office of Naval Research
800 North Quincy Street
Arlington, VA 22217-5000

By

D. Marshall, B.N. Cox,
W.C. Oliver, A.G. Evans

OCTOBER 1986

Approved for public release; distribution unlimited

Rockwell International
Science Center

REPORT DOCUMENTATION PAGE

1a. REPORT SECURITY CLASSIFICATION
Unclassified

1b. RESTRICTIVE MARKINGS

2a. SECURITY CLASSIFICATION AUTHORITY

2b. DECLASSIFICATION/DOWNGRADING SCHEDULE

3. DISTRIBUTION/AVAILABILITY OF REPORT
Approved for public release; distribution unlimited.

4. PERFORMING ORGANIZATION REPORT NUMBER(S)
SC5432.AR

5. MONITORING ORGANIZATION REPORT NUMBER(S)

6a. NAME OF PERFORMING ORGANIZATION
Rockwell International
Science Center

6b. OFFICE SYMBOL *(If applicable)*

7a. NAME OF MONITORING ORGANIZATION

6c. ADDRESS *(City, State and ZIP Code)*
1049 Camino Dos Rios
Thousand Oaks, CA 91360

7b. ADDRESS *(City, State and ZIP Code)*

8a. NAME OF FUNDING/SPONSORING ORGANIZATION
Office of Naval Research

8b. OFFICE SYMBOL *(If applicable)*

9. PROCUREMENT INSTRUMENT IDENTIFICATION NUMBER
Contract No. N00014-85-C-0416

8c. ADDRESS *(City, State and ZIP Code)*
Scientific Officer
Program Manager Non-Metallic Materials
800 North Quincy Street
Arlington, VA 22217-5000

10. SOURCE OF FUNDING NOS.

PROGRAM ELEMENT NO.	PROJECT NO.	TASK NO.	WORK UNIT NO.

11. TITLE *(Include Security Classification)* FIBER MATRIX INTERFACE EFFECTS IN FAILURE OF CERAMIC MATRIX FIBER COMPOSITES

12. PERSONAL AUTHOR(S)
Marshall, D.

13a. TYPE OF REPORT
Annual Report

13b. TIME COVERED
FROM 07/15/85 TO 07/14/86

14. DATE OF REPORT *(Yr., Mo., Day)*
OCTOBER 1986

15. PAGE COUNT
122

16. SUPPLEMENTARY NOTATION

17. COSATI CODES

FIELD	GROUP	SUB. GR.

18. SUBJECT TERMS *(Continue on reverse if necessary and identify by block number)*

19. ABSTRACT *(Continue on reverse if necessary and identify by block number)*

Mechanical behavior of ceramic fiber composites has been investigated. Methods were developed for measuring mechanical properties of the fiber/matrix interface at individual fibers and micromechanics models were developed to analyze debonding and sliding at the interface. A fracture mechanics model for tensile failure of composites has been developed. Solutions from this model define several different failure mechanisms and provide relations between strength, toughness and conditions for transition in failure mechanism in terms of microstructural properties of the composite.

20. DISTRIBUTION/AVAILABILITY OF ABSTRACT
UNCLASSIFIED/UNLIMITED ☒ SAME AS RPT. ☐ DTIC USERS ☐

21. ABSTRACT SECURITY CLASSIFICATION
Unclassified

22a. NAME OF RESPONSIBLE INDIVIDUAL

22b. TELEPHONE NUMBER *(Include Area Code)*

22c. OFFICE SYMBOL

TABLE OF CONTENTS

1.0 INTRODUCTION

The goal of this research is to develop a basic scientific understanding of the relation between the macroscopic mechanical properties of ceramic composites and the properties of the microstructure, especially the fiber-matrix interface. The work is directed to two main topics. One is to devise experiments that are capable of measuring the properties of the fiber-matrix interface directly, and the other is to develop micromechanics models that relate the interface properties quantitatively to the strength, toughness and failure mechanisms of the composite.

The detailed results of the research are contained in four papers which are included as Sections 2 to 5 of this report, and which have been submitted to, or published in the journals and books noted on the title pages. The results are briefly summarized below.

In the studies of fiber/matrix interface properties, novel methods were developed for investigating bonding at the interface, and to measure sliding resistance (Sections 2 and 3). These are based on an indentation technique (developed previously in our IR&D) in which the ends of individual fibers are pushed with a diamond indenter. The method was analyzed theoretically to determine the range of frictional stresses that can be measured. This range was found to be more than three orders of magnitude (Section 2). Theoretical analyses were also developed for combined debonding and frictional sliding and for frictional sliding during loading, unloading and load cycling (Section 3). Measurements were done on an SiC/glass-ceramic composite (LAS III, UTRC) using two indentation instruments; a microhardness tester which provided continuous measurements of force as a function of time during loading (at relatively high loading rates), and an ultralow load instrument (collaboration with W. Oliver, ORNL) which provided continuous force-displacement measurements during loading, unloading and load cycling at lower loading rates (Section 3). The results provided an upper-bound estimate for the fracture energy of the interface (0.04 $J{\bullet}m^{-2}$, similar to the energy of Van der Waals bonds) and a measure of the magnitude of the frictional stress (2.5 ± 1 MPa). They also indicated that for a given fiber, the frictional stresses were very uniform over fiber lengths up to 1 mm, that the frictional stress decreases slightly upon reverse sliding, but remains constant thereafter during cyclic sliding, and that the frictional stress is not sensitive to load rate for loading times in the range 100 ms to 100 s (Section 3). Experiments were also done in the presence of an applied transverse compression to evaluate the friction coefficient at the interface and the influence of Poisson's contraction or expansion on frictional stresses (Section 2). Changes of interface properties at high temperatures were also evaluated and a very simple method using a Knoop indenter was developed for measuring reverse fiber sliding.

The fracture mechanics modeling (Sections 4 and 5) addressed the problem of tensile failure of composites containing aligned fibers with weak frictional stresses at the fiber/matrix interface, and with fiber strengths in the range where fiber failure can accompany matrix cracking. This modeling is expected to provide the basis for further development of more advanced analyses of toughening in many whisker composite systems. The general solution to this problem can be quite complicated because failure may initiate with either growth of a crack in the matrix or fracture of fibers that bridge the matrix crack. Morever, both of these failure modes may continue either unstably at constant applied stress or stably with increasing applied stress. An approximate analytical approach that we developed recently was further expanded (Section 4) and numerical solutions have been obtained (Section 5). The solutions define several different failure mechanisms, specify conditions for transitions between mechanisms and provide strength/crack-size relations for each mechanism. The results were obtained in terms of normalized stresses and crack lengths, with two microstructural variables, the normalized fiber strength and the area of unbroken or missing fibers in the initial crack. The most important transition in failure mechanism is from a noncastrophic mode of failure (involving periodic matrix cracking at a stress that is independent of crack length) to a catastrophic mode. Explicit relations have been derived for composite properties such as matrix cracking stress (noncatastrophic mode), the condition for transition to catastrophic failure mode, and fracture toughness in the region of catastrophic failure, in terms of the interface characteristics, the fiber strength and the other microstructural properties of the composite.

2.0 MEASUREMENT OF INTERFACE PROPERTIES IN CERAMIC COMPOSITES

Submitted to J. Am. Ceram. Soc.

MEASUREMENT OF INTERFACE PROPERTIES IN CERAMIC COMPOSITES

D.B. Marshall

Rockwell International Science Center
Thousand Oaks, CA 91360

W.C. Oliver

Metals and Ceramics Division
Oak Ridge National Laboratory
Oak Ridge, TN 37831

ABSTRACT

Properties of the fiber/matrix interface in a SiC/glass-ceramic composite are investigated using an indentation method in which a pyramidal indenter is used to push on the fibers and cause sliding at the interface. An ultralow-load indentation instrument was used to measure force and displacement continuously during loading, unloading, and load cycling. Frictional sliding and combined debonding/frictional sliding at the interface was analyzed. The analysis enabled the results to be used to provide a measure of the debond fracture energy, the magnitude of the frictional sliding stress, a measure of the uniformity of the frictional stress, and an indication of the sensitivity of the frictional stress to repeated sliding, varying load rate, and exposure to high temperatures.

1.0 INTRODUCTION

A method was developed recently for measuring the magnitude of frictional stresses at the interface between fibers and matrix in composites.[1] A pyramidal indenter was used to push on the ends of individual fibers and the resulting displacement of the surface of the fiber below the matrix surface (due to sliding) was measured. The frictional stress was calculated from the force-displacement relation obtained by analysis of the frictional sliding. The force and displacement measurements were obtained only at the peak of the load cycle and the sliding analysis was based on sliding at constant shear resistance at the interface, with the assumption that the length over which sliding occurred between the fiber and matrix was large compared to the fiber diameter. These experiments provided measurements of average frictional stress at individual fibers, which were consistent with values inferred independently from fracture measurements.[1,2] However, they left open several questions concerning the nature of the interface which are important for understanding the detailed role of the interface in fracture processes.[3,4] These include whether or not there is any bonding at the interface in addition to frictional forces (i.e., whether fiber displacement involves debonding followed by frictional sliding), whether the static and dynamic friction coefficients differ, whether the frictional stress is constant along the slipping region of fiber, and whether the sliding resistance remains constant during reverse sliding upon unloading (and subsequent load cycling).

In this paper we present direct measurements of the forces and displacements during loading, unloading, and subsequent load cycling in a SiC/glass-ceramic composite. The measurements are correlated with analysis of combined debonding and frictional sliding and analysis of reverse and cyclic sliding to answer some of these questions. Results of additional preliminary experiments to investigate effects of loading rate and high temperature degradation of the interface properties are discussed.

2.0 EXPERIMENTS

The indentation experiment is shown schematically in Fig. 1. In the previous work[1] sufficient force was applied to a Vickers indenter to make its edges contact the matrix, thereby allowing the depth u corresponding to the peak load, to be obtained from subsequent measurements of surface contact dimensions and the known geometry of the indenter. In the present experiments the forces and displacements were measured continuously during loading, unloading, and load cycling, mostly at loads sufficiently low that the indenter did not touch the matrix.

The composite used for these experiments was a lithium-aluminosilicate glass-ceramic matrix reinforced by SiC (Nicalon) fibers,* which has been used in previous studies of interface properties and mechanical behavior.[1,2,5,6] The composite was tested in both the as-received state and after heat treatment in air and argon at temperatures between 900°C and 1250°C. Heat treatment was done in air by inserting the specimen into a preheated furnace for a specified time, and in argon by heating and cooling at a constant rate, 10°C/min. The heat treatments provided a limited indication of the influence of high temperatures on the sliding resistance of the interface. They also provided a convenient means for calibrating some of the force-displacement measurements.

---

*United Technologies Research Center, East Hartford, CT, SiC/LAS III.

Most experiments were done using an ultralow-load indentation instrument* which allowed forces and displacements to be measured with resolutions of 0.5 μN and 0.2-0.3 nm.[7] The indenter in this instrument is a triangular pyramid with the same depth-to-area ratio as the Vickers (square) pyramid. A coil and magnet assembly is used to move the indenter toward the surface and to apply the load, and the position of the indenter is measured using a capacitor displacement gage. In the present experiments loads up to 0.12 N were applied by moving the indenter at constant velocity 10 nm s^{-1}, giving typical loading times ~ 100 s. A scanning electron micrograph of a fiber after indentation is shown in Fig. 1(b).

The frictional stress was also measured using a second indentation instrument in which the load was applied gravitationally with a dashpot resistance.** This system allowed more rapid loading (loading times as small as ~ 10 ms) so that comparison of the two sets of measurements allowed a preliminary estimate of the influence of loading rate on the sliding resistance. A transducer load cell was used to measure the force as a function of time during loading but displacements were not measured. The F(t) measurements are not readily amenable to quantitative analysis, but they do provide qualitative information on the fiber sliding at the higher loading rates.

---

*Nanoindenter, Nano Instruments.
**Zwick.

3.0 RESULTS

Force and displacement measurements obtained from the Nanoindenter during indentation of the fiber shown in Fig. 1(b) are plotted in Fig. 2(a). The force was increased monotonically from 0 to 0.10 N, decreased to 0.002 N, and then cycled between these two values five times. All force changes were effected by moving the indenter at a constant speed of 10 nm s^{-1}. The decreasing slope of the loading curve and the hysteresis in the unload/reload curves are both a result of frictional sliding at the fiber/matrix interface.

The results of a similar experiment done on a fiber in another piece of the same composite that had been heat treated for 10 min at 1000°C in air are shown in Fig. 2(b). In this case the loading curve has a continuously increasing slope (the curve is close to parabolic), with shape similar to that of curves obtained from indenting homogeneous materials.[7] Moreover, the reloading curve retraced the unloading path without any sign of the hysteresis that is evident in Fig. 2(a). These results suggest that the heat treatment caused oxidation and strong bonding at the interface, which prevented sliding of the fiber during indentation. Subsequent observation of the fiber by scanning electron microscopy confirmed that sliding had not occurred.

The directly measured displacements in Fig. 2(a) represent the displacement of the indenter (u_T in Fig. 2(a)), which is the sum of the sliding distance u and the penetration, u_0 (elastic and plastic), of the indenter into the fiber. The results in Fig. 2(b) for the heat-treated composite which does not exhibit sliding provide a convenient calibration of the indenter penetration u_0.

The true fiber sliding distances obtained by subtracting the displacements in Fig. 2(b) from those in Fig. 2(a) are plotted in Fig. 3 for one load-unload-reload cycle. After unloading, the fiber remained depressed below the matrix surface a distance nearly half of the peak load displacement, whereas reloading to the peak load restored the original displacement. Subsequent load cycling caused the first unload/reload path to be retraced. Measurements on 15 such fibers produced very similar results.

Measurements of force as a function of time during loading with the Zwick instrument are shown in Fig. 4, for both the as-received and the heat-treated composite. The effect of fiber sliding in the as-received material is clearly evident. The peak load (0.24 N) was sufficiently high for the edges of the indenter to touch the matrix in the as-received specimen (contact occurred at force of 0.17 N as indicated in Fig. 4). In these measurements the indenter approached the surface at a fixed velocity, but after contacting the surface its deceleration was dictated by the sum of the gravitational force, the reaction of the indented material, and the dashpot resistance.

The measurements of Figs. 2(b) and 4 indicate that short exposure to air at 1000°C causes strong bonding at the interface. Similar results were obtained for 5 min exposure at 900°C (a wider range of temperatures was not investigated). In contrast, indentation experiments after heat treatment in argon at temperatures up to 1250°C did not reveal any bonding; the average room temperature frictional stress based on peak-load measurements was not changed by the heat treatment. However, observations of fibers that had been indented before the heat treatment indicated that relaxation of the sliding resistance occurred at high temperatures. After heat treatment at 1250°C the residual displacements of the indented fibers (see Fig. 2(a)) had completely relaxed. After treatment at 1170°C the residual displacement had relaxed to about half of its original value. This is the temperature range where the viscosity of the glass-ceramic matrix decreases rapidly and the matrix creeps under small loads.[8]

4.0 ANALYSIS OF FORCE-DISPLACEMENT RELATIONS

4.1 Frictional Sliding

If we assume that sliding occurs between matrix and fibers wherever the shear stress parallel to the interface exceeds a constant value τ, then application of a force F to the end of the fiber causes sliding beginning at the surface and extending to a depth ℓ (Fig. 5). With a shear-lag approximation in which only normal stresses σ exist within the fiber (shear stress concentrated at the interface), equilibrium of the fiber at $z < \ell$ requires

$$d\sigma/dz = 2\tau/R \tag{1}$$

where R is the radius of the fiber. If we assume that $\ell >> R$, then the elastic stresses at $z > \ell$ may be neglected[1] and Eq. (1) with the boundary conditions $\sigma(\ell) = 0$ and $\sigma(0) = F/\pi R^2$ defines the sliding distance

$$\ell = F/2\pi R\tau \tag{2}$$

and the strain distribution in the fiber (Fig. 5)

$$\epsilon(z) = (F/\pi R^2 E_f)(1 - z/\ell) \quad , \tag{3}$$

where E_f is the Young's modulus of the fiber. The displacement of the fiber surface below the original specimen surface, obtained by integration of Eq.

(3) over the range $z = 0$ to $z = \ell$, is

$$u = F^2/4\pi^2R^3\tau E_f \tag{4}$$

4.2 Interface Debonding and Frictional Sliding

More generally, fiber sliding may be expected to entail extension of a debonding crack at the fiber/matrix interface followed by frictional sliding over the crack surfaces. In this case the sliding depth is dictated by the length, c, of the debond crack (Fig. 6). For $c \gg R$ the strain distribution in the region $z \leq c$ in the fiber is given by Eq. (3), but the displacement of the fiber surface below the matrix is given by integration between $z = 0$ and $z = c$:

$$u = (F/\pi R^2E_f)(c - c^2/2\ell) \tag{5}$$

Therefore, evaluation of u requires knowledge of the debond length c.

The debond length can be calculated from an energy balance analysis for incremental crack growth. If the crack extends by dc at constant applied force F, then the strain energy of the specimen increases by dU_E, the potential energy of the loading system decreases by dU_L, work, dU_F, is done against frictional forces, and there is additional energy dU_Γ associated with the new crack area. For large debond cracks ($c \gg R$) these energy changes are given by (Appendix)

$$dU_E = (F^2/2\pi R^2 E_f)(1 - 2c/\ell + c^2/\ell^2)dc \tag{6a}$$

$$dU_F = (F^2/\pi R^2 E_f)(c/\ell - c^2/\ell^2)dc \tag{6b}$$

$$dU_L = (F^2/\pi R^2 E_f)(1 - c/\ell)dc \tag{6c}$$

and

$$dU_\Gamma = 4\pi R\Gamma dc \quad , \tag{6d}$$

where 2Γ is the fracture surface energy per unit area of interface. The net energy change of the system is

$$\begin{aligned} dU &= dU_E - dU_L + dU_f + dU_\Gamma \\ &= -(F^2/2\pi R^2 E_f)(1 - c/\ell)^2 dc + 4\pi R\Gamma dc \end{aligned} \tag{7}$$

With the fracture criterion $dU/dc \le 0$, Eq. (7) gives an expression for the equilibrium crack length in terms of the applied force and other microstructural parameters.

$$(1 - c/\ell)^2 = 8\pi^2 R^3 \Gamma E_f/F^2 \tag{8}$$

Equation (8) represents stable crack growth with increasing force. This implies that debonding does not cause a discontinuity (load drop) in the force-displacement relation. However, the analysis applies only to well-developed cracks with $c \gg R$. Crack initiation could involve instability which would be reflected in the force-displacement relation. In the limit of no bonding at the interface ($\Gamma = 0$), Eq. (8) reduces to the result $c = \ell$ of Section 4.1. In the limit of a bonded interface without friction ($\tau = 0$, i.e., $\ell \to \infty$), the crack length dependence disappears, implying that at a critical applied force given by Eq. (7), the debond crack extends without limit under mechanical equilibrium.

The fiber displacement at the surface, given by Eqs. (5) and (8) is

$$u = F^2/4\pi^2 R^3 \tau E_f - 2\Gamma/\tau \tag{9}$$

Comparisons of Eqs. (4) and (9) indicates that under combined debonding and sliding the displacement of the fiber surface is smaller than it is for pure sliding by a constant amount $2\Gamma/\tau$.

4.3 Reverse Sliding

If the force applied to the end of a fiber is increased to a maximum, F_m, and then decreased, sliding occurs in the reverse sense during unloading, beginning at the surface and extending a distance s along the interface (Fig. 7). The resulting strain distribution in an unbonded fiber is shown in Fig. 7. Assuming that the frictional stress τ remains the same during loading and unloading the fiber displacement (shaded area in Fig. 7) is

$$u = u_m[1 - (1 - F/F_m)^2/2] \quad . \tag{10}$$

where u_m is the displacement at the maximum load, given by Eq. (4) with $F = F_m$. After completely unloading ($F = 0$) the displacement is one half of the peak load displacement. If, on the other hand, the frictional stresses during forward and reverse sliding are unequal, then the displacement after unloading becomes

$$u = u_m/(1 + \tau_1/\tau_2) \tag{11}$$

where τ_1 and τ_2 are the frictional stresses during forward and reverse sliding. For the fiber considered in Section 4.2, which undergoes combined debonding and sliding, the displacement during unloading is smaller than that in Eq. (10) by the constant amount $2\Gamma/\tau$.

4.4 Reloading

The strain distribution in the fiber during reloading is shown in Fig. 8. The displacement of the fiber surface, given by the shaded area in Fig. 8, is

$$u = (u_m/2)[1 + (F/F_m)^2] \tag{12}$$

If the frictional stress decreases after the first loading but remains constant thereafter, Eq. (12) becomes

$$u/u_m = (1 + \tau_1/\tau_2)^{-1} + (\tau_1/\tau_2)(F/F_m)^2/2 \tag{13}$$

5.0 DISCUSSION

The results in Fig. 3 and the analysis of Section 4.2 allow an upper bound to be estimated for the fracture energy associated with any bonding that may exist at the interface. The data from Fig. 3 are plotted in Fig. 9 in the form F^2 vs u, for which Eq. (9) predicts a linear relation for the first loading. A line fitted to the data for displacements larger than ~ 0.1 μm extrapolates through the origin, suggesting that the fracture energy is $\Gamma \approx 0$. The maximum departure of the data from this result is $2\Gamma/\tau < 0.01$ μm. With the measured fiber radius $R = 8.0$ μm and elastic modulus $E_f = 200$ GPa, the measured slope of the line in Fig. 9 with Eq. (9) gives $\tau \approx 3.6$ MPa. Therefore, the fracture energy is $2\Gamma < 4 \times 10^{-2}$ J/m^2. This is in the range of energies associated with Van der Waals forces and is consistent with observations by Brennan[6] of a thin layer of carbon at the fiber/matrix interface in this composite.

For displacements larger than ~ 0.1 μm the data in Fig. 9 follow the prediction of Eq. (4) very closely. Since the sliding distance increases in proportion to the applied force (Eq. (2)), each force increment causes a new area of fiber to begin sliding and contribute to the total fiber displacement. Therefore, the results suggest that the frictional stress is very uniform along the fiber and is not influenced by irregularities of fiber shape or thickness that occur over lengths comparable to or larger than the fiber radius.

At small forces the displacements in Fig. 9 are smaller than predicted by Eq. (4), and for forces ≤ 0.01 N no displacement was resolved. Deviation at low loads is expected because Eq. (9) is based on an assumption that sliding occurs over a large distance compared with the fiber radius. The sliding distances calculated from Eq. (2) for the linear region of Fig. 9 are $\ell/R \sim 10$ to 70. A rigorous analysis for small sliding distances is not available. However, we can see that the sign of the deviation is consistent with expectations: the boundary condition $\sigma(\ell) = 0$ leading to Eq. (2) becomes $\sigma(\ell) > 0$ for small ℓ, so that Eqs. (2) and (4) give overestimates of ℓ and u. A modified shear-lag analysis for fiber sliding in composites where all fibers are loaded simultaneously was developed recently by Budiansky et al,[9] but this analysis becomes invalid as the volume fraction approaches zero (single fiber). However, it is worth noting that the analysis predicts that, for purely frictional sliding, sliding does not occur until a critical load is exceeded, as observed in Fig. 3. The shear stresses at the interface at the onset of sliding are estimated in Appendix B. The calculation suggests that at the observed onset of sliding ($F \sim 0.01$ N) the shear stresses exceed the frictional stress, $\tau = 3.6$ MPa, over a region beneath the surface with length about equal to the fiber diameter.

With the observation that debonding does not influence the sliding characteristics, the data for unloading and reloading can be compared with the predictions of Eqs. (10) and (12). These are plotted in Fig. 9 with the measured values $u_m = 0.793$ μm and $F_m = 0.108$ N. The extent of reverse sliding is larger than predicted, suggesting that the frictional stress is smaller during reverse sliding than during the first forward sliding. The measured displacement at full unload ($u/u_m \approx 0.4$) with Eq. (11) implies a reduction ~ 30%. A similar frictional stress is obtained from the slope of the reloading curve with Eq. (13). Measurements on fifteen other fibers in this specimen gave results very similar to those in Fig. 9, with a calculated reduction of τ in the range 20-40% during reverse sliding. The magnitudes of the frictional stresses calculated from the slopes of the initial loading curves (Eq. (4)) for these specimens fell within the range 2.7 MPa to 3.3 MPa.

The frictional stresses calculated from the peak load measurements for 70 fibers using the Zwick instrument were $\tau = 2.1 \pm 1.5$ MPa. These stresses include the range of values obtained by the Nanoindenter, thus, for the corresponding range of loading times, ~ 10 ms to 100 s, there does not appear to be an influence of load rate on sliding resistance.

The heat treatment experiments indicate that bonding at the interface occurs very rapidly upon exposure to air at 900°-1000°C. Brennan[6] has observed that the thin layer of carbon at the interface disappears with similar heat treatment. The present results support Brennan's suggestion that the weak interfacial bonding in this composite is caused by the carbon layer. The results also bear on the embrittlement that has been observed in this composite when tested at high temperatures in air.[6,10] Two mechanisms have been suggested to account for the embrittlement. One is the rapid oxidation and bonding at fibers behind a moving crack, and the other is an increased frictional stress at high temperature. The difference is important in predicting the high temperature toughness of the composite. The present results lend credence to the bonding argument, but increases in frictional stress have also been measured.[10] Further studies of the oxidation kinetics are needed to distinguish which mechanism is dominant.

The question of whether the static friction stress exceeds the sliding resistance cannot be answered with the present analysis and data. The approximation $\ell \gg R$ used in the analysis of Section 4.0 is tantamount to neglecting elastic strains at $z > \ell$, so that the displacements are not influenced by the static frictional stress. The data would be influenced only in the region of small ℓ where a rigorous analysis to interpret the data is not available.

Finally, it is noted that an estimate was made recently of the contribution of Poisson's expansion of the fibers to measured frictional stresses.[11] From experiments (with the same composite used here) in which frictional stresses were measured by the indentation method in the presence of applied transverse compressive stress, a coefficient of friction $\mu \approx 0.01$ was obtained. Calculation of the average compressive strain in the region of fiber that slipped during indentation allowed the normal stress at the interface to be calculated (≈ 8 MPa), assuming that the fibers and matrix were initially in intimate contact. These two results imply an additional frictional stress $\Delta\tau \approx 0.1$ MPa due to Poisson's contraction. This is small compared with the total measured value $\tau \approx 2$ MPa. Tensile strains in fibers that bridge cracks during composite failure are of similar magnitude to the strains in the indentation experiments. Therefore, the compressive nature of the indentation experiment should not cause the measured frictional stress to differ significantly from the value appropriate to fiber pullout in tension during cracking. This conclusion is consistent with independent measurements of τ in tension, which agree well with the indentation measurements.[2]

6.0 ACKNOWLEDGMENT

This research was supported by the U.S. Office of Naval Research under Contract No. N00014-85-C-0416 and by the Department of Energy.

7.0 REFERENCES

1. D.B. Marshall, "An Indentation Method for Measuring Matrix/Fiber Frictional Stresses in Ceramic Composites," J. Am. Ceram. Soc. 67[12] C259-60 (1984).

2. D.B. Marshall and A.G. Evans, "Failure Mechanisms in Ceramic-Fiber/Ceramic-Matrix Composites," J. Am. Ceram. Soc. 68[5] 225-31 (1985).

3. J. Aveston, G.A. Cooper and A. Kelly, "Single and Multiple Fracture," pp. 15-26 in Properties of Fiber Composites, Conf. Proc. Nat. Physical Lab. IPC Science and Technology Pres. Ltd., Surrey, England, 1971.

4. D.B. Marshall and A.G. Evans, "The Tensile Strength of Uniaxially Reinforced Ceramic Fiber Composites," pp. 1-15 in Fracture Mechanics of Ceramics, 7, Ed., R.C. Bradt, A.G. Evans, D.P.H. Hasselman and F.F. Lange, Plenum.

5. J.J. Brennan and K.M. Prewo, "Silicon Carbide Fiber Reinforced Glass-Ceramic Matrix Composites Exhibiting High Strength and Toughness," J. Mater. Sci. 17[8] 2371-83 (1982).

6. J.J. Brennan, "Interfacial Chemistry and Bonding in Fiber Reinforced Glass and Glass-Ceramic Matrix Composites," in Ceramic Microstructures '86: Role of Interfaces, Ed., J.A. Pask and A.G. Evans, Plenum, in press.

7. W.C. Oliver, R. Hutchings and J.B. Pethica, "Measurement of Hardness at Indentation Depths as Low as 20 Nanometers," in Microindentation Techniques in Materials Science and Engineering, Ed., P.J. Blau and B.R. Lawn, ASTM STP 889, 1985.

8. M. Borom and C.A. Johnson, "Thermomechanical Mismatch in Ceramics-Fiber-Reinforced Glass Ceramic Composites."

9. B. Budiansky, J.W. Hutchinson and A.G. Evans, "Matrix Fracture in Fiber-Reinforced Ceramics," J. Mech. Phys. Solids 34[2] 167 (1986).

10. A.G. Evans, M.D. Thouless, D.B. Johnson-Walls, E. Luh and D.B. Marshall, "Some Structural Properties of Ceramic Matrix Fiber Composites," in Proc. 5th Int'l Conf. on Composite Materials ICCM-V, Ed., W.C. Harrigan, J. Strife and A.K. Dhingra, Metallurgical Soc. PA, 1985.

11. D.B. Marshall, "Interfaces in Ceramic Fiber Composites," in Ceramic Microstructures '86: Role of Interfaces, Ed., J.A. Pask and A.G. Evans, Plenum, in press.

APPENDIX A

Energy Changes with Growth of a Debond Crack

With the condition c >> R, strain energy changes in the matrix during growth of a debond crack are negligible and we need consider only the strain energy in the fiber at $x \leq c$, which is given by

$$U_E = (\pi R^2 E_f/2) \int_0^c \varepsilon^2(z)dz \qquad \text{(A1)}$$

Substitution of Eq. (3) into Eq. (A1) gives the result

$$U_E = (F^2/2\pi R^2 E_f)(c - c^2/\ell + c^3/3\ell^2) \qquad \text{(A2)}$$

and differentiation leads to

$$dU_E/dc = F^2/2\pi R^2 E_f(1- 2c/\ell + c^2/\ell^2) \qquad \text{(A3)}$$

The work done against frictional forces is

$$U_F = 2\pi R\tau \int_0^c u(z)dz \qquad \text{(A4)}$$

where u(z) is the displacement of the fiber at z. Integration of Eq. (3) and substitution into Eq. (A4) gives

$$u_f = (F^2/\pi R^2 E_f)(c^2/2\ell - c^3/3\ell^2) \quad , \qquad \text{(A5)}$$

and differentiation leads to

$$dU_f/dc = (F^2/\pi R^2 E_f)(c/\ell - c^2/\ell^2) \qquad \text{(A6)}$$

The potential energy of the loading system is

$$U_L = Fu(0) \qquad \text{(A7)}$$

where $u(0)$ is the fiber displacement at the surface. Substitution from Eq. (5) followed by differentiation yields

$$dU_L/dz = (F^2/\pi R^2 E_f)(1 - c/\ell) \qquad \text{(A7)}$$

Finally, the increase in surface energy is

$$dU_\Gamma/dc = 4\pi R\Gamma \qquad \text{(A8)}$$

where 2Γ is the fracture surface energy per unit area of interface.

APPENDIX B

Estimate of Shear Stress at Interface at Onset of Sliding

A rough indication of the magnitude of shear stress at the interface before sliding begins can be obtained from Mindlins solutions for a point force applied to a half-space (this would be exact for a composite with fibers and matrix of equal elastic moduli). If a force, F, is applied at the center of a fiber of radius R the shear stress along the interface is

$$\sigma_{xz} = (3F/2\pi R^2)(z/R)^2/[1 + (z/R)^2]^{5/2} \tag{B1}$$

where z is the distance below the surface. The variation of σ_{xz} with z/R is plotted in Fig. B1. The onset of fiber sliding occurred at a force of 0.01 N for the data in Fig. 2(A). With this force and with R = 8 μm, the plot of Fig. B1 indicates that $\sigma_{xz} > \tau$ over the range z/R ~ 0.3 to 2.3, i.e., over a distance of 2R.

FIGURE CAPTIONS

Fig. 1 (a) Schematic diagram of indentation experiment used to measure interfacial sliding resistance. (b) Scanning electron micrograph of fiber in SiC/lithium-alumino-silicate composite after indentation with the triangular pyramid of the Nanoindenter instrument.

Fig. 2 (a) Force and displacement measurements obtained during indentation of the fiber in Fig. 1(b). (b) Force and displacement measurements obtained during indentation of a fiber in a specimen of the same composite as in (a) but after heat treatment at 1000°C in air for 10 min.

Fig. 3 Fiber sliding distances obtained by subtraction at the displacements in Fig. 2(b), (i.e., u_0) from the displacements in Fig. 2(a) (i.e., u_T).

Fig. 4 Measurements of force as a function of time during indentation with the Zwick instrument.

Fig. 5 (a) Schematic diagram showing sliding distance ℓ, frictional stresses, τ, exerted by the matrix on the fiber during initial loading and the distribution of compressive strain in the fiber.

Fig. 6 (a) Schematic diagram of combined debonding and frictional sliding, showing debond crack length, c, stresses applied by the matrix to the section of fiber at $z < c$, and the distribution of compressive strain in the fiber. Shaded area is fiber displacment, u.

Fig. 7 (a) Schematic diagram showing frictional stresses exerted by the matrix on the fiber during unloading and the distribution of compressive strain in the fiber. Shaded area is fiber displacement, u.

Fig. 8 (a) Schematic diagram showing frictional stresses exerted on the fiber by the matrix during reloading and the distribution of compressive strain in the fiber. Shaded area is fiber displacement, u.

Fig. 9 Comparison of data from Fig. 3 with theoretical analysis. Solid curves are representations of Eq. (4) for initial loading, Eq. (10) for unloading, and Eq. (12) for reloading.

Fig. B1 Variation of shear stress at fiber interface with depth below surface for nonsliding fiber and equal elastic moduli in fiber and matrix.

SC37582

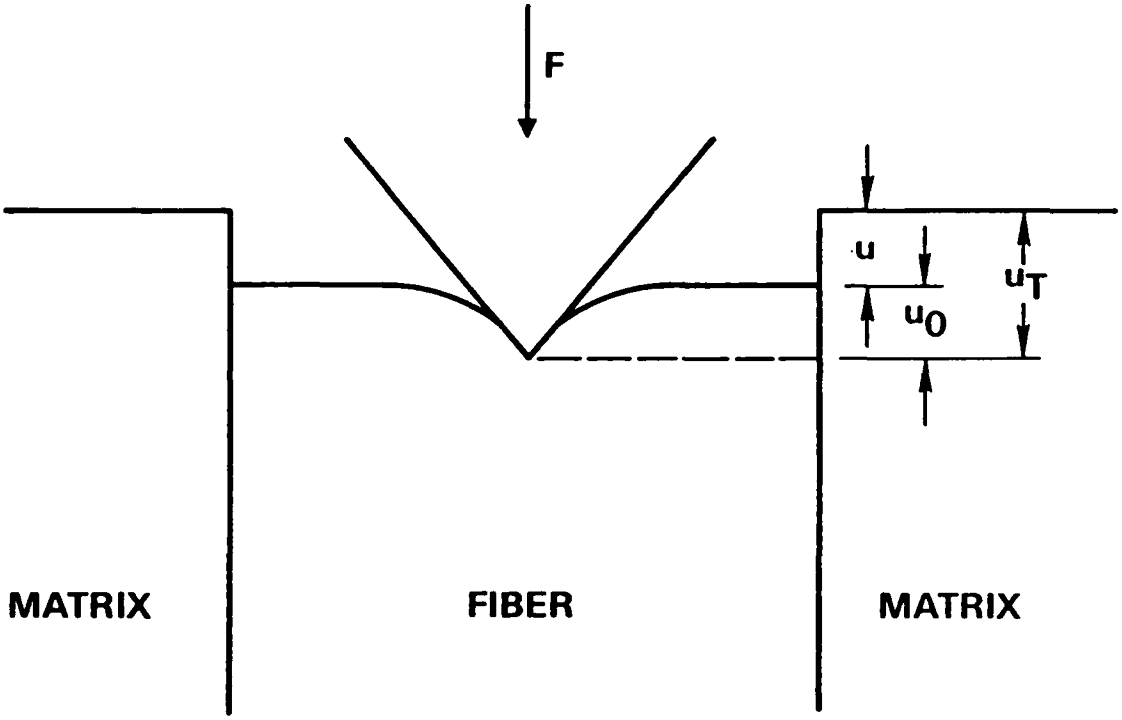

Figure 1a

Figure 1b

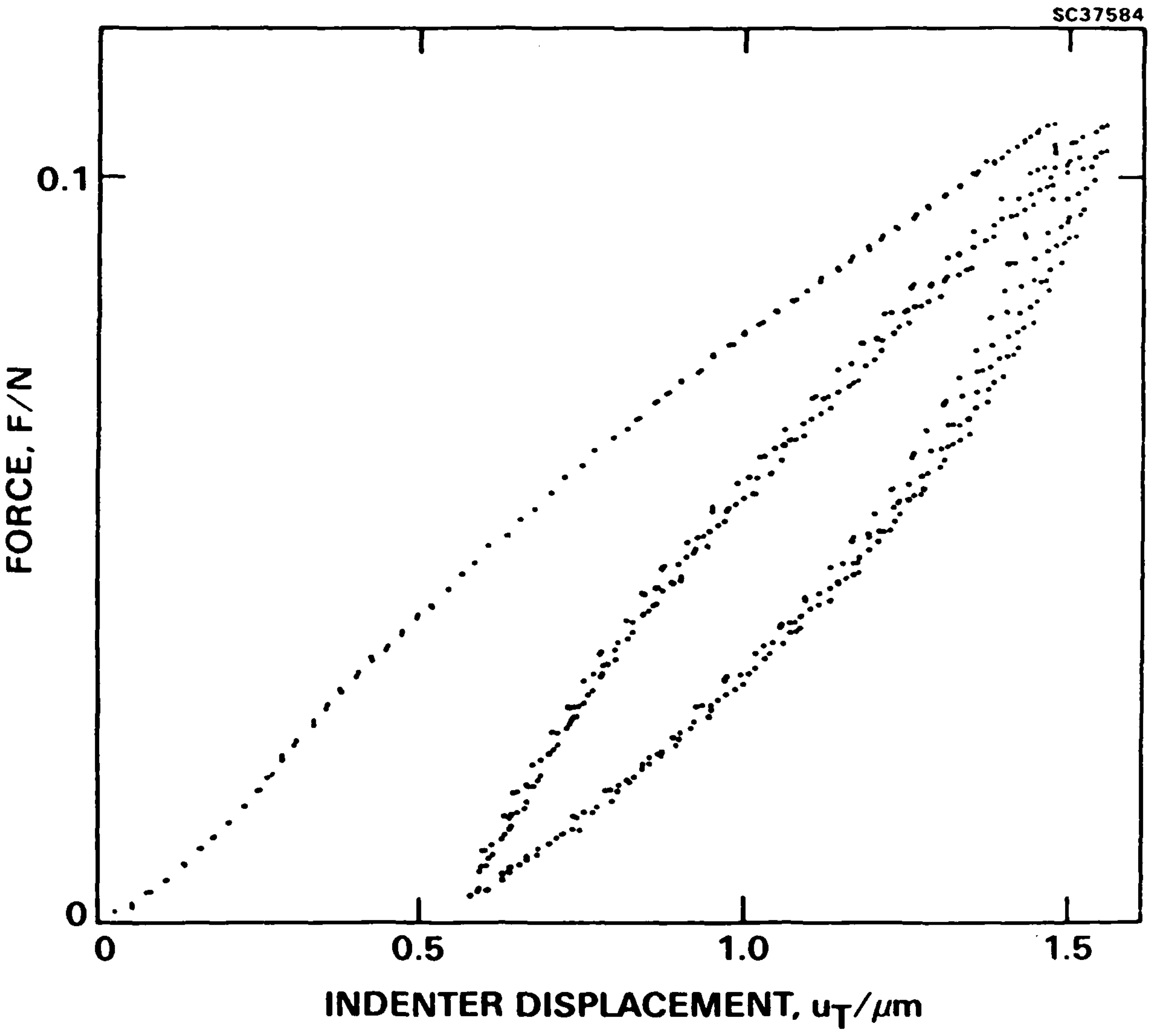

Figure 2a

SC37578

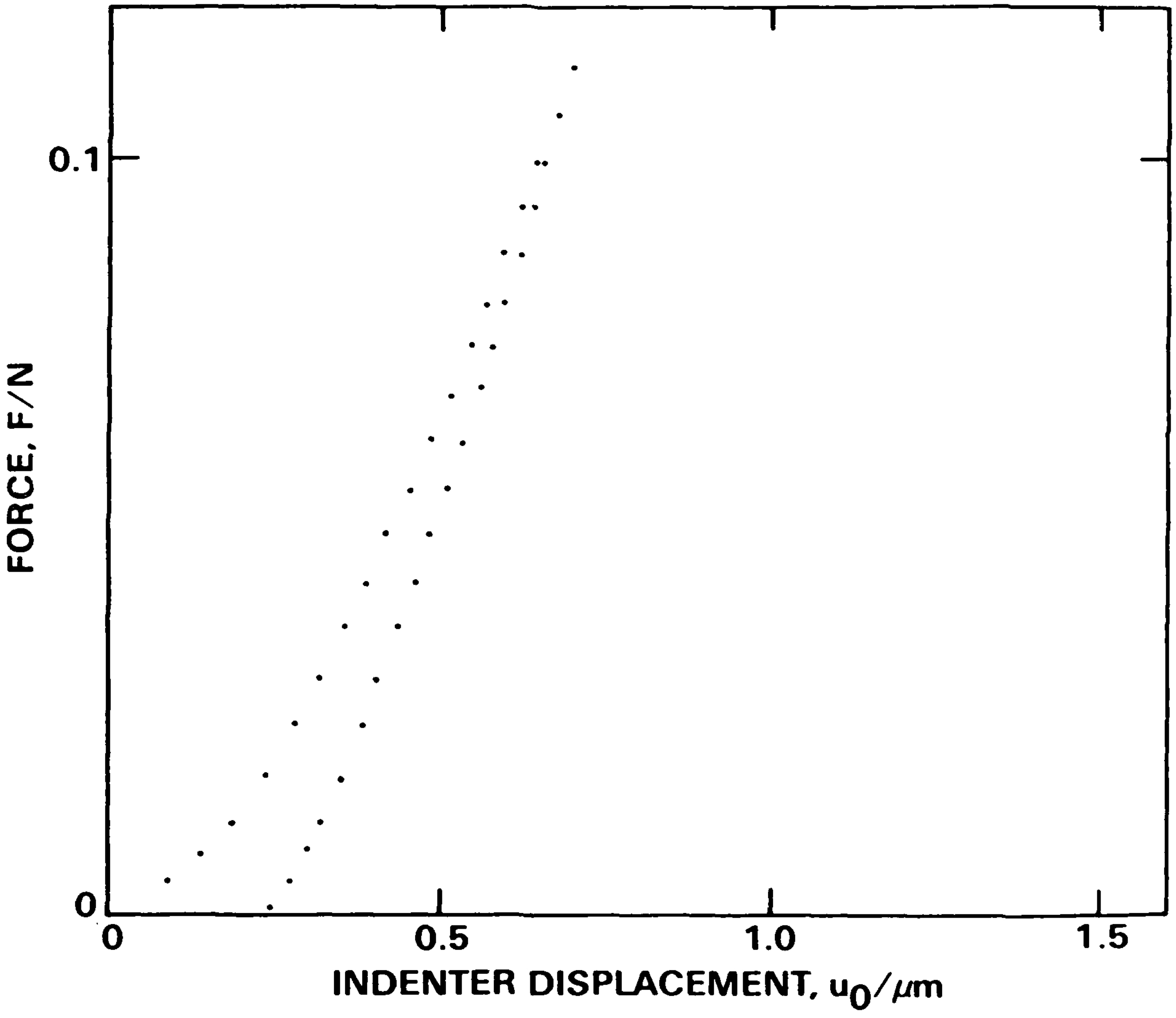

Figure 2b

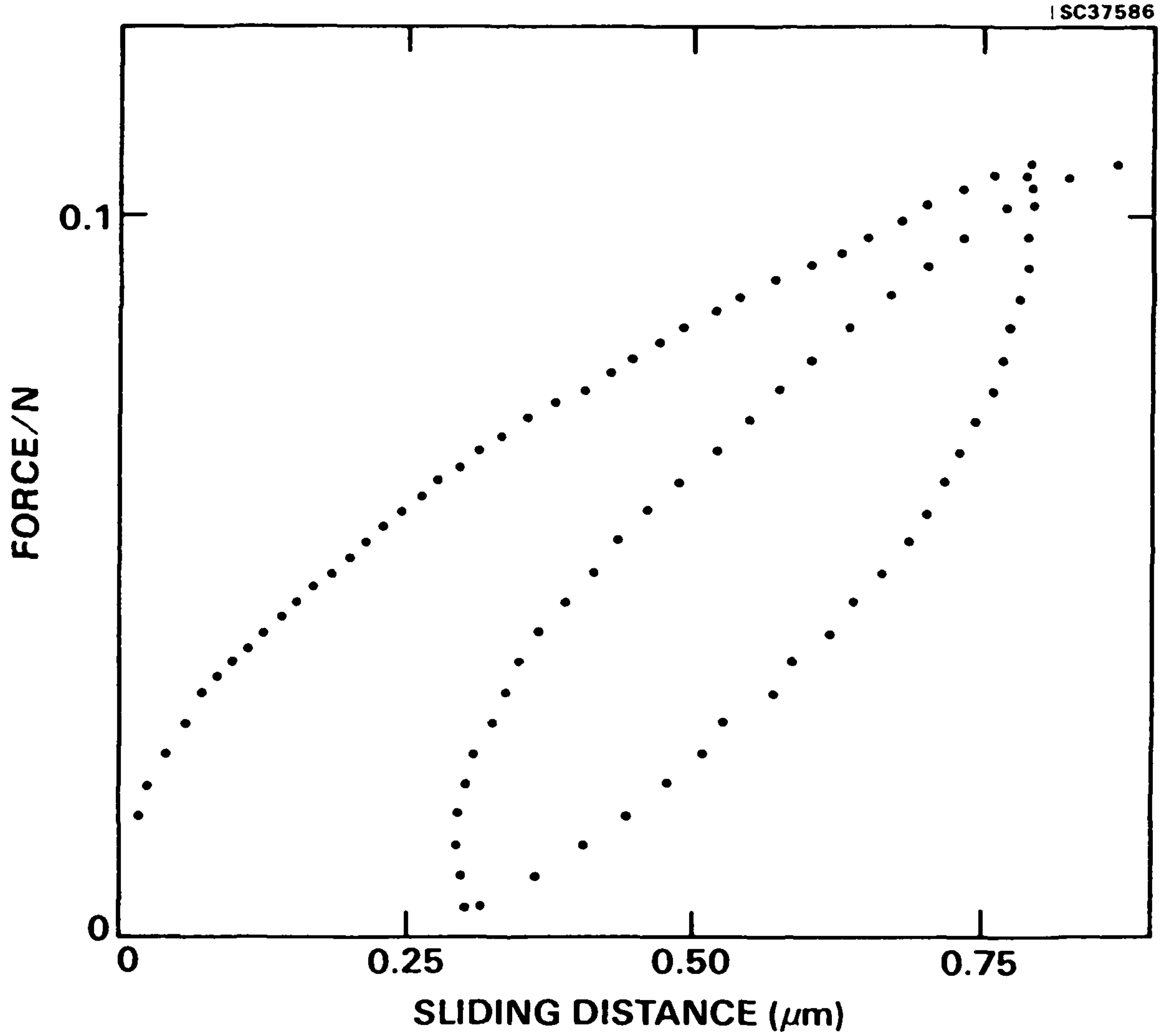

Figure 3

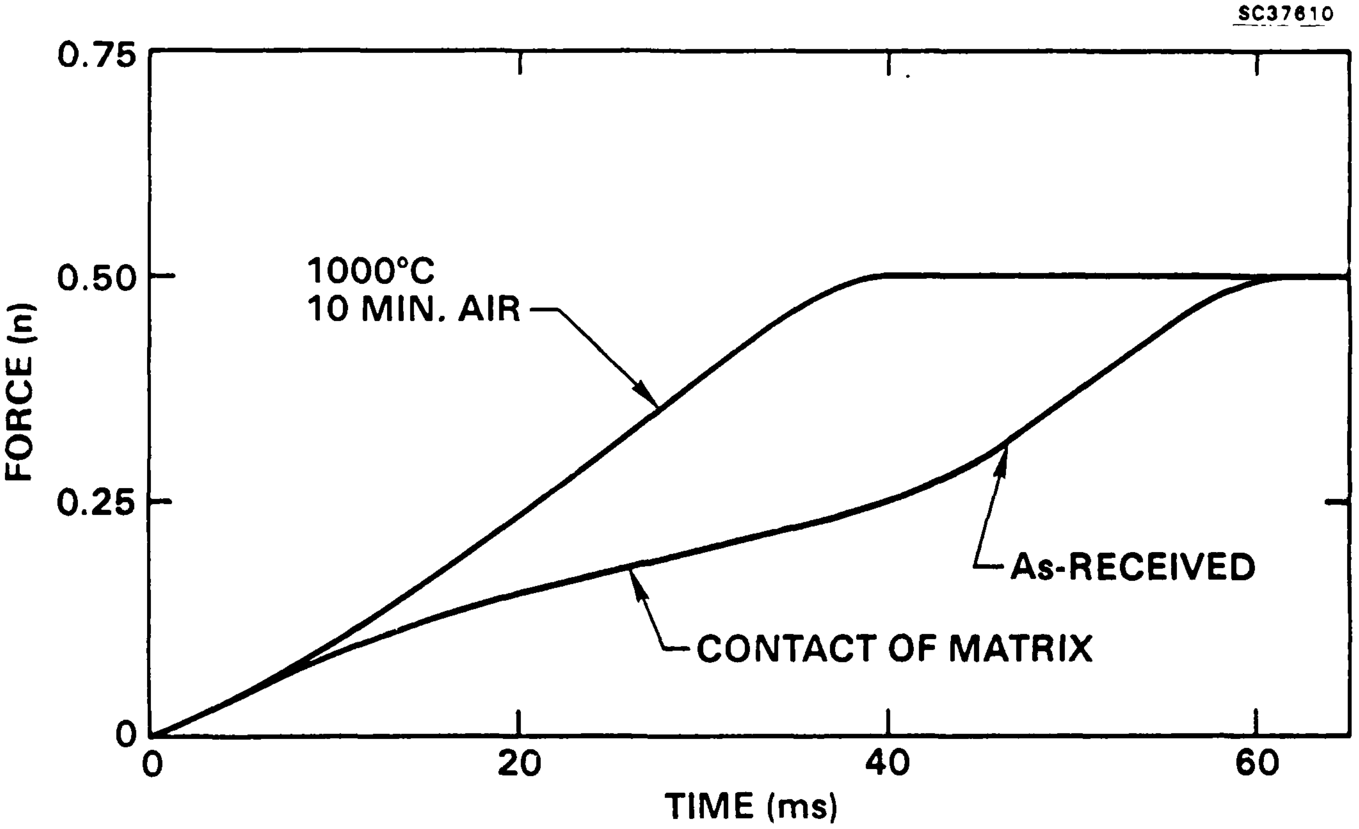
SC37610
0.75
0.50
0.25
0
FORCE (n)
0
20
40
60
TIME (ms)
1000°C
10 MIN. AIR
As-RECEIVED
CONTACT OF MATRIX

Figure 4

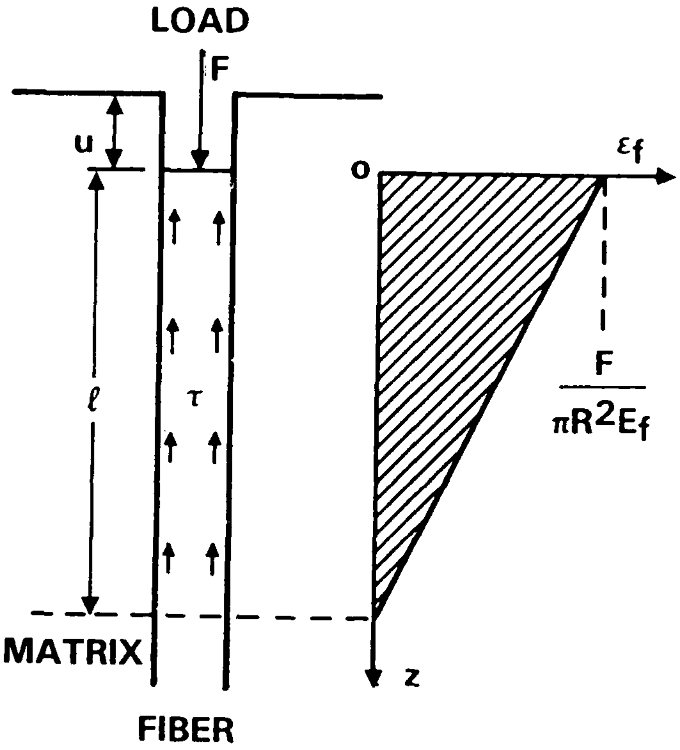

Figure 5

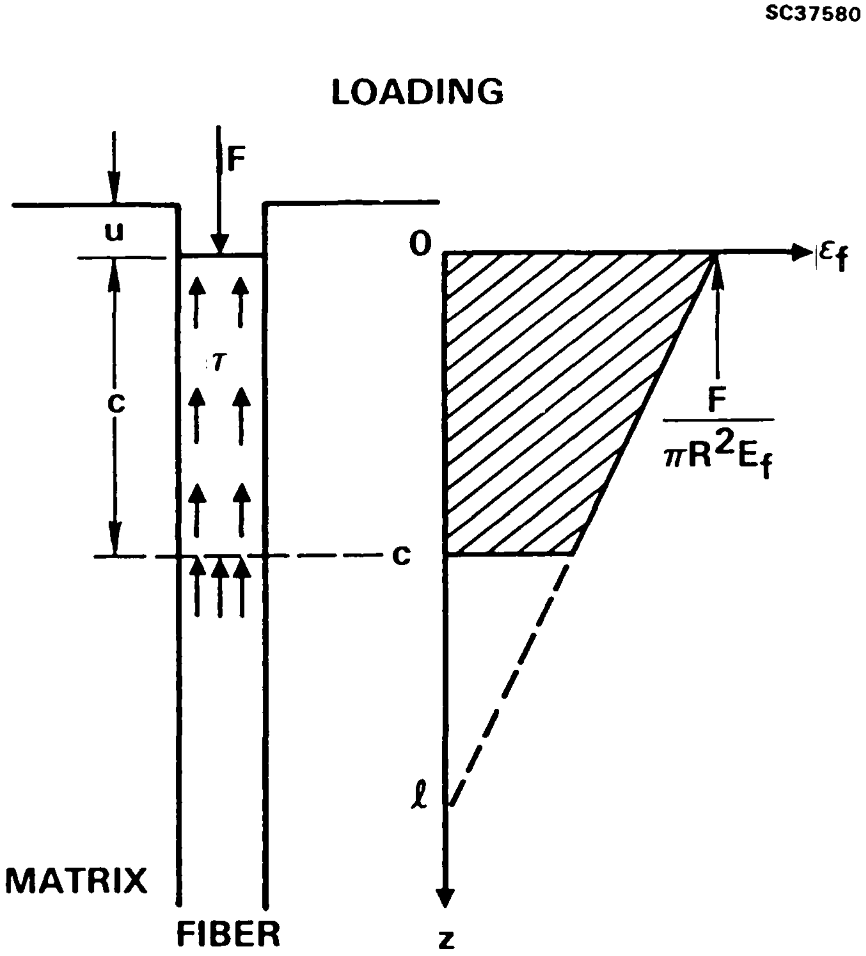
SC37580
LOADING
F
u
c
τ
c
0
ε_f
$\frac{F}{\pi R^2 E_f}$
ℓ
z
MATRIX
FIBER

Figure 6

SC37579

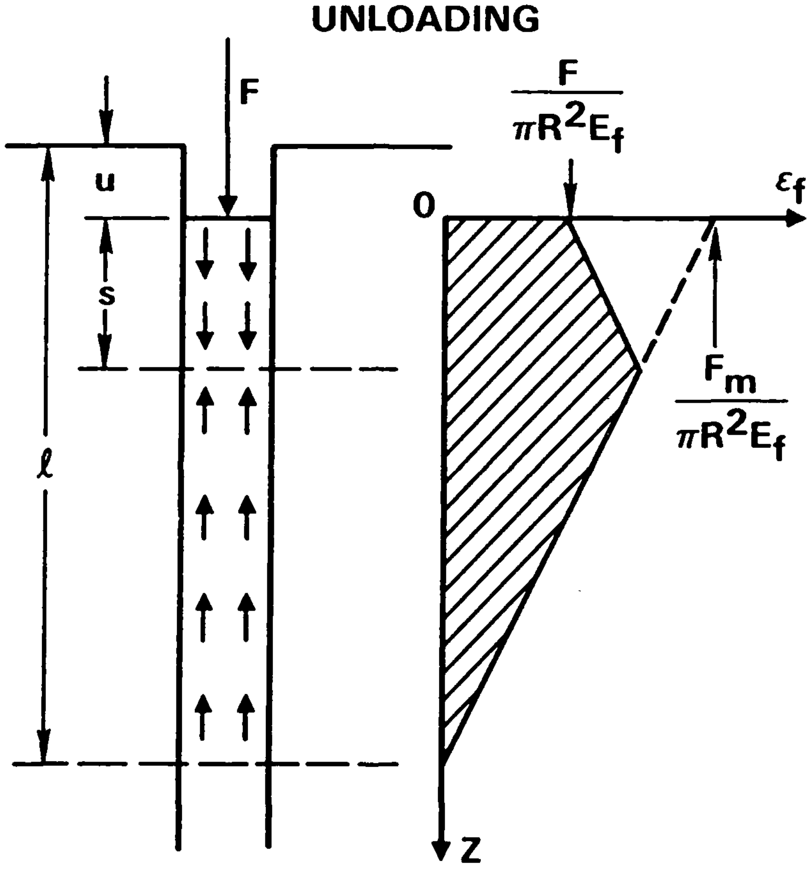

Figure 7

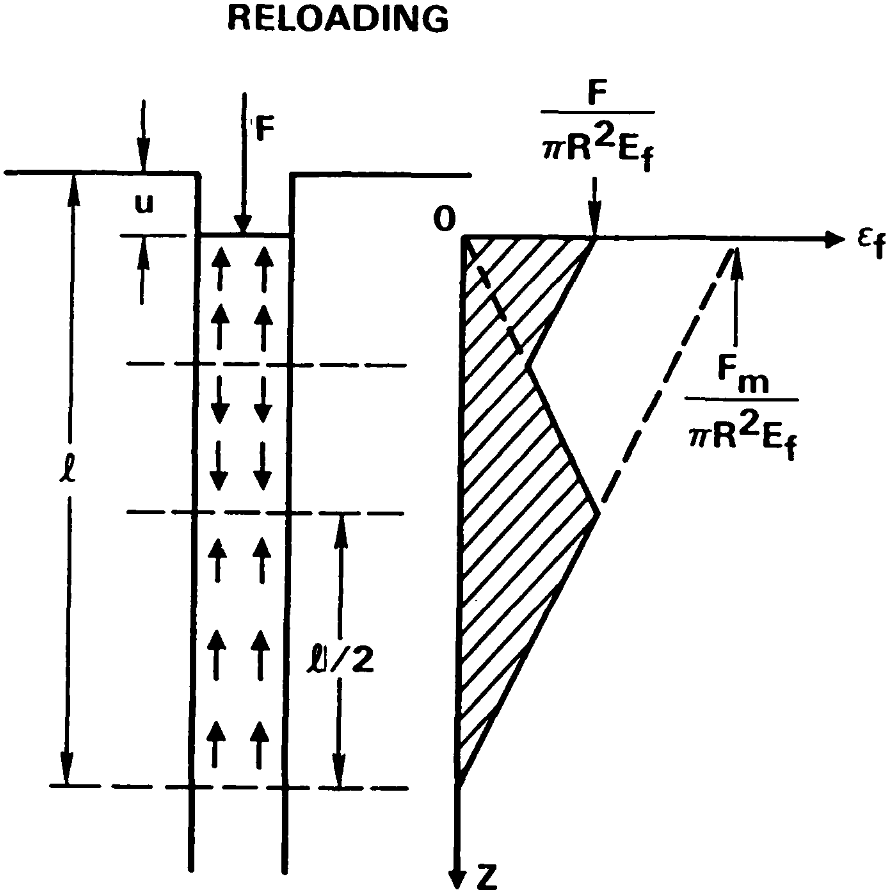
RELOADING
u
F
ℓ
ℓ/2
O
$\frac{F}{\pi R^2 E_f}$
ε_f
$\frac{F_m}{\pi R^2 E_f}$
Z

Figure 8

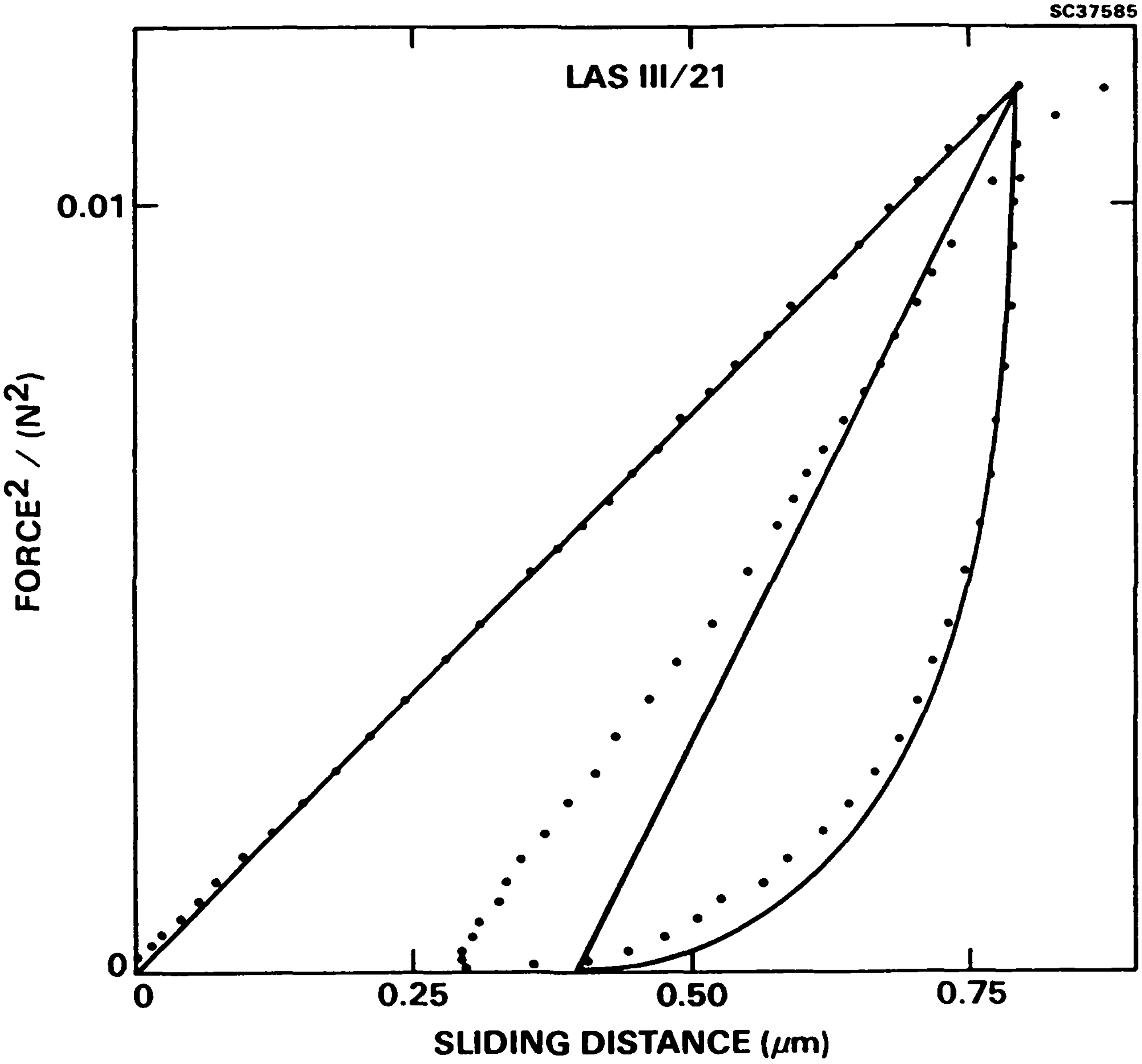
SC37585
LAS III/21
FORCE^2 / (N^2)
0.01
0
0
0.25
0.50
0.75
SLIDING DISTANCE (μm)

Figure 9

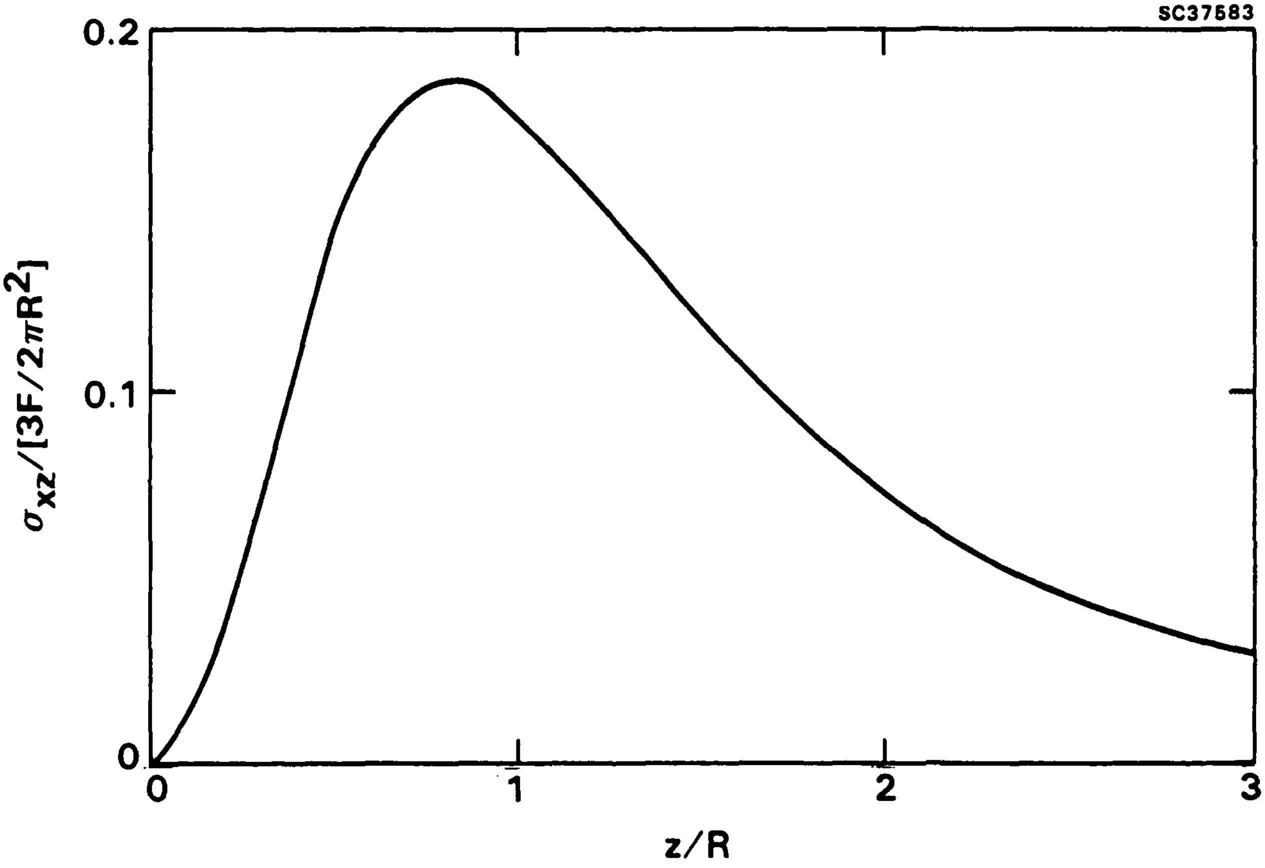

Figure B1

3.0 INTERFACES IN CERAMIC FIBER COMPOSITES

in Ceramic Microstructures '86: The Role of Interfaces, ed. J. Pask, Plenum, in press.

INTERFACES IN CERAMIC FIBER COMPOSITES

D.B. Marshall

Rockwell International Science Center
1049 Camino Dos Rios
Thousand Oaks, CA 91360

ABSTRACT

Fiber/matrix interface properties in frictionally bonded ceramic composites are examined. Relations between the sliding resistance of the interface and the mechanical properties of the composite are discussed. Then measurements of interface sliding, obtained using an indentation technique are presented. Experiments in the presence of transverse compressive stress and measurements of reverse sliding provide further insight into the nature of the interface. The range of composite properties for which the indentation method can be used to measure frictional stresses is assessed.

1. INTRODUCTION

The nature of the interface between fibers and matrix is the most critical factor in determining the mechanical properties of ceramic composites. If the interface is strongly bonded, matrix cracks can cross the interface and the composite fails in a brittle manner. However, if the interface is weakly bonded, then debonding and fiber pullout can lead to nonbrittle response of the composite, with a nonlinear stress-strain curve, large strain to failure, and load-carrying capacity beyond the peak load.[1-7]

The purpose of this paper is to quantify this notion of a "weak" interface. For composites in which relative sliding of the fibers and matrix is resisted only by frictional forces, fracture mechanics models have been developed recently to analyze the influence of bridging fibers on matrix crack growth.[1,8-10] Explicit relations have been obtained for strength, toughness and conditions for transitions in failure mechanisms in terms of frictional sliding resistance. Some of these results will be summarized in Section 2 to illustrate the role of the interface. In the following sections some new direct measurements of the mechanical characteristics of interfaces at individual fibers in a SiC/glass ceramic composite, which has interfacial properties dominated by frictional forces, will be presented.

2. INFLUENCE OF INTERFACES ON MECHANICAL PROPERTIES

2.1 Failure Mechanics

The tensile properties of unidirectionally reinforced brittle matrix composites are determined by the response of the fibers during growth of matrix cracks.[11] This response is dictated by the properties of the fiber/matrix interface. In strongly bonded systems, growth of the matrix crack causes fiber failure at, or near, the crack plane, and the composite fails catastrophically. However, if the interface is sufficiently weak, the fibers remain intact and bridge the matrix crack when it extends completely through the test section.[12] Then matrix cracking is followed by a region of nonlinear load increase and continued load support beyond the peak. The nonlinear load increase is associated with additional, periodic matrix cracks and pullout of fibers from the resultant blocks of matrix. The peak load is then determined by fiber failure, and continued load support results from pullout of the broken fibers prior to separation. This noncatastrophic mode of failure has been obtained in glass and glass-ceramics reinforced by carbon and SiC fibers.[1-7]

2.2 Fracture Mechanics Analysis

The major influence of the reinforcing fibers on the growth of the first matrix crack arises from fibers that remain intact across the crack plane and restrain the opening of the crack surfaces. By modeling the influence of the fibers as crack closure forces, the reduction of crack tip stresses due to the fibers can be calculated.[8,9]

An essential requirement for this analysis is knowledge of the force-displacement relation for fiber pullout, which is determined by the properties of the fiber-matrix interface. In the case of a SiC/glass-ceramic composite,* frictional sliding at the interface has been identified from measurements of hysteresis in crack opening displacements during load cycling experiments[12] (other measurements are discussed in the following sections).

For composites with frictionally bonded fibers that do not fail during matrix cracking, the fracture mechanics analysis predicts that the stress for matrix cracking is given by[8-10]

$$\sigma_1 = [6(1 - \nu^2)K_o^2 \tau f^2 E_f E_c^2 / R(1 - f)E_m^3]^{1/3} \qquad (1)$$

where τ is the sliding frictional stress at the interface, K_o is the toughness of the interface, E_m, E_f and E_c are the elastic moduli of the matrix, fibers and composite, R is the fiber radius and f is the volume fraction of fibers. It is noted that this stress is independent of the crack size and is therefore a damage-tolerant property of the composite. The requirement for this mode of failure is that the fiber strengths, S, satisfy the relation $Sf > \sigma_1$, which, for given fiber strength defines a maximum allowable value of τ.[9]

For larger values of τ, fiber failure occurs at a location behind the crack tip and failure of the composite is catastrophic. However, the

---

*United Technologies Research Center, lithium-alumino-silicate glass-ceramic matrix (LASIII), with Nicalon fibers.

limited zone of bridging fibers can lead to significant toughening of the composite. In general the events leading to failure are dependent upon the initial crack configuration (crack area and area of initially broken fibers). Failure can begin with stable fiber fracture or matrix cracking.[6] However, for a wide range of initial conditions, the crack configuration at the point of unstable composite failure is that for which the matrix crack growth and fiber failure conditions are satisfied simultaneously. In this case the strength is given by[9]

$$\sigma = (E_c/E_m)[1 + (Sf/\sigma_1)^3]K_o/(\pi c)^{1/2} \tag{2}$$

where c is the crack length. The strength in this case is sensitive to pre-existing crack size and the effect of the fibers is to increase the fracture toughness by the factor $[1 + (Sf/\sigma_1)^3]E_c/E_m$.

These results indicate that, for composites that fail noncatastrophically, the matrix cracking stress increases with increasing τ (Eq. (1)). However, there is a maximum value of τ that will allow this mode of failure, defined by the condition $Sf > \sigma_1$. For larger values of τ failure is catastrophic and the toughening effect of the fibers diminishes as τ increases further. Therefore, it is evident that intermediate values of τ give optimum properties.

3. MEASUREMENT OF INTERFACE PROPERTIES COMPOSITE

3.1 Indentation Method

Direct measurement of properties of individual fiber/matrix interfaces in the SiC/glass-ceramic composite have been obtained using the indentation method illustrated in Fig. 1.[13] In this technique a Vickers indenter is used to push on the end of a fiber, and the magnitude of the interfacial stress that resists sliding is obtained from measurement of the force, F, applied to the fiber, and the resultant displacement, u, of the fiber surface below the matrix surface. In a composite with frictional forces between the fibers and matrix, sliding begins at the specimen surface and extends a distance below the surface which is dependent upon the magnitude of the applied force. If the sliding distance is smaller than the specimen thickness (i.e., measured depression of the fiber below the matrix is due to elastic compression of the fiber) but large compared with the fiber radius, the frictional stress is given by[13]

$$\tau = F^2/4\pi^2 u R^3 E_f \tag{3}$$

and the sliding distance is given by

$$\ell = 2\pi R^2 u E_f/F \tag{4}$$

During unloading, sliding occurs in the reverse sense so that the fiber displacement after unloading is smaller than at the peak load (Section 3.3).

A simple method for obtaining the peak load displacement required in Eqs. (3) and (4) is to allow the edges of the indenter to touch the matrix as in Fig. 1. Then the displacement of the fiber is calculated from measurements of dimensions parallel to the surface and the known angle of the indenter;

$$u = (b - a)\cot\psi \tag{5}$$

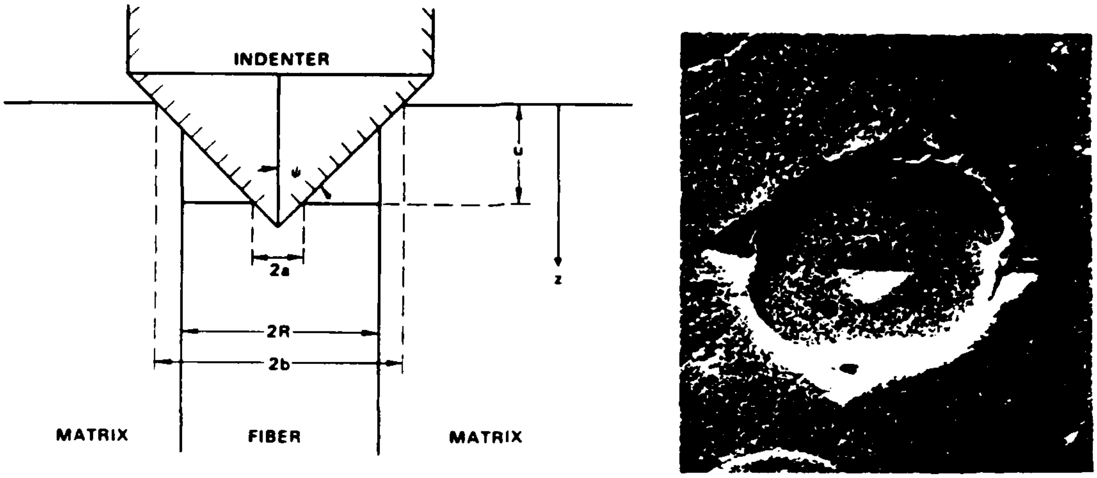

(a) (b)

Fig. 1. (a) Schematic of indentation method used for measuring matrix/fiber frictional stress. (b) Scanning electron micrograph showing fiber indentation with Vickers pyramid. Width of field 32 μm. (After Ref. 10).

where the dimensions a and b and the angle ψ are defined in Fig. 1(a) ($\psi = 74°$ for the Vickers indenter). The force applied to the fiber is obtained from the contact dimension, a, and the hardness, H, of the fiber

$$F = 2a^2H \tag{6}$$

Measurements of frictional stresses using this method in the SiC/glass-ceramic composite are shown in Fig. 2. Most values fall within the range $\tau = 2.1 \pm 1$ MPa, and there is no systematic variation of τ with the fiber diameter. Several measurements fall in the range 10 to 15 MPa. The fibers in this composite are not all perfectly aligned and the diameters of individual fibers are not perfectly uniform. Therefore, these relatively high values of τ could result from fiber misalignment below the surface (ellipticity of the fiber cross sections due to misalignment was not evident at the surface) or from relatively large irregularities in fiber diameter below the surface.

It is of interest to examine the range of fiber sizes and frictional stresses for which this method provides sensitive measurements of τ. (Changing τ alters the contact dimension, a, when the indenter first touches the matrix; in the limits $a \to 0$ and $a \to R$ the method becomes inaccurate.) This range can be assessed by expressing τ and ℓ in terms of the dimensions a and b rather than F and u (Eqs. (3) to (6));

$$\tau = [H^2/\pi^2E_f \cot\psi](a/R)^3/[(b/R)(R/a) - 1] \tag{7}$$

$$\ell/R = [\pi \cot\psi\ E_f/H][(b/R)(R/a) - 1]/(a/R) \tag{8}$$

Geometrical similarity is evident in the dimensions b, a, R and ℓ in Eqs. (7) and (8); for a given material the ratios a/R and ℓ/R are fixed once b/R is specified. This implies that the sensitivity of the technique is not influenced by the fiber size (except for practical considerations of measurement resolution). Equations (7) and (8) are plotted in Fig. 3,

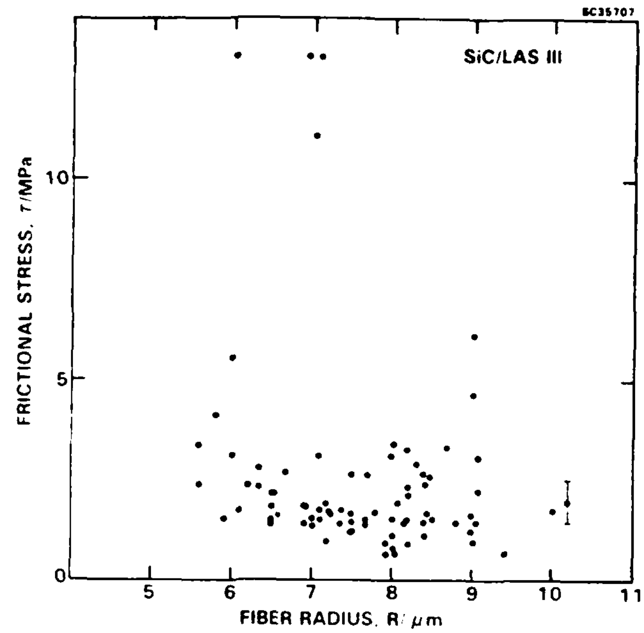

Fig. 2. Indentation measurements of frictional stresses acting on SiC fibers in a lithium-alumino-silicate glass-ceramic matrix.

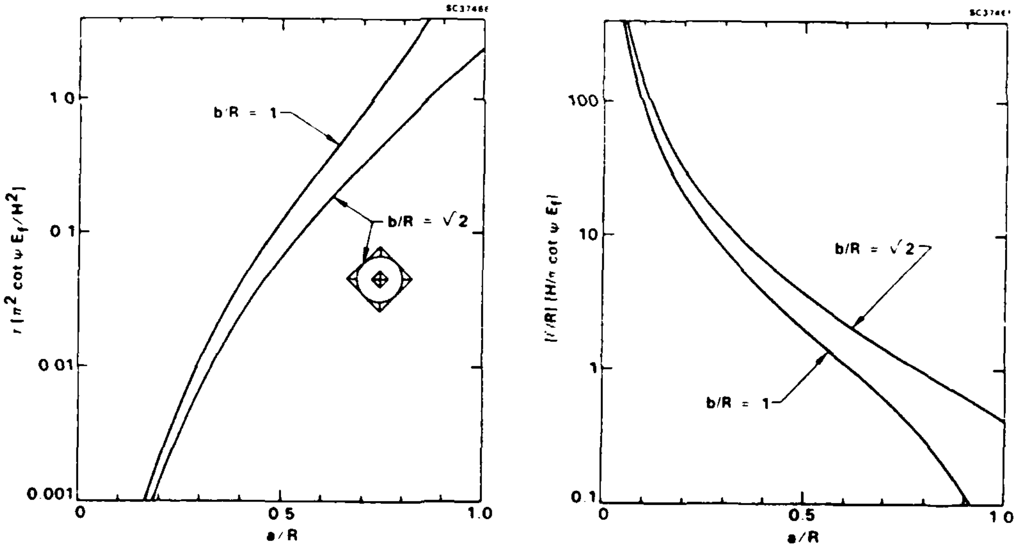

(a) (b)

Fig. 3. Plots showing the relation between contact geometry in the indentation experiment and the properties of the composite.

for two values of b/R which bound the range usually used for measuring τ. The smaller value, $b/R = 1$, corresponds to the case where the edges of the indenter just touch the matrix, whereas the larger value, $b/R = \sqrt{2}$, corresponds to the indenter faces touching the matrix in a continuous line (see Fig. 3). For the SiC/glass-ceramic composite, (E_f = 200 GPa, H = 13 GPa, $\tau(\pi^2 \cot\psi\ E_f/H^2) = 0.01$ and $\pi \cot\psi\ E_f/H = 13.9$), Fig. 3 gives $a/R \simeq 0.30$ and 0.34 and $\ell/R \simeq 140$ for these values of b/R. Variation of τ over 3 orders of magnitude would keep a/R within the range 0.2 to 0.8 and ℓ/R within the range 1000 to 10. Therefore, the technique would appear to be applicable to a wide range of microstructures.

3.2 Effect of Normal Stress on Interface Sliding

The sliding resistance of a frictionally bonded interface should be sensitive to stresses normal to the interface (such stresses in composites arise from thermal contraction mismatch between fibers and matrix). A preliminary estimate of this sensitivity was obtained by measuring the frictional stress in the SiC/glass-ceramic composite in the presence of applied compressive stress. This was done by applying biaxial pressure normal to the fibers with a fixture mounted on the table of the indentation equipment. The specimen was a rectangular beam (2 × 2 × 25 mm) with the fibers parallel to the longest dimension. The beam was embedded in epoxy (dimensions with epoxy 6 × 6 × 25 mm) to prevent crushing, and the load was applied through four steel anvils placed against the sides of the specimen). The resulting strain in the composite was measured with a strain gage attached to one end of the beam and the friction measurements were obtained by indenting fibers at the opposite end.

The results of measurements obtained at zero stress and at compressive stress 300 MPa (transverse elastic modulus of composite 110 GPa, strain 2×10^{-3}) are summarized in Fig. 4. Care was taken in these experiments to avoid systematic errors that might arise from spatial variations of τ, or from bias in selecting fibers of particular diameters or locations for testing. Using the micrometer table of the indenting equipment, the fibers tested were those closest to the intersections of a rectangular grid, with alternate rows being tested at zero stress and under compression. The results in Fig. 4 indicate that the applied compression caused the frictional stress to increase from $\tau = 2.1 \pm 1$ MPa to $\tau = 4.8 \pm 2.5$ MPa. If Coulomb's friction law is assumed,[14]

$$\tau = A + \mu\sigma_n \qquad (9)$$

where σ_n is the normal stress at the interface and A is a constant, then the friction coefficient would be $\mu = 0.01$.

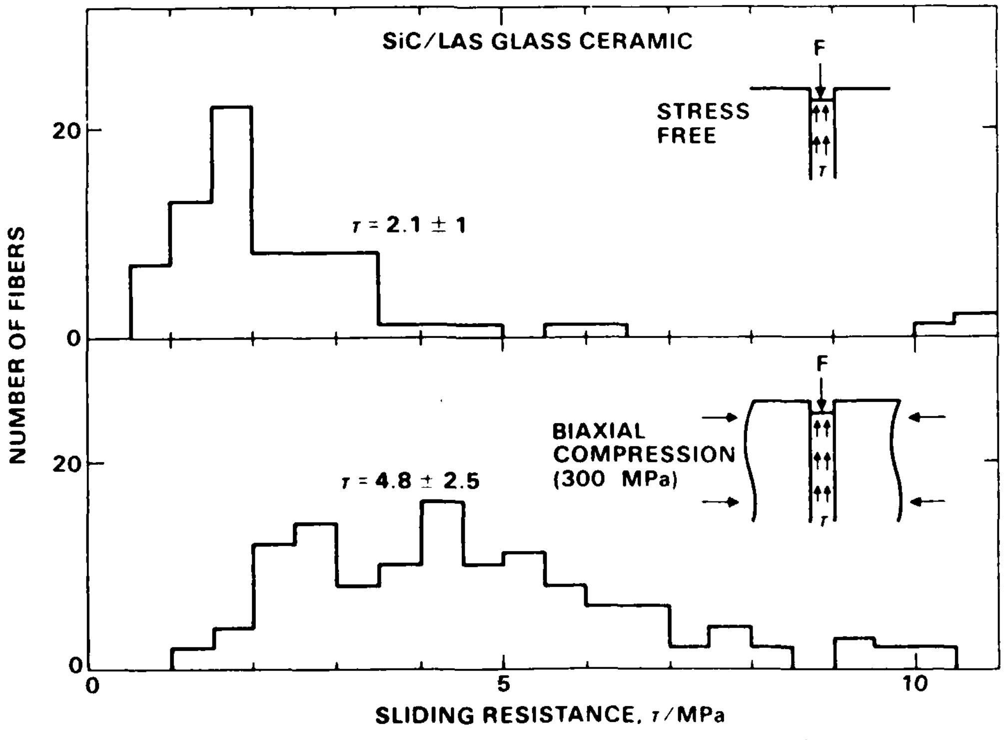

Fig. 4. Distributions of frictional stresses in SiC/glass-ceramic composite with and without transversely applied compressive stress.

3.3 Reverse Sliding

When the force applied to the end of a fiber is decreased, sliding occurs in the direction opposite to that during loading (Fig. 5). Consequently, the displacement of the fiber surface below the matrix is smaller after the indenter is removed than it is at the peak load. Measurement of the relaxed displacement provides further insight into the nature of the interface.

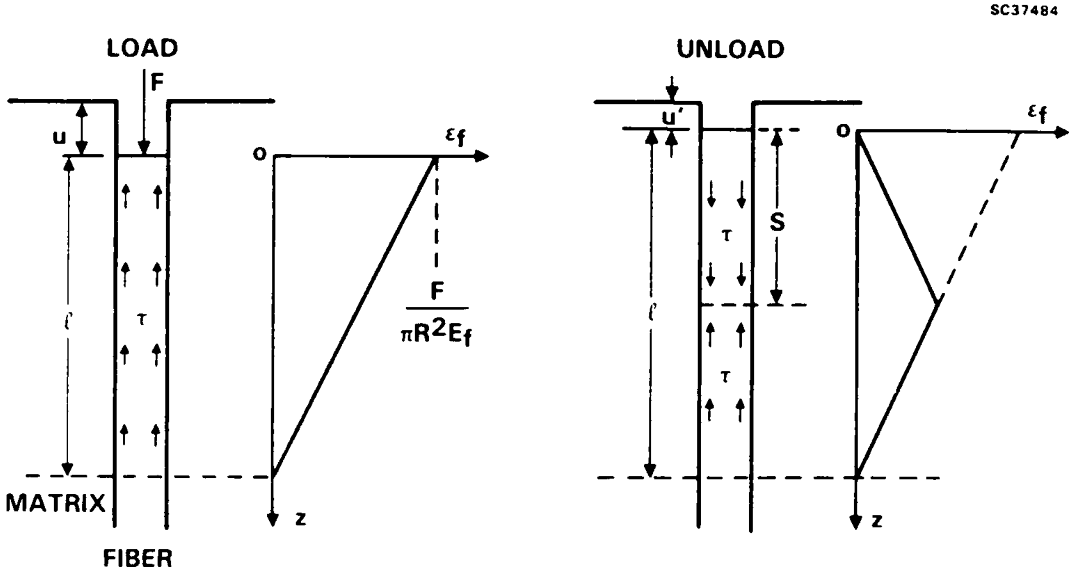

Fig. 5. Distributions of compressive strains within the region of a fiber that slides relative to the matrix.

The relative values of the fiber displacements at peak and zero loads can be calculated from Fig. 5. The peak load displacement is obtained by integration of the compressive strains, $\varepsilon_f(z)$, within the section of fiber over which sliding occurs between the fiber and matrix

$$u = \int_0^{\ell} \varepsilon_f(z)dz \tag{10}$$

The strain distribution, obtained from the relation $d\varepsilon_f/dz = \tau/RE_f$ and the boundary condition $\varepsilon_f(0) = F/\pi R^2 E_f$, is shown in Fig. 5(a) (this, with Eq. (10) leads to Eq. (3)). During unloading, sliding begins in the reverse sense at the fiber surface and extends a distance s (Fig. 5(b)) after complete unloading. The resultant strain distribution, defined by the boundary condition $\varepsilon_f(0) = 0$, is shown in Fig. 5(b). The reverse sliding distance is $s = \ell/2$, and the fiber displacement, u' (Eq. (10)) is half of the peak load displacement, u.

This result is based on the assumption that elastic strains at $z > \ell$ are negligible and that the frictional stresses are equal during forward and reverse sliding. However, if forward sliding degrades the interface, resulting in a lower frictional stress τ' during reverse sliding, or if the sliding distance ℓ is dictated by the length of a debond crack in an initially bonded interface, then $s > \ell/2$, and the displacement after unloading is smaller than u/2. For the case of unequal frictional stresses during forward and reverse sliding, the displacement after unloading is given by[15]

$$u' = u/(1 - \tau/\tau') \tag{11}$$

The displacements at peak and zero loads were measured in the SiC/glass-ceramic composite using the simple method shown in Fig. 6. After loading a fiber with the Vickers pyramid the same fiber was loaded with a Knoop indenter with the specimen rotated so that the diagonals of the two indentations were at 45°. Because the angle between opposite edges of the Knoop indenter is larger than that for the Vickers, the edge of the Knoop indenter touched the matrix before the tip touched the fiber (Fig. 6(a). Moreover, the elongated shape of the Knoop indenter allowed a measurable impression to be left on the fiber surface with a relatively small load and, consequently, a relatively small displacement of the fiber. For the case shown in Fig. 6(b) the force applied to the fiber by the Knoop indenter was < 0.2 of the original force applied to the Vickers indenter, and the displacement caused by the Knoop indenter was < 0.02 of that caused by the Vickers (analysis of reloading displacements will be published elsewhere[15]). Therefore, measurement of the fiber displacement at the peak load for the Knoop indenter, using Eq. (5) and the measured Knoop contact dimensions (with ψ = 86.25°), provides a good approximation to the displacement after unloading the Vickers indenter.

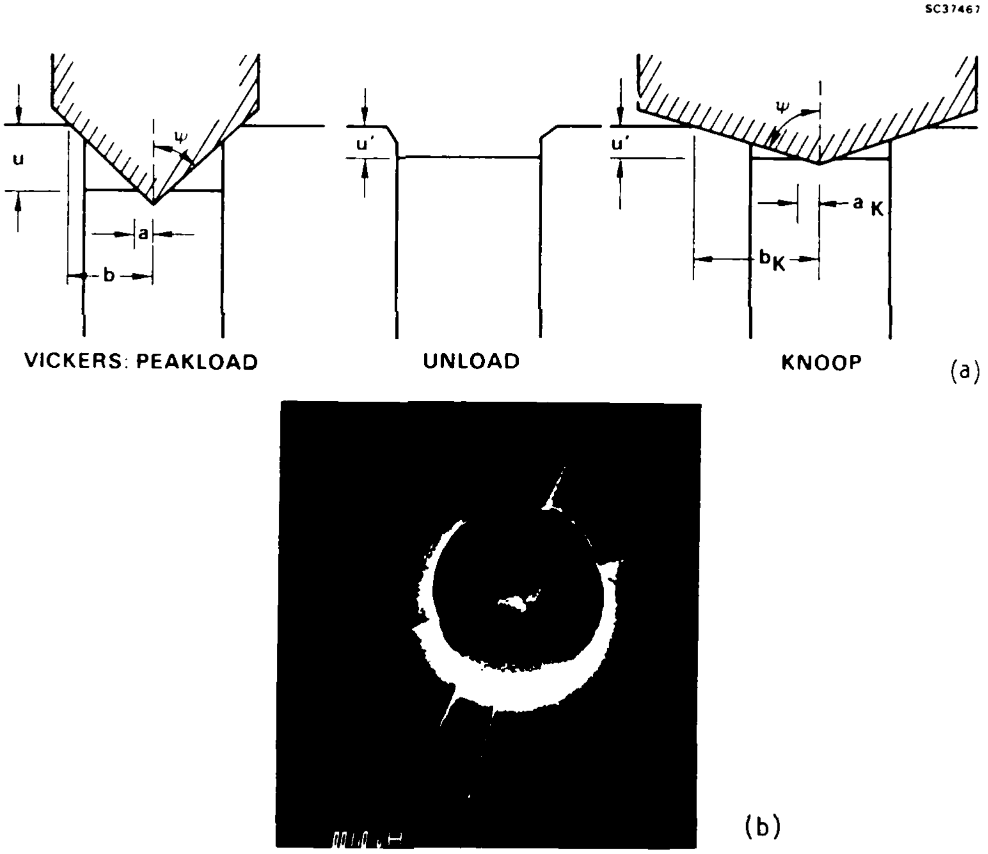

Fig. 6. Measurement of reverse sliding distance due to unloading: (a) schematic of method, (b) scanning electron micrograph of fiber indenter by a Vickers pyramid and then a Knoop indenter.

Measurements of the ratios of the peak and zero load displacements for 20 fibers in the SiC/glass-ceramic composite gave the result $u'/u = 0.46 \pm 0.03$. This is close to the value 0.5 predicted for frictional sliding of an unbonded interface. The result suggests that the interface may degrade slightly on the first sliding, but Eq. (11) indicates that the reduction in the frictional stress is less than 10%.

4. DISCUSSION

The experiments described in Section 3 provide insight into the nature of the fiber/matrix interface, as well as providing direct measurements the frictional stress, τ, which dictates strength, toughness and failure mechanism of the composite (Eqs. (1) and (2)). The measurements in the presence of applied transverse compression in the SiC/glass ceramic composite suggest a friction coefficient $\mu \approx 0.01$. This value is lower than that of graphite sliding on graphite $\mu = 0.1$ (Brennan has observed a thin layer of carbon at the fiber/ matrix interface in this composite[16]). This very low value of μ suggests that a gap may exist at the interface, in which case the true friction coefficient in Eq. (9) would be larger than 0.01. Further experiments over a range of applied stresses would clarify this question (stresses in the present experiments were limited by flow of the epoxy used to prevent crushing). The reverse sliding experiments indicate that there is not sufficient bonding at the interface to influence the sliding, and that the frictional stress is similar during forward and reverse sliding. This result has been confirmed by experiments, to be reported elsewhere,[15] in which forces and displacements were measured at all stages of loading and unloading (and subsequent cyclic loading).

The results of the experiments with transverse compression allow an estimate to be made of the contribution of Poisson's expansion of the fibers to measured frictional stresses. The force applied to the ends of the fibers in these experiments (≈ 0.2N) caused average compressive strain ≈ 0.0015 over the region of fiber that underwent sliding, and average transverse expansion ≈ 0.0004. If the fiber and matrix were initially in intimate contact, this would result in compressive stress ≈ 8 MPa across the interface. With the measured friction coefficient, 0.01, the resultant additional frictional stress is $\tau_v \approx 0.1$ MPa. This is small compared with the total measured value, $\tau \approx 2$ MPa. Tensile strains in the fibers that bridge cracks are of similar magnitude to the strains in the indentation experiments. Therefore, the compressive nature of the indentation experiment should not cause the measured frictional stress to differ significantly from the value appropriate to fiber pullout in tension during cracking. This conclusion is consistent with independent measurements of τ in tension, which agree well with the indentation measurements.[13]

ACKNOWLEDGMENT

Funding for this work was provided by the U.S. Office of Naval Research under Contract No. N00014-85-C-0416. The author is indebted to J.J. Petrovic for suggesting experiments using applied transverse compression.

REFERENCES

1. J. Aveston, G.A. Cooper and A. Kelly, pp. 15-26 in the Properties of Fiber Composites, Conf. Proc. Nat. Physical Lab., IPC Science and Technology Pres. Ltd., Surry, England, 1971.
2. R.A.J. Sambell, A. Briggs, D.C. Phillips and D.H. Bowen, J. Mater. Sci. 7:6, 676-681 (1972).
3. D.C. Phillips, J. Mater. Sci. 9:11, 1847-54 (1974).
4. D.C. Phillips, J. Mater. Sci. 7:10, 1175-91 (1972).
5. K.M. Prewo and J.J. Brennan, J. Mater. Sci. 15:2, 463-8 (1980).
6. K.M. Prewo and J.J. Brennan, J. Mater. Sci. 17:4, 1201-6 (1982).
7. J.J. Brennan and K.M. Prewo, J. Mater. Sci. 17:8, 2371-83 (1982).

8. D.B. Marshall, B.N. Cox and A.G. Evans, Act. Met. 33:11, 2013-21 (1985).
9. D.B. Marshall and A.G. Evans in Fracture Mechanics of Ceramics, Vol. 7, Ed., R.C. Bradt, A.G. Evans, D.P.H. Hasselman and F.F. Lange, Plenum, in press.
10. B. Budiansky, J.W. Hutchinson and A.G. Evans, to be published in J. Appl. Mech.
11. A.G. Evans, M.D. Thouless, D.B. Johnson-Walls, E. Luh, and D.B. Marshall, in proceedings of 5th Int'l. Conf. on Composite Materials. Ed., W.C. Harrigan, J. Strife, A.K. Dingra, Metallurgical Soc. 1985.
12. D.B. Marshall and A.G. Evans, J. Amer. Ceram. Soc. 68:5, 225-21 (1985).
13. D.B. Marshall, J. Am. Ceram. Soc. 67:12, C259-60 (1984).
14. F.P. Bowden and D. Tabor, Friction and Lubrication of Solids, Parts I and II, Clarendon, Oxford, 1950, 1964.
15. W. Oliver and D.B. Marshall, to be published in J. Am. Ceram. Soc.
16. J.J. Brennan, this volume.

4.0 TENSILE STRENGTH OF BRITTLE MATRIX COMPOSITES: INFLUENCE OF FIBER STRENGTH

to be submitted to Acta. Met.

TENSILE STRENGTH OF BRITTLE MATRIX COMPOSITES: INFLUENCE OF FIBER STRENGTH

D.B. Marshall and B.N. Cox

Rockwell International Science Center
1049 Camino Dos Rios
Thousand Oaks, CA 91360

ABSTRACT

A stress intensity approach is used to analyze tensile failure of brittle matrix composites that contain unidirectionally aligned fibers held in place by friction. In general, failure may initiate either by growth of a crack in the matrix, or by fracture of fibers that bridge the matrix crack. Subsequently, these failure processes may continue either unstably or stably with increasing applied stress. Solutions to the fracture mechanics analysis are obtained numerically in normalized form, with one microstructural variable, the normalized fiber strength. The analysis defines transitions between failure mechanisms and provides strength/crack-size relations for each mechanism. Explicit relations are derived for the matrix cracking stress (noncatastrophic failure mode), the condition for transition to a catastrophic failure mode, and the fracture toughness in a region of catastrophic failure, in terms of microstructural properties of the composite.

1.0 INTRODUCTION

Two distinct tensile failure mechanisms are exhibited by brittle materials that are reinforced with unidirectionally aligned fibers.[1,2] If the fiber strength is sufficiently large, the first damage to occur during tensile loading is a crack which extends completely through the matrix and remains bridged by unbroken fibers over its entire area. Further loading causes periodic matrix cracking, followed by failure of the composite at a stress equal to the fiber-bundle fracture stress. This failure mechanism has been observed in several ceramic composites (glass and glass ceramics reinforced by SiC and carbon fibers)[3-7] and in fiber reinforced cements.[8] On the other hand, if the fiber strength is lower than a critical value, fiber failure occurs behind the tip of a growing crack. In that case matrix cracking causes complete failure of the composite. However, the zone of unbroken fibers behind the crack tip can lead to substantial toughening.

The critical stress for matrix cracking has been evaluated using fracture mechanics for composites containing unbonded high-strength fibers in which fiber/matrix sliding is resisted by friction and fiber failure does not occur. Analyses using energy balance approaches have provided steady state (i.e., large-crack) solutions, initially in the work of Aveston et al[4,9] for the limits of large and small frictional stresses and more recently by Budiansky et al[10] for intermediate values. Solutions for a range of initial matrix crack sizes (nonsteady-state cracks) have also been obtained recently[11] for the case of small frictional stress, using a stress intensity approach in which a closure stress intensity factor due to the bridging fibers was calculated. This solution confirms the existence of a steady state for large cracks, provides the same solution as the energy balance analysis for the steady-state critical stress, and defines a minimum initial matrix crack size at which the steady state solution is a reasonable approximation.

In this paper the stress intensity approach is extended to analyze matrix cracking in composites in which fiber failure accompanies matrix cracking. The analysis provides a relation for the critical fiber strength at which the change in failure mechanism occurs, in terms of the microstructural properties of the composite. It also defines strength/crack-size relations for composites in which the fiber strength is lower than the critical value. For certain initial crack configurations, failure is preceded by stable matrix crack growth or fiber failure with increasing applied load. Therefore, consideration of crack stability is an important part of assessing the conditions for failure.

2.0 FRACTURE MECHANICS MODEL

2.1 Fracture Criteria

The present analysis is directed to the crack configuration of Fig. 1, where continuous reinforcing fibers are aligned normal to the plane of a penny shaped crack of radius c. (Results for straight cracks are very similar and are summarized in Appendix I). The composite is loaded monotonically with a remote uniform stress σ_∞ normal to the crack plane. The fibers within a distance d of the crack tip remain intact and bridge the crack, whereas the remainder of the fibers, over an area of radius c_0, are broken and do not contribute to bridging. Failure of the composite may initiate with either matrix crack growth or fiber failure.

Fiber failure occurs when the stress σ_f in the bridging fiber exceeds the fiber strength, S. For composites in which the fibers and matrix are not chemically bonded, sliding between the matrix and fibers is resisted by friction. Sliding occurs over a distance from the crack surface determined by the length over which the interfacial shear stresses exceed the frictional stress τ. The tensile stress in a bridging fiber is maximum in the section of the fiber between the crack surfaces and decreases linearly with distance along the region that has slipped. In general, a statistical distribution of fiber strengths would allow some fiber failure within the region embedded in the matrix. However, the present calculations assume a single valued fiber strength S, so that fiber failure occurs only between the crack surfaces and broken fibers do not contribute to crack bridging. A single-valued fiber strength also implies that fiber failure occurs first at the trailing edge of the bridging zone because the crack opening displacements always increase monotonically away from the crack tip (this is confirmed in the calculations in Section 3.0).

The criterion for growth of the crack in the matrix is not as clear-cut. Previously, both energy-balance and stress-intensity criteria have been used.[2,4,9-11] In certain cases these criteria give identical results (homogeneous materials, steady-state fully-bridged matrix cracks in composites[17]), but in general the results differ (Section 5.0). The energy-balance criterion gives a lower bound fracture stress whereas the stress intensity criterion represents an upper bound. To remain consistent with our previous work the stress-intensity criterion is used here. The condition for crack growth is that the stress intensity factor associated with the stresses in the matrix near the crack tip equal the critical value K_o for the unreinforced matrix. The influence of the bridging fibers is to restrain the opening of the crack and, consequently, cause a reduction in the crack tip stresses.

2.2 Crack Opening Displacements and Crack Tip Stresses

The relation between the applied load and the crack-tip stresses can be evaluated by replacing the bridging section of each fiber by crack surface tractions equal to the stress, σ_f, in that section of fiber (Fig. 1). In a continuum approximation (crack radius, c >> fiber spacing) this is equivalent to applying a distribution of closure pressure, p(x) to the surface of the crack:

$$p(x) = f\ \sigma_f(x) \qquad (1)$$

where x represents the position on the crack surface and f is the volume fraction of fibers. The influence of the remotely applied stress, σ_∞, on the crack tip stress can be calculated by regarding the stress as a uniform opening pressure acting over the crack surface. Therefore, the net crack surface pressure is $\sigma_\infty - p(x)$, and a composite stress intensity factor can be defined as[12]

$$K = 2(c/\pi)^{1/2} \int_0^1 \frac{[\sigma_\infty - p(X)]XdX}{\sqrt{1 - X^2}} \qquad (2)$$

where X = x/c. If there is no sliding between the fibers and matrix ahead of the crack tip, the composite stresses, σ_c, and the matrix and fiber stresses, σ_m and σ_f are related by

$$\sigma_m/E_m = \sigma_c/E_c = \sigma_f/E_f \qquad (3)$$

where

$$E_c = fE_f + (1 - f)E_m \qquad (4)$$

and E, E_m and E_f are the Young's Moduli of the composite, the matrix, and the fibers. Moreover, since the matrix and composite stress intensity factors scale with the stresses, the stress intensity factor in the <u>matrix</u>, K^m, is related to K by

$$K^m = K\,E_m/E_c \quad . \tag{5}$$

A relation between the closure pressure p(x) and the crack opening u(x); is provided by analysis of fiber pullout from the matrix[11]

$$p(x) = \begin{cases} \alpha\,\sqrt{u(x)} & (x > c_0) \quad (6a) \\ 0 & (x < c_0) \quad (6b) \end{cases}$$

where

$$\alpha = \left[\frac{4\tau f^2 E_f E_c}{R\,E_m(1 - f)}\right]^{1/2} \quad , \tag{7}$$

and R is the radius of the fibers. Equation (7) is a limiting solution for large slip, obtained by neglecting the effect of interfacial shear stresses beyond the region of fiber/matrix sliding. From the analysis of steady state cracking by Budiansky et al[10] it can be shown that this approximation is valid for

$$\tau \lesssim (K_0/R^{1/2})(E/E_f)^{1/4} g(f) \tag{8}$$

where

$$g(f) = (1 - f)^{7/4}/f^{1/2}[2 \log f + (1 - f)(3 - f)]^{3/4}$$

The crack opening at a given location is determined by the entire distribution of crack surface pressure[13]

$$u(X) = \frac{4(1 - \nu^2)c}{\pi E} \int_X^1 \frac{1}{\sqrt{s^2 - X^2}} \int_0^s \frac{[\sigma_\infty - p(t)]tdt}{\sqrt{s^2 - t^2}} ds \qquad (9)$$

where s and t are normalized position coordinates and ν is Poisson's ratio for the composite. Therefore calculation of the crack tip stresses requires solution of Eqs. (6) and (9) followed by evaluation of the integral in Eq. (2). An analytical solution, based on an assumed crack profile and valid for small bridging zones, was obtained previously[2] (Appendix II). In the present work numerical solutions are presented. For convenience, the equations can be expressed in the normalized form

$$U(X) = 3(C/\Sigma_\infty) \int_X^1 \frac{1}{\sqrt{s^2 - X^2}} \int_0^s \frac{F(u)\ t\ dt}{\sqrt{s^2 - t^2}} ds \qquad (10)$$

and

$$K/K_C = 3\Sigma_\infty\sqrt{C} \int_0^1 \frac{F(U)XdX}{\sqrt{1 - X^2}} \qquad (11)$$

where

$$F(u) = \begin{cases} 1 - \sqrt{U} & X > C_0 \\ 1 & X < C_0 \end{cases} \qquad (12)$$

and the dimensionless parameters $\Sigma_\infty = \sigma_\infty/\sigma_n$, $C = c/c_n$, $C_o = c_o/c_n$, and $U = u/u_n$ are defined by*

$$\sigma_n = \left[3\alpha^2 K_c^2 \, (1 - \nu^2)/E\right]^{1/3} \quad , \tag{13}$$

$$c_n = (\pi/4)\left[9EK_c/\alpha^2(1 - \nu^2)\right]^{2/3} \quad , \tag{14}$$

$$u_n = \sigma_\infty^2/\alpha^2 \quad , \tag{15}$$

and $K_c = K_o E_c/E_m$ is the critical value of K for matrix crack growth (Eq. (5) with $K^m = K_o$). The stress in the bridging fibers is $\Sigma_f = \Sigma_\infty \sqrt{U}/f$ (Eqs. (1), (6) and (15)) and the failure condition for the fibers is

$$\Sigma_\infty \sqrt{U(C_o)} = fS/\sigma_n \tag{16}$$

---

*It is noted that Eqs. (10) and (11) can be further simplified to eliminate the factor of 3 which appears in both equations by defining the normalization parameters $\sigma_n = \sigma_n/3^{1/3}$ and $C_n = C_n/9^{2/5}$. However the present normalization is retained for consistency with previous work (Refs. 2 and 11).

3.0 NUMERICAL SOLUTIONS

Equations (10) and (12) were solved by iteration to self consistency in the function $U(X)$, after making the transformations $t = s \sin \theta$ and $s = X \cosh \phi$. The effective dimension of the integral equation was reduced by evaluating the inner integral for all t at the beginning of each iteration, and storing the results on a suitable grid. Then as the outer integral was evaluated for each value of X_0, values of the inner integral were found by interpolation over the stored values. This procedure, combined with integration using cubic splines, yielded well-behaved solutions (increasing grid density always increased accuracy) and rapid covergence. A typical crack profile is shown in Fig. 2.

After obtaining a self-consistent crack profile for each crack configuration (i.e., given C_0 and C) and applied stress, the stress in the last bridging fiber was calculated ($\Sigma_f = \Sigma_\infty \sqrt{U(C_0)}/f$) and the matrix stress intensity factor was computed from Eq. (11). Then, from sets of solutions at various Σ_∞, C, and C_0, the critical applied stress for matrix crack growth Σ_k, was evaluated for various C and C_0, and the critical applied stress for fiber failure, Σ_s, was evaluated for various C, C_0 and Sf/σ_n. The results are exemplified in Fig. 3, where Σ_k, and Σ_s are plotted as a function of the unbridged crack radius for four representative values of the total crack size.

Some effects of changing the length of bridging zone or the crack radius on the stresses at the crack tip and in the remaining bridging fibers are readily deduced from Fig. 3. If the fiber furthest from the crack tip (i.e., at $X = C_o$) is broken, with the applied stress and total crack size held constant, the crack tip stresses always increase (i.e., $\partial\Sigma_k/\partial C_o|_c < 0$). This result is expected intuitively because removal of a bridging fiber allows the crack opening to increase. This also causes the stress in each remaining fiber to increase. For initially fully-bridged cracks this increase is sufficient to cause failure of the next fiber (i.e., $\partial\Sigma_s/\partial C_o|_c < 0$), but for cracks with smaller bridging zones (i.e., larger C_o) the increase is not sufficient to cause further fiber failure ($\partial\Sigma_s/\partial C_o|_c > 0$). If the crack radius c is increased at constant c_o/c and applied stress, both the crack tip stresses and the fiber stresses increase (i.e., Σ_s and Σ_k decrease).

4.0 COMPOSITE FAILURE MECHANICS

Failure of the composite initiates when the applied stress exceeds the smaller of Σ_k and Σ_s. Subsequently, the failure process (at constant applied stress) may involve either stable or unstable matrix cracking and/or fiber failure, depending on the signs of the partial derivatives of Σ_s and Σ_K with respect to C_o and C. Consequently, the sequence of events leading to complete failure of the composite depends on the initial crack configuration, c and c_o and the fiber strength, Sf/σ_n.

4.1 Initially Fully-Bridged Crack

The critical applied stresses for matrix cracking (Σ_K) and fiber failure (Σ_S) for fully bridged cracks (i.e., $C_o = 0$) are plotted as a function of crack size in Fig. 4. For large cracks, both critical stresses approach steady-state values, $\Sigma_k = 0.794$ and $\Sigma_s = Sf/\sigma_n$. In general the first failure event to occur is dependent upon both the fiber strength and the initial crack length.

For fiber strengths, Sf/σ_n, larger than 0.794, unstable matrix crack extension always occurs before fiber failure, but subsequent events are dependent upon the initial crack size. If the initial crack is sufficiently large that the stress Σ_k is smaller than the steady-state fiber failure stress Sf/σ_n, the crack grows unstably completely through the matrix without causing fiber breakage. Further increase of applied load is then needed to cause fiber failure. This is the mode of failure that leads to mutiple matrix cracking and large nonlinear strains before complete failure of the composite. For smaller cracks, where Σ_k exceeds Sf/σ_n, unstable fiber failure accompanies matrix cracking after some unstable growth of the matrix crack. This causes catastrophic failure of the composite at the applied stress Σ_k.

For smaller fiber strengths ($Sf/\sigma_n < 0.8$) the curves for Σ_k and Σ_s intersect at crack length C*. Initial cracks that are smaller than C* respond in the same manner as the small cracks described above (unstable matrix crack growth followed by fiber failure). For larger initial cracks, fiber failure occurs first ($\Sigma_s < \Sigma_k$). Over most of the range of crack sizes and fiber strengths fiber failure is unstable and is followed by matrix failure, but over a small range of C and S stable fiber failure occurs at increasing applied stress. These two responses can be inferred directly from Fig. 3, as shown in Fig. 5. In Fig 5(a), where the stress for fiber failure (at $c_0 = 0$) is larger than the intersection stress Σ^*, unstable fiber failure occurs initially without matrix crack growth (path A-B). But, once fibers break beyond position B, unstable matrix crack extension accompanies further fiber failure and the strength of the composite is given by Σ_s. For fiber strengths ≤ 0.6 there is a small range of crack lengths for which the fiber failure stress (at $C_0 = 0$) is smaller than Σ^*, as shown in Fig. 5(b). In this case, unstable fiber failure occurs along AB, but further load increase is required to proceed along BD. At position D simultaneous matrix crack growth and fiber fracture occur, so that the strength of the composite is given by Σ^*.

4.2 Cracks with Partial Bridging Zones

The general form of the counterpart of Fig. 4 for cracks with an initial area of broken fibers is shown schematically in Fig. 6. The introduction of an unbridged area reduces the stress for matrix cracking. The magnitude of the reduction decreases with increasing c/c_0 (see Fig. 3). A maximum appears in the function $\Sigma_k(c)$, but the limiting solution at large c/c_0 is the same as for the fully-bridged crack. The stress for fiber failure is reduced at large c/c_0 but is increased for $c/c_0 \rightarrow 1$.

Failure from a crack that initially has no bridging fibers (i.e., $c = c_0$) always begins with growth of the crack in the matrix. Moreover, the growth is initially stable with increasing applied stress. In this case the closure effect of the developing bridging zone outweighs the increased opening effect of the applied load. If the fiber strength is smaller than S_2 in Fig. 6 stable growth continues until the stress in the last bridging fiber exceeds the fiber strength, whereupon both fiber failure and matrix crack growth become unstable. This instability condition ($C = C^*$, $\Sigma_\infty = \Sigma^*$) is defined by the intersections of the curves $\Sigma_k(C)$ and $\Sigma_s(C)$ in Fig. 6. On the other hand, if the fiber strength exceeds S_2, instability of the matrix crack occurs before fiber failure, at stress Σ^+ corresponding to the peak in the $\Sigma_k(C)$ curve. Provided the steady-state (i.e., $C \rightarrow \infty$) fiber-failure stress is smaller than Σ^+ (i.e., fiber strength less than S_4 in Fig. 6), fiber failure occurs after some unstable matrix crack growth, and failure of the composite is catastrophic at $\Sigma = \Sigma^+$. However, if the fiber strength exceeds S_4, the fibers remain intact after the crack passes completely through the matrix and the composite exhibits the high-strain, multiple-cracking failure mechanism.

Cracks with an initial bridging zone (i.e., $C > C_0$) behave in a similar manner provided the initial crack is smaller than C^* and the intersection (C^*, Σ^*) falls to the left of the peak in the matrix cracking stress (i.e., $S < S_2$). If the intersection falls to the right of the peak (i.e., $S > S_2$) and the initial crack lies between C^+ and C^* the crack extends unstably in the matrix without precursor stable growth at $\Sigma = \Sigma_k(C)$, and is followed by fiber failure if the steady state fiber failure stress is smaller than $\Sigma_k(C)$. This condition is always satisfied for $S < S_3$ (i.e., catastrophic failure of the composite), never satisfied for $S > S_4$ (noncatastrophic composite failure), and satisfied for certain initial crack lengths for $S_3 < S < S_4$.

If the initial crack size is larger than C^* then fiber failure occurs before matrix crack growth. The response in this region is similar to that of initially fully bridged cracks, with fiber failure being unstable and followed by matrix failure over most of the range of C and S, but with a limited region where stable fiber failure precedes matrix failure.

Numerical solutions for the matrix cracking stress corresponding to Fig. 6 are shown for various C_0 in Fig. 7 as a function of crack extension, i.e., $d/c_n = C - C_0$. In this figure the left axis corresponds to a crack that initially has no bridging fibers. Also plotted in Fig. 7 are the loci of the intersection points (C^*, Σ^*) for various fiber strengths. A rapid transition is evident between two types of $\Sigma_k(C)$ curve. At small C_o (≤ 0.2) the peak in the curve occurs very close to the left axis, so the extent of stable matrix cracking for an initially unbridged crack is small. But, at large C_o (≥ 0.2) the peak falls at larger C and at a stress very close to the large crack length limit ($\Sigma_k = 0.794$). In this region the stable cracking is more extensive and the strength of the composite containing an initially unbridged crack is given by Σ_k^*. The variation of the intersection stress Σ_k^* with total crack length is shown in Fig. 8. The broken portions of the curves in Fig. 8 represent the second (left hand) intersections which occur for some of the curves in Fig. 3.

5.0 FRACTURE TOUGHNESS

In the present analysis the bridging effect of the fibers is viewed as a crack shielding mechanism, in which the fibers reduce the crack tip stresses and crack growth is dictated by a critical value of these local stresses. The composite stress intensity factor (Eq. (2)) can be expressed as

$$K = K^{\infty} - K_p \tag{17}$$

where $K^{\infty} = 2\,\sigma_{\infty}(c/\pi)^{1/2}$ is the applied stress intensity factor and K_p represents the shielding due to the fibers. The failure condition is taken as $K = K_c = E_c K_o / E_m$ where K_c is the intrinsic toughness of the composite without shielding (i.e., zero strength fibers). Therefore the critical value of the <u>applied</u> stress intensity factor, which is the quantity usually referred to as the facture toughness, is

$$K_c^{\infty} = K_c + K_p \tag{18}$$

and the relative toughness increment due to bridging is

$$K_p/K_c = (K_c^{\infty} - K_c)/K_c \tag{19}$$

The total increase in toughness, ΔK_c, relative to the unreinforced matrix is influenced by the relative moduli of the composite and matrix addition to the bridging:

$$\Delta K_c = K_c^\infty - K_o = K_o(E_c/E_m - 1) + K_p \tag{20}$$

The composite toughness is a material property *only* if K_p is independent of crack size. In this case the strength/crack-size relation is

$$\sigma_\infty c^{1/2} = K_c^\infty \pi^{1/2}/2 \tag{21}$$

or, in normalized form,

$$\Sigma_\infty c^{1/2} = (1/3)K_c^\infty/K_c = (1 + K_p/K_c)/3 \tag{22}$$

It is clear from Figs. 4 and 7 that this relation does not hold in general. Indeed, for initially fully bridged cracks (Fig. 4), the *strength* for large pre-existing cracks is constant and is therefore the material property which is independent of pre-existing defects. On the other hand, an initially unbridged crack grows stably with increasing applied stress (i.e., increasing K_∞), a response that is characterized by a crack growth resistance curve (R-curve) rather than a single-valued toughness.[2]

However, a constant toughness increment is obtained for the special crack configuration with a bridging zone of length d*, for which fiber failure and matrix crack growth occur simultaneously (i.e., $d^* = c^* - c_0$ in Fig. 6). This is the crack configuration at the instability point on the crack growth resistance curve for an initially unbridged crack. The constant toughness increment is demonstrated by plotting the curves of Fig. 8 in logarithmic coordinates (Fig. 9). The toughness increases, obtained by fitting Eq. (22) to the curves in Fig. 9 are plotted as a function of normalized fiber strength in Fig. 10.

Analytical solutions can also be obtained for the crack with $d = d^*$. One approximate solution, which is valid for small bridging zones, was obtained previously[2] by substituting an assumed crack profile into Eq. (10) (Appendix II). This solution predicted a crack-size-independent toughness increase for this crack configuration:

$$K/K_c = 2(Sf/\sigma_n)^3 \tag{23}$$

The other solution derives from recent work of Budiansky[14] who used a J-integral approach, but employed an energy balance fracture criterion. The analysis can be modified to incorporate the stress-intensity criterion used here. The analysis begins by evaluating the J-integral for the path shown in Fig. 11,[12]

$$J_\infty = J_{tip} + J_P \tag{24}$$

where $$J_\infty = K^{\infty 2}(1 - \nu^2)/E_c \tag{25}$$

$$J_p = 2 \int_0^{u_d} p(u)du \tag{26}$$

and u_d is the crack opening at the end of the bridging zone. Budiansky set $J_{tip} = 2\gamma_m(1 - f)$, where $\gamma_m = K_o^2(1 - \nu^2)/2E_m$ is the fracture surface energy of the unreinforced matrix, to obtain

$$K^{\infty 2} = K_o^2(1 - f)E_c/E_m + J_pE_c/(1 - \nu^2) \tag{27}$$

If instead we evaluate J_{tip} for the circular path shown,[12] taking into account the stress in the matrix and fibers (with corresponding stress intensity factors K_m and K_f) we get

$$J_{tip} = K_m^2(1 - \nu^2)(1 - f)/E_m + K_f^2(1 - \nu^2)f/E_f \tag{28}$$

$$= K_m^2(1 - \nu^2)E_c/E_m^2 \tag{29}$$

Then setting $K_m = K_o$ as the condition for crack growth and combining Eqs. (24)-(25) and (29) yields

$$K^{\infty 2} = K_o^2E_c^2/E_m^2 + J_pE_c/(1 - \nu^2) \tag{30}$$

Thus, the predictions resulting from the energy balance and stress intensity criteria differ by a factor $E_m (1 - f)/E_c$ in the term that derives from

J_{tip}. Equation (30) can be expressed alternatively in terms of K_p (using Eq. (19)):

$$K_p/K_c = [1 + E_m^2 J_p/(1 - \nu^2)E_c K_o^2]^{1/2} - 1 \qquad (31)$$

Equation (31) holds for the general crack configuration, but evaluation of J_p (from Eq. (26)) requires solution of Eq. (10) for the crack opening displacements to obtain u_d. However, for the crack with $d = d^*$ a straightforward analytical solution is obtained because u_d is the displacement at which fiber failure occurs, given by Eq. (6a) with $p(u_d) = S$. In this case Eq. (31) becomes

$$K_p/K_c = [1 + 4(Sf/\sigma_n)^3]^{1/2} - 1 \qquad (32)$$

For small bridging zones (i.e., $4(Sf/\sigma_n)^3 << 1$) Eq. (32) reduces to the approximate solution of Eq. (23). The analytical solution is plotted in Fig. 10; the results agree well with the numerical computations.

6.0 DISCUSSION

Normalization of the crack opening and stress intensity equations in the forms of Eqs. (10)-(12) has enabled the mechanics of failure for unbonded composites to be examined with only one material or microstructural variable - the normalized fiber strength, Sf/σ_n. The analysis yields strength/crack size relations for several failure mechanisms (Figs. 4 and 7), and defines conditions for transitions between mechanisms. Relations between these quantities and microstructural properties of specific composites are obtained by evaluation of the normalization parameters defined in Eqs. (7), (13) and (14).

6.1 Transitions in Failure Mechanisms

The most important failure mechanism transition is from the "high-strength" fiber behavior, which involves periodic matrix cracking followed by fiber failure at a higher applied load (and consequently a large strain to failure), to the "lower strength" behavior where fiber failure accompanies matrix cracking and failure is catastrophic. This transition occurs at fiber strengths between S_3 and S_4, illustrated in Fig. 6, and plotted as a function of the unbridged crack size in Fig. 12. Fiber strengths larger than S_4 always give rise to the noncatastrophic failure mechanism, whereas fiber strengths smaller than S_3 always lead to catastrophic failure. For fiber strengths between S_3 and S_4, either failure mechanism can occur, depending on the total crack size (with large c/c_n favoring noncatastrophic failure). For

$c_o/c_m \geq 0.5$, S_3 and S_4 are almost identical, but at smaller values of c_o/c_m the two strengths diverge.

The failure mechanisms for specific composites can be conveniently predicted from Fig. 12 by evaluating the material parameter Sf/σ_n (Eqs. (7) and (13)):

$$Sf/\sigma_n = \left[\frac{S^3 R\, f(1 - f) E_m{}^3}{12 \tau K_o{}^2 (1 - \nu^2) E_f E_c{}^2}\right]^{1/3} \tag{33}$$

For example, in a composite composed of a glass-ceramic matrix with unidirectionally aligned SiC fibers,[2,3] the following microstructural parameters have been measured:[5,15] $K_o = 2$ MPa•m$^{1/2}$, $\tau = 2$ MPa, $R = 8$ μm, $S = 1$ GPa, $f = 0.5$, $E_f = 200$ GPa, $E_m = 70$ GPa. Substitution of these values into Eq. (33) gives $Sf/\sigma_n \simeq 1.5 \pm 0.2$. This value falls within the field of noncatastrophic failure (in Fig. 12) for $0.02 \leq C_o/C_n \leq 2$. Moreover, for $C_o/C_n < 0.02$ the fiber strength is in the transition range $S_2 < S < S_4$. Comparison with Fig. 4 indicates that, even for a fully bridged crack ($C_o = 0$), the failure is noncatastrophic for this value of Sf/σ_n provided the total crack length C/C_n exceeds $\simeq 0.03$. The absolute crack dimensions corresponding to these bounds are obtained by expressing C_n in terms of microstructural parameters (Eqs. (7) and (14)):

$$c_n = (9\pi/4)\left[\frac{K_0 R(1 - f)E_c}{12\tau(1 - \nu^2)f^2 E_f}\right]^{2/3} \tag{34}$$

With the measured parameters for this composite Eq. (34) gives $c_n = 300\ \mu m$. Therefore, the small-crack limit corresponds to a total crack size $c \simeq 10\ \mu m$ and the large-crack limit to an unbridged crack size $c_0 \simeq 600\ \mu m$. Flaws in this composite are expected to fall within this range; the average fiber spacing is larger than the lower limit but more than an order of magnitude smaller than the upper limit. Therefore the nonctastrophic mode of failure is expected, consistent with experimental observations.[5] However, it would, in principle, be possible to increase C_0 and cross into the region of catastrophic failure by cutting a large saw notch or by introducing a large processing defect. In practice this transition is generally not observed because such unidirectionally reinforced composites are weak in shear loading and large notches cause failure by splitting parallel to the fibers rather than by cracking normal to them. However, there is a reported instance in a similar composite (carbon-reinforced glass) where splitting was inhibited by using a circumferentially notched test specimen and the transition to the catastrophic failure mode was apparently observed.[7]

The influences of microstructural properties on failure mechanisms are readily deduced from Eq. (33). Noncatastrophic failure is most likely in composites with large values of Sf/σ_n, i.e., large S, R and E_m, and small τ, K_0 and E_f. The influence of the volume fraction of fibers is dependent on the ratio E_f/E_m. Increasing f causes Sf/σ_n to increase for $E_f/E_m < (1 - f)/f$.

6.2 Noncatastrophic Failure Mechanism

Within the region of noncatastrophic failure the first damage to occur is the matrix cracking. The stress for matrix cracking can be dependent upon crack length at small c/c_n, but at large c/c_n it approaches a lower bound, $\sigma/\sigma_n = 0.794$, independent of crack size. In terms of specific microstructural properties, this steady state stress becomes (Eqs. (7), (13) and (16)

$$\sigma = \left[\frac{6(1 - \nu^2)K_0^2\tau f^2 E_f E_c^2}{R(1 - f)E_m^3}\right]^{1/3} \tag{35}$$

Comparison of Eqs. (33) and (35) indicates that, with the exception of the volume fraction of fibers, any microstructural change that increases the matrix cracking stress also makes the transition to the catastrophic failure mode more likely. Increasing f always causes the matrix cracking stress to increase but can cause Sf/σ_n either to increase or to decrease depending on the value of E_f/E_m.

The strength of the <u>composite</u> in this region is higher than the matrix cracking stress, and is dictated by fiber failure after the matrix crack has extended completely through the composite.

6.3 Catastrophic Failure Mechanism

The mechanism of catastrophic failure is dependent on the initial crack configuration. Failure of composites containing large fully-bridged cracks is controlled by the fracture of bridging fibers, and the strength is dictated by the product of the fiber strength and volume fraction, Sf. On the other hand, failure of composites containing cracks with substantial areas of broken or missing fibers involves stable matrix crack growth at increasing applied stress (described by a crack growth resistance curve), with instability occurring when the crack develops a bridging zone with critizal size, d = d*. The fracture toughness of the composite at the instability point is (Eqs. (20) and (32))

$$K_c^{\infty}/K_o = (E_c/E_m)[1 + 4(Sf/\sigma_n)^3]^{1/2} \qquad (36)$$

where Sf/σ_n is given in terms of microstructural properties by Eq. (33).

The critical zone size d*, is of interest, for this is a parameter that could be measured. In general, d* is dependent upon both the total crack size and the normalized fiber strength (Fig. 7). However, for large cracks, d* becomes independent of crack size. This limiting value is plotted in Fig. 13. For small fiber strengths the limiting zone size is approximately

$$d^*/c_n = 0.5\ (Sf/\sigma_n)^4 \qquad (37)$$

in agreement with the previous approximate analytical solution (Appendix II). At larger fiber strengths the limiting zone size is smaller than predicted by the analytical approximation (Fig. 13). Comparison of Eqs. (36) and (37) indicates that there is a direct relation between the normalized limiting zone size and the corresponding toughness increment.

Equations (36) and (33) indicate that the toughness is increased by increasing S and R or decreasing τ and K_0. The influence of these parameters on ΔK_c is opposite to their influence on the stress for steady state matrix cracking in the noncatastrophic failure mode. This dependence arises because any microstructural change that decreases σ_n leads to a smaller fiber bridging zone (Eq. (37)) and thus a smaller toughness increment due to bridging. As a result, there are optimum values of microstructural properties to give either maximum toughness of the composite in the region of catastrophic failure or maximum matrix cracking stress in the region of noncatastrophic failure. The optimum combination of properties exists at the transition condition defined by Eq. (33) and Fig. 12.

The inverse relation between K_c^∞ and K_0 in Eq. (36) warrants qualification. The baseline matrix toughness K_0 is the toughness in the absence of <u>any</u> crack shielding mechanisms, i.e., it is the intrinsic matrix toughness, or the critical stress intensity factor locally at the crack tip required to cause crack extension. Therefore, the measured matrix toughness in the absence of reinforcing fibers could be increased by introducing a second shielding mechanism, such as transformation toughening, without changing K_0 and hence without decreasing ΔK_c. In fact, it has recently been suggested that synergistic effects with multiple crack shielding mechanisms could increase the toughening increment due to each individual mechanism.[16]

Finally, the influence of elastic modulus and fiber volume fraction on K_c^∞ are dependent upon the values of the other parameters. This dependence is evaluated by rewriting Eq. (36) (using Eq. (33)):

$$K^\infty/K_o = \left[[1 + f(E_f/E_m - 1)]^2 + \left(\frac{S^3R}{4\tau K_o^2(1 - \nu^2)}\right) \frac{f(1 - f)E_m}{E_f} \right]^{1/2} \tag{38}$$

For composites in which the toughening due to fiber bridging is small (i.e., second term in Eq. (37) small) the toughness of the composite increases with increasing E_f/E_m. However, if the toughening due to bridging is large the dependence on E_f/E_m is reversed. Increasing f causes K_c^∞ to increase for both high and low toughness composites, provided $f < 0.5$ and $E_f/E_m > 1$. However, if $E_f/E_m < 1$ the opposite variation occurs for composites with low toughness.

ACKNOWLEDGMENTS

Funding for this work was supplied by the U.S. Office of Naval Research, Contract No. N00014-85-C-0416. Parts of this work were stimulated by discussions with A.G. Evans and B. Budiansky at the Winter Study Group meeting at the University of California, Santa Barbara in January 1986.

APPENDIX I

ANALYSIS FOR STRAIGHT CRACKS

Analysis of straight cracks is the same as for the penny cracks considered in the text, except that the equations for the crack opening displacement and the stress intensity factor (Eqs. (10) and (11)) become

$$U(X) = 3(C/\Sigma_\infty) \int_x^1 \frac{s}{\sqrt{s^2 - X^2}} \int_u^s \frac{F(U)dt}{\sqrt{s^2 - t^2}} ds \tag{A1}$$

and

$$K/K_C = 2\Sigma_\infty C^{1/2} \int_0^1 \frac{F(U)dX}{\sqrt{1 - X^2}} \tag{A2}$$

The solutions of these equations are very similar to those of Eqs. (10) and (11), so that the description of the mechanics of failure (Section 4.0) is the same as for penny cracks. However the magnitudes of corresponding strengths at small crack sizes differ slightly, as summarized in Figs. A1 and A2 which correspond to Figs. 7 and 12.

APPENDIX II

APPROXIMATE ANALYTICAL SOLUTION

Some of the results in this paper were foreshadowed by an approximate analytical solution to Eqs. (10 and (11), obtained by assuming an approximate form for the crack profile.[2] The profile was taken as the solution of Eq. (9) for a crack subject to uniform stress, but with the magnitude of the opening governed by the net stress intensity factor:

$$u(X) = 2(1 - \nu^2)Kc^{1/2}(1 - X^2)^{1/2}/E\pi^{1/2} \tag{B1}$$

This approximation is expected to be reasonable for small bridging zones (i.e., small Sf/σ_n), but it is expected to yield an overestimate of the closure pressure for large bridging zones. The stress intensity factor for a crack with fiber closure tractions over a zone of length d was calculated from Eq. (11) with the crack surface pressure, $F(U) = 1 - \sqrt{U}$, dictated by Eq. (B1):

$$\frac{K}{K_c} = 3\Sigma_\infty C^{1/2} - 2(K/K_c)^{1/2}C^{3/4}(d/c)^{3/4}(2 - d/c)^{3/4} \tag{B2}$$

The applied stress, Σ_∞, required to cause matrix crack growth was then evaluated from Eq. (B2) by setting $K = K_c$. The results, plotted in the same form as Fig. 7, were very similar to the numerical solutions, but with stresses generally about 20% higher. The condition at which both fiber failure and matrix cracking occur simultaneously was also obtained by calculating the critical bridging zone size d* from Eqs. (6) and (B1) with p(x) = Sf at $x = c - d^*$:

$$\frac{d^*}{c}\left(2 - \frac{d^*}{c}\right) = \left(\frac{Sf}{\sigma_n}\right)^4 \left(\frac{c_n}{c}\right) \tag{B3}$$

In the limit of large cracks (i.e., $\left(\frac{Sf}{\sigma_n}\right)^4 \frac{c_n}{c} << 1$), Eq. (B3) becomes

$$d^*/c_n = (Sf/\sigma_n)^4/2 \tag{B4}$$

The corresponding stress intensity factor due to the bridging zone, obtained from the second term of Eq. (B2) with $d = d^*$ from Eq. (B3) is

$$K_p/K_c = 2(Sf/\sigma_n)^3 \tag{B5}$$

Since K_p is independent of crack length, the closure effect of the fibers represents an increase in fracture toughness, $\Delta K_c = K_p$, for this crack configuration.

REFERENCES

1. A.G. Evans, M.D. Thouless, D.B. Johnson-Walls, E. Luh and D.B. Marshall, "Some Structural Properties of Ceramic Matrix Fiber Composites," in Proceedings of the Fifth International Conference on Composite Materials, Ed., W.C. Harrigan and J. Strife, AIME (1985).

2 D.B. Marshall and A.G. Evans, "Tensile Strength of Uniaxially Reinforced Ceramic Fiber Composites," in Fracture Mechanics of Ceramics, 7, Ed., R.C. Bradt, A.G. Evans, D.P.H. Hasselman and F.F. Lange, Plenum, in press.

3. J.J. Brennan and K.M. Prewo, "Silicon Carbide Fiber Reinforced Glass-Ceramic Matrix Composites Exhibiting High Strength and Toughness," J. Mater. Sci. 17(8), 2371-83 (1982).

4. J. Aveston, G.A. Cooper and A. Kelly, "Single and Multiple Fracture," pp 15-26 in the Properties of Fiber Composites, Conf. Proc. Nat. Physical Lab., IPC Science and Technology Pres. Ltd., Surrey, England, 1971.

5. D.B. Marshall and A.G. Evans, "Failure Mechanisms in Ceramic-Fiber/ Ceramic-Matrix Composites," J. Amer. Ceram. Soc. 68(5), 225-31 (1985).

6. R.A.J. Sambell, A. Briggs, D.C. Phillips and D.H. Bowen, "Carbon Fiber Composites with Ceramic and Glass Matrices, Part 2 - Continuous Fibers," J. Mater. Sci. 7(6), 676-81 (1972).

7. D.C. Phillips, "Interfacial Bonding and the Toughness of Carbon Fiber Reinforced Glass and Glass-Ceramics," J. Mater. Sci. 9(11), 1847-54 (1974).

8. J. Aveston, R.A. Mercer and J.M. Sillwood, "Fiber Reinforced Cements-Scientific Foundations for Specifications," Proceedings of Conference on Standards, Testing and Design.

9. J. Aveston and A. Kelly, "Theory of Multiple Fracture of Fibrous Composites," J. Mat. Sci. 8, 352-62 (1973).

10. B. Budiansky, J.W. Hutchinson and A.G. Evans, "Matrix Fracture in Fiber-Reinforced Ceramics" J. Mech. Phys. Solids 34[2], 167 (1986).

11. D.B. Marshall, B.N. Cox and A.G. Evans, "The Mechanics of Matrix Cracking in Brittle-Matrix Fiber Composites," Acta Met. 33(11), 2013-21 (1985).

12. B.R. Lawn, "Fracture of Brittle Solids," Cambridge University Press (1975).

13. I.N. Sneddon and M. Lowengrub, "Crack Problems in the Classical Theory of Elasticity," Wiley, New York (1969).

14. Budiansky, Micromechanics II

15. K.M. Prewo, private communication.

16. A.G. Evans, Z.B. Ahmed, D.G. Gilbert and P.W.R. Beaumont, "Mechanisms of Toughening in Rubber Toughened Polymers."

FIGURE CAPTIONS

Fig. 1 Schematic of crack configuration analyzed in Sections 2.0 to 5.0.

Fig. 2 Typical solution for the crack opening displacement and the corresponding closure pressure due to bridging fibers. Total crack radius $= c/c_n = 1.0$, unbridged radius $= c_o/c_n = 0.156$, applied stress $\sigma/\sigma_n = 0.9$

Fig. 3 Solutions for the applied stresses required to cause matrix crack growth, Σ_k, and fiber failure, Σ_s, for various crack configurations and fiber strengths. The left axis of each plot represents a fully bridged crack whereas the right axis represents an unbridged crack. Solutions for Σ_s are plotted for fiber strengths Sf/σ_n at intervals of 0.1.

Fig. 4 Solution for Σ_k and Σ_s for fully bridged matrix cracks ($c_o = 0$ in Fig. 3) plotted as a function of crack length.

Fig. 5 Examples of Σ_k and Σ_s curves from Fig. 3, illustrating two different sequences of failure from fully-bridged cracks: (A) unstable fiber fracture (A → B) followed by simultaneous matrix and fiber failure; (B) unstable fiber fracture (A → B) followed by stable fiber fracture (B → D) then simultaneous matrix and fiber failure.

Fig. 6 Schematic of the variations of Σ_k and Σ_s (for several values of fiber strength, S) with total crack length for a crack with an <u>unbridged</u> zone of radius C_o.

Fig. 7 Numerical solutions for Σ_k corresponding to Fig. 6, but plotted as a function of $(C - C_o)$, i.e., the length of bridging zone, so that the left axis represents a completely unbridged crack of length C_o. The set of broken curves represent the intersections, $\Sigma^* = \Sigma_s = \Sigma_k$, depicted in Fig. 6 for various fiber strengths.

Fig. 8 Plot of the intersection stress Σ^* as a function of total crack length.

Fig. 9 Plot of results from Fig. 8 in logarithmic coordinates.

Fig. 10 Toughness increase for crack with critical bridging zone of length d*. Round symbols represent numerical solutions obtained by fitting Eq. (22) to the results of Fig. 9. Solid curve represents the analytical solution, Eq. (32).

Fig. 11 J-integral path used for analytical solution in Section 5.0.

Fig. 12 Variation of the critical fiber stresses S_3 and S_4 (represented schematically in Fig. 6) with unbridged crack length c_0/c_n. This plot defines the transition between catastropic and noncatastropic failure modes.

Fig. 13 Bridging zone size d* for simultaneous fiber failure and matrix cracking at large C.

Fig. A1 Numerical solutions for straight crack corresponding to Fig. 7.

Fig. A2 Numerical solutions for straight crack corresponding to Fig. 12.

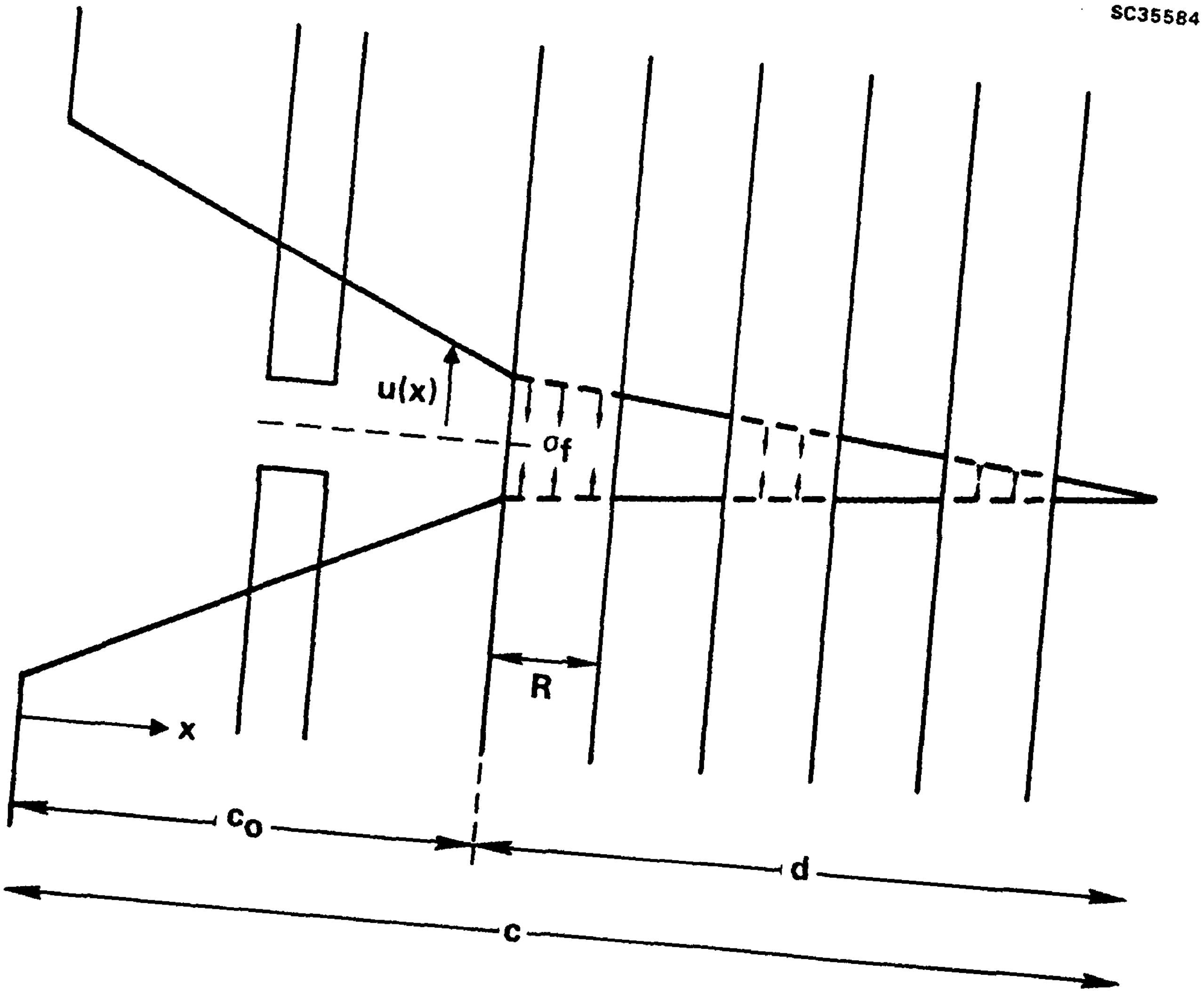

Figure 1

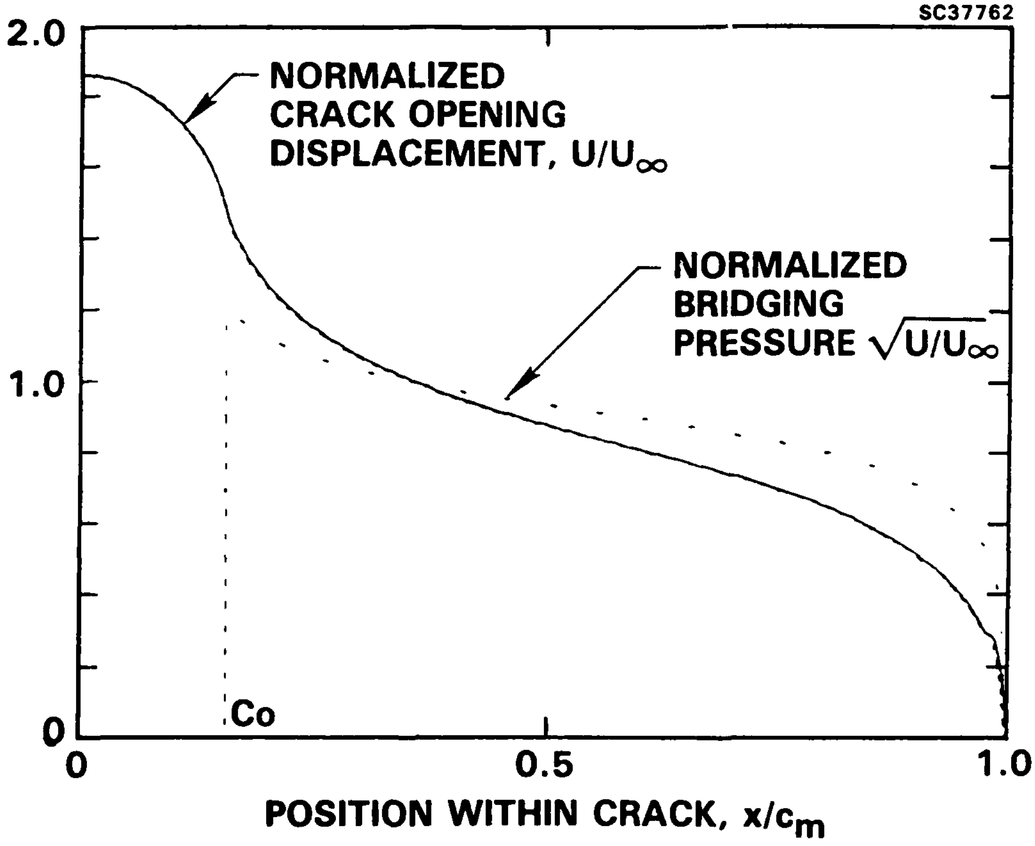
SC37762
2.0
1.0
0
0
0.5
1.0
NORMALIZED CRACK OPENING DISPLACEMENT, U/U_∞
NORMALIZED BRIDGING PRESSURE $\sqrt{U/U_\infty}$
Co
POSITION WITHIN CRACK, x/c_m

Figure 2

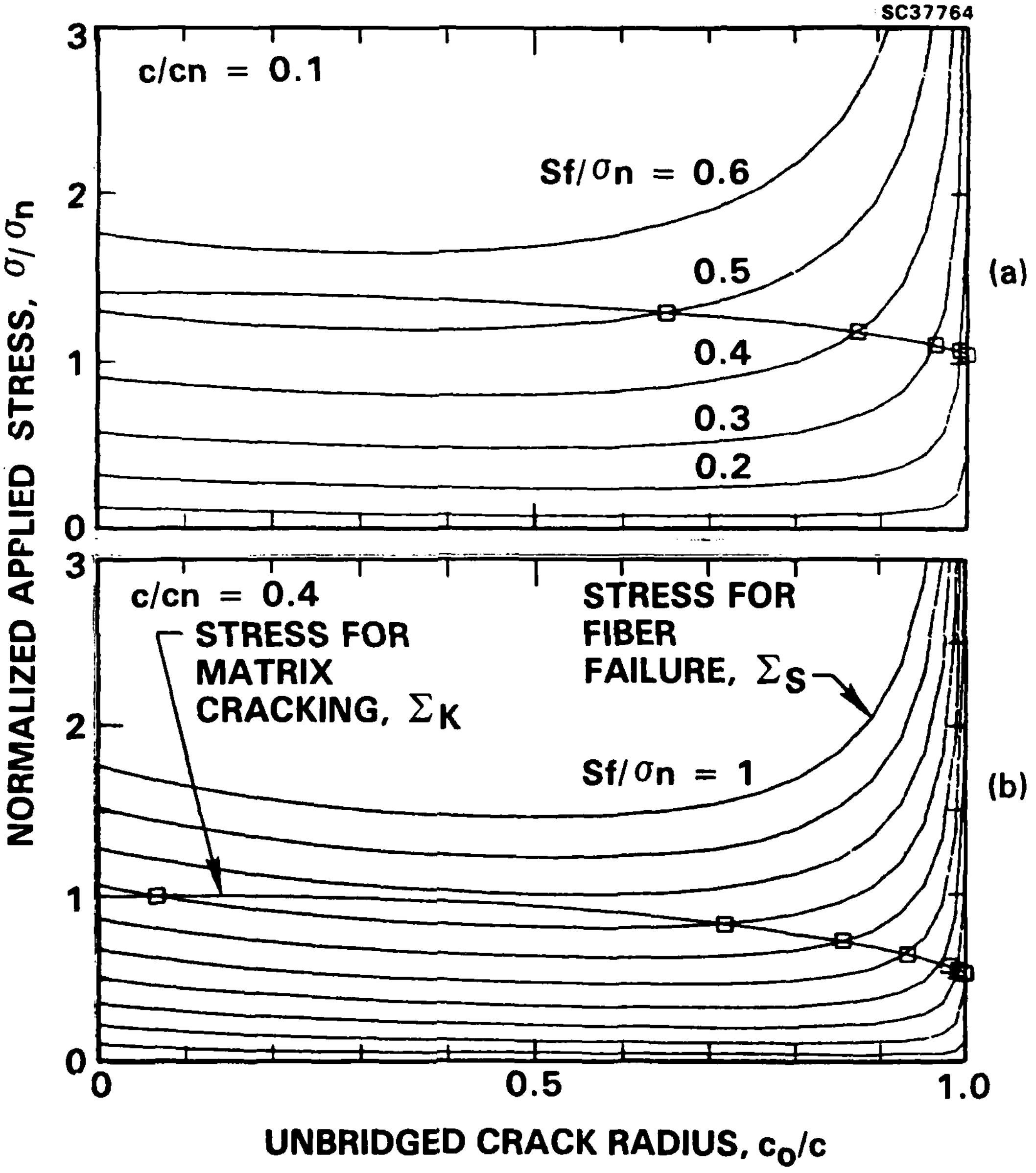
SC37764
c/cn = 0.1
Sf/σn = 0.6
0.5
0.4
0.3
0.2
(a)
c/cn = 0.4
STRESS FOR MATRIX CRACKING, ΣK
STRESS FOR FIBER FAILURE, ΣS
Sf/σn = 1
(b)
NORMALIZED APPLIED STRESS, σ/σn
0
1
2
3
0
0.5
1.0
UNBRIDGED CRACK RADIUS, co/c

Figure 3

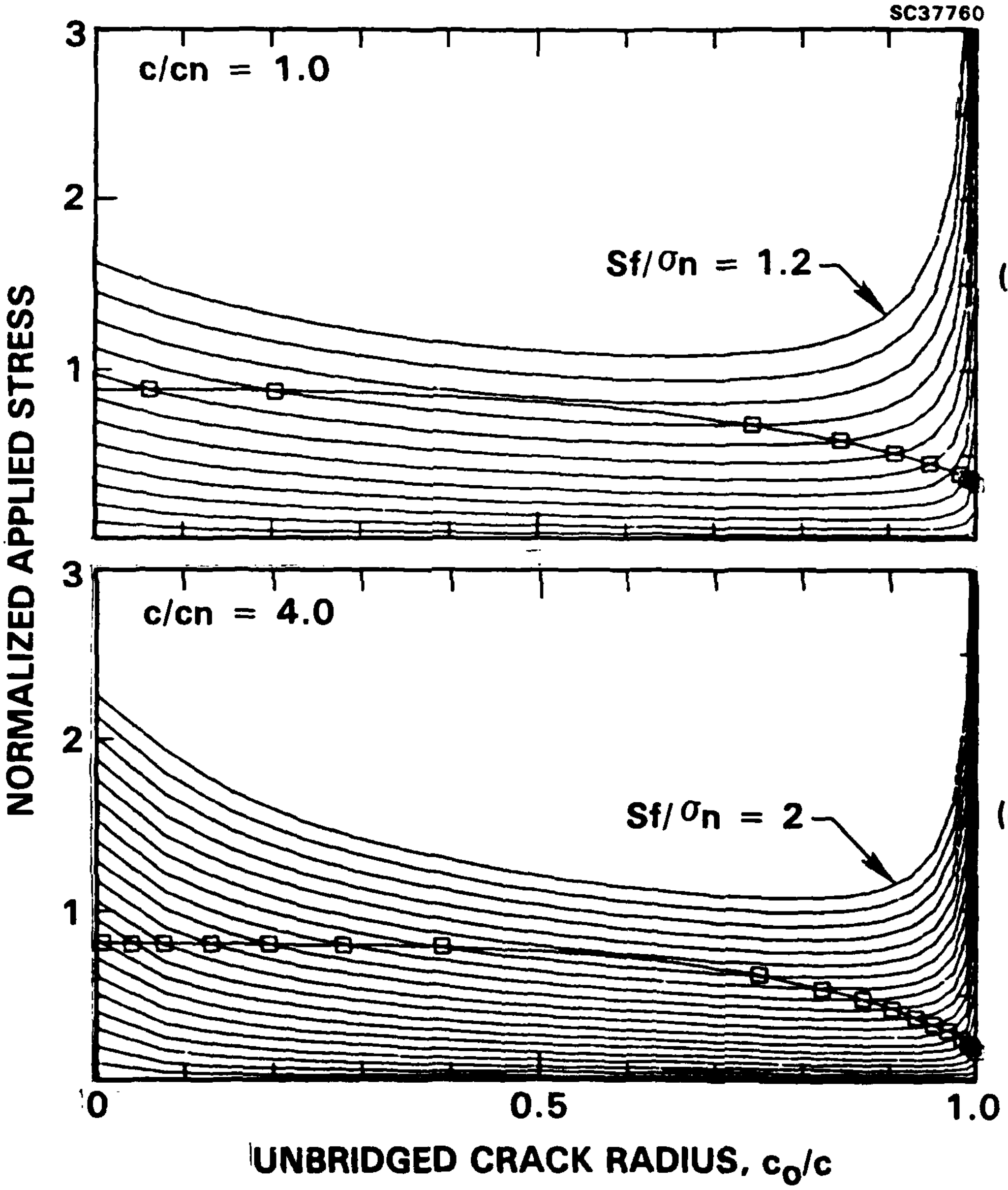
SC37760
c/cn = 1.0
Sf/σn = 1.2
(c)
c/cn = 4.0
Sf/σn = 2
(d)
NORMALIZED APPLIED STRESS
3
2
1
3
2
1
0
0.5
1.0
UNBRIDGED CRACK RADIUS, c_o/c

Figure 3

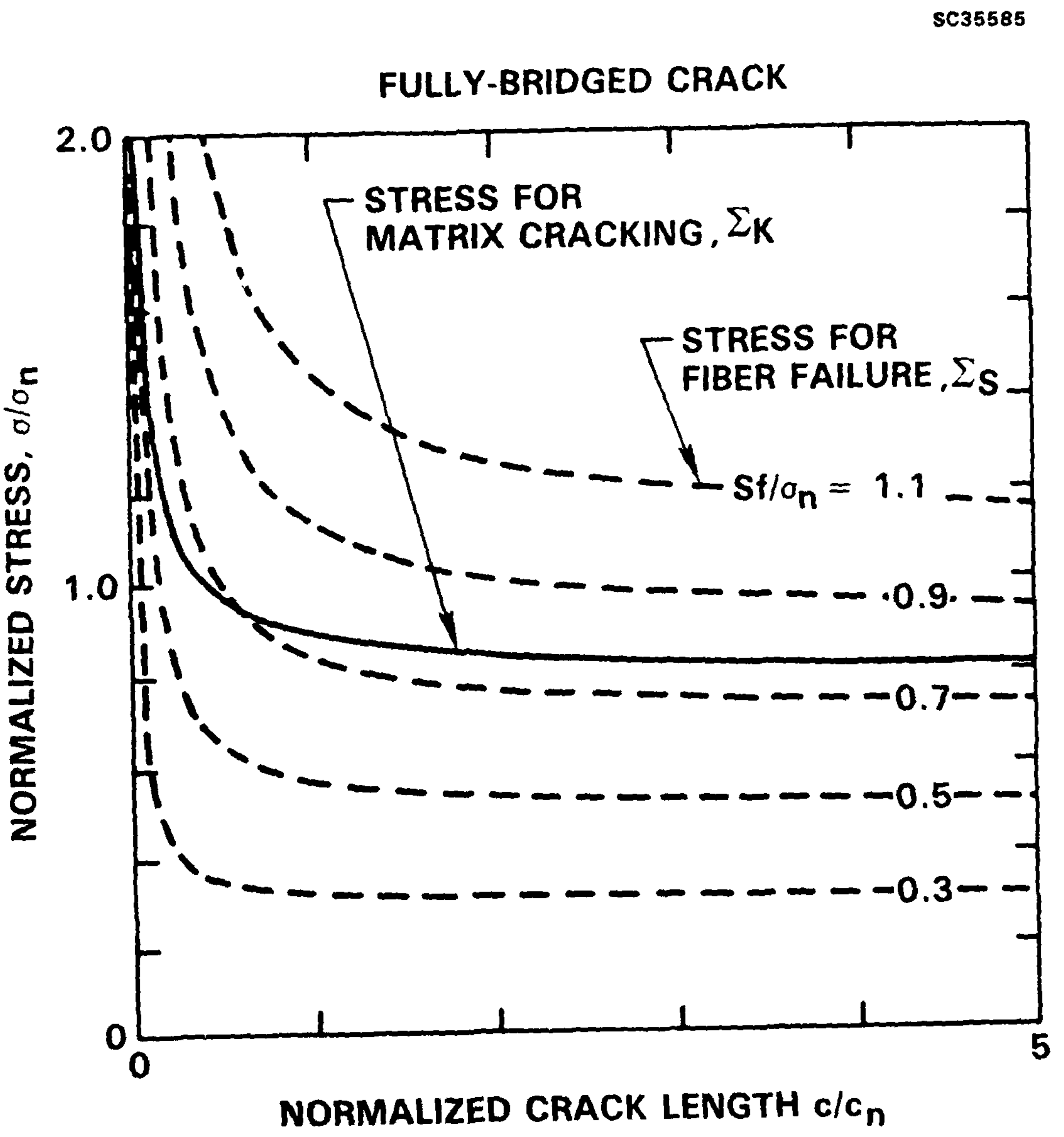
SC35585
FULLY-BRIDGED CRACK
STRESS FOR MATRIX CRACKING, Σ_K
STRESS FOR FIBER FAILURE, Σ_S
Sf/σ_n = 1.1
0.9
0.7
0.5
0.3
2.0
1.0
0
0
5
NORMALIZED STRESS, σ/σ_n
NORMALIZED CRACK LENGTH c/c_n

Figure 4

AD-A174 146 FIBER MATRIX INTERFACE EFFECTS IN FAILURE OF CERAMIC 2/2
MATRIX FIBER COMPOSI (U) ROCKWELL INTERNATIONAL
THOUSAND OAKS CA SCIENCE CENTER D MARSHALL ET AL
UNCLASSIFIED OCT 86 SC5432 AR N00014-85-C-0416 F/G 11/4 NL

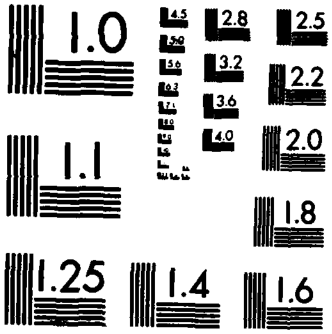

MICROCOPY RESOLUTION TEST CHART
NATIONAL BUREAU OF STANDARDS-1963-A

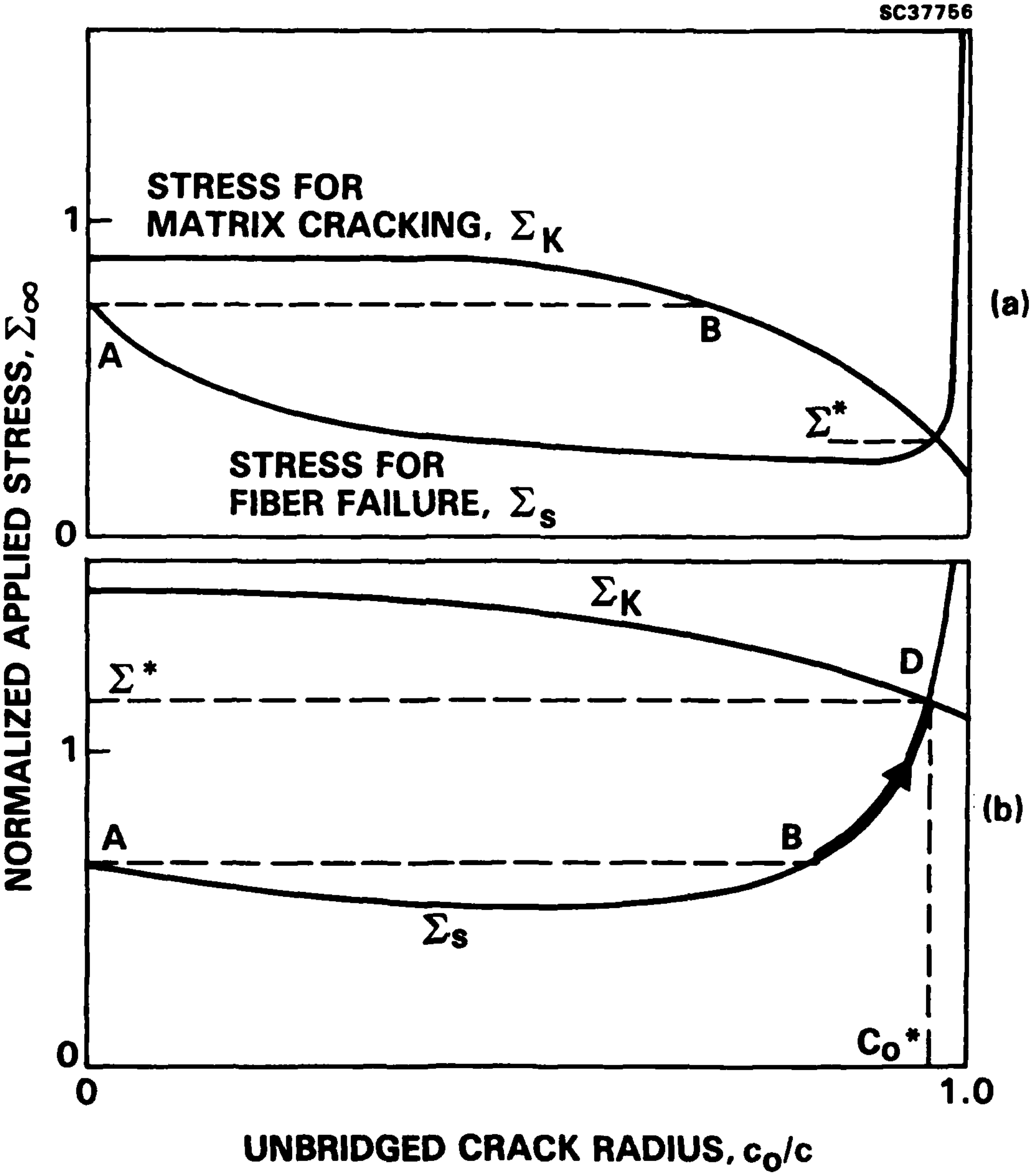
SC37756
STRESS FOR
MATRIX CRACKING, Σ_K
STRESS FOR
FIBER FAILURE, Σ_s
A
B
Σ^*
(a)
Σ_K
Σ^*
D
A
B
Σ_s
C_o^*
(b)
1
0
1
0
0
1.0
NORMALIZED APPLIED STRESS, Σ_∞
UNBRIDGED CRACK RADIUS, c_o/c

Figure 5

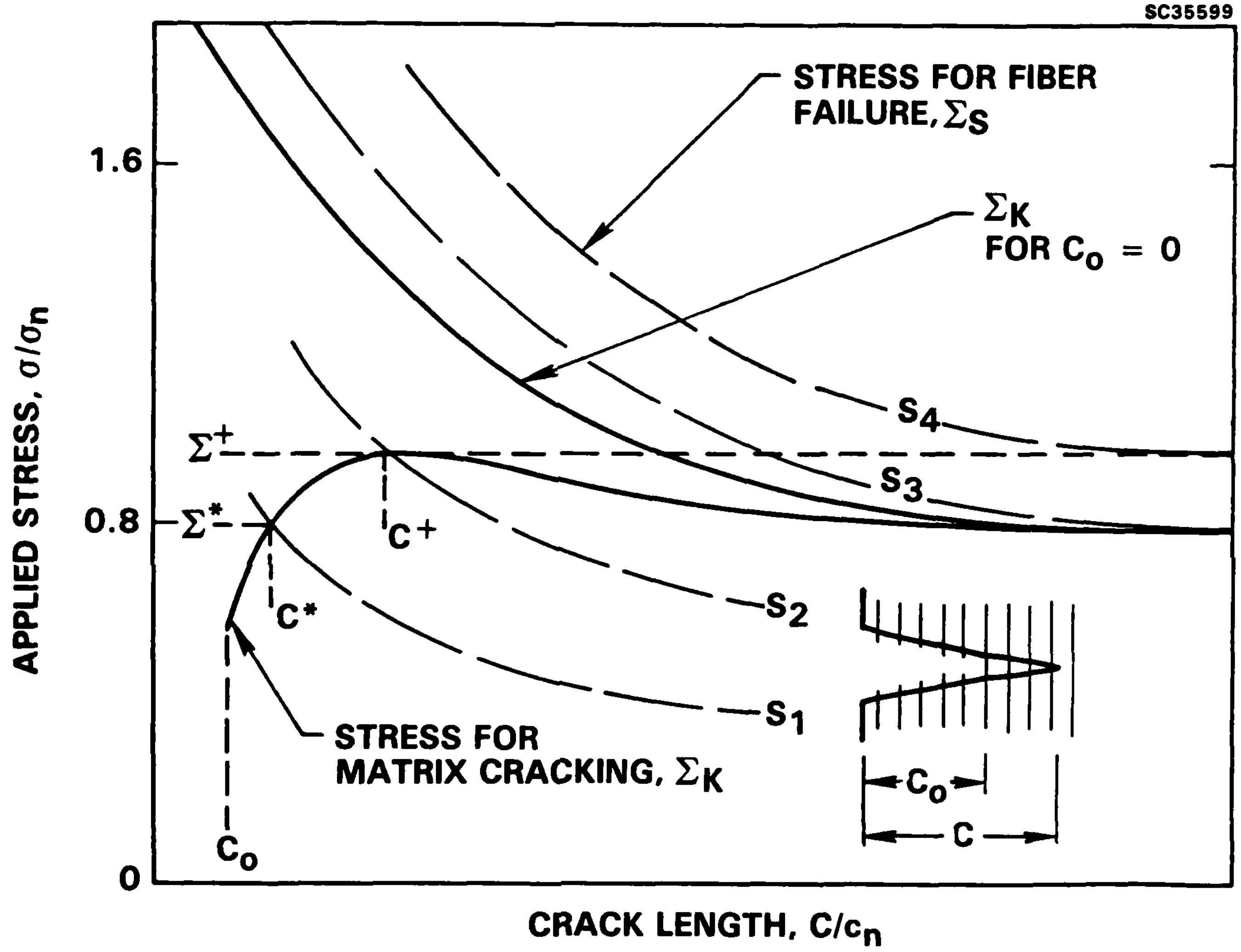
SC35599
STRESS FOR FIBER FAILURE, Σ_S
Σ_K FOR $C_o = 0$
1.6
0.8
0
Σ^+
Σ^*
C^+
C^*
S_4
S_3
S_2
S_1
STRESS FOR MATRIX CRACKING, Σ_K
C_o
C
APPLIED STRESS, σ/σ_n
CRACK LENGTH, C/c_n

Figure 6

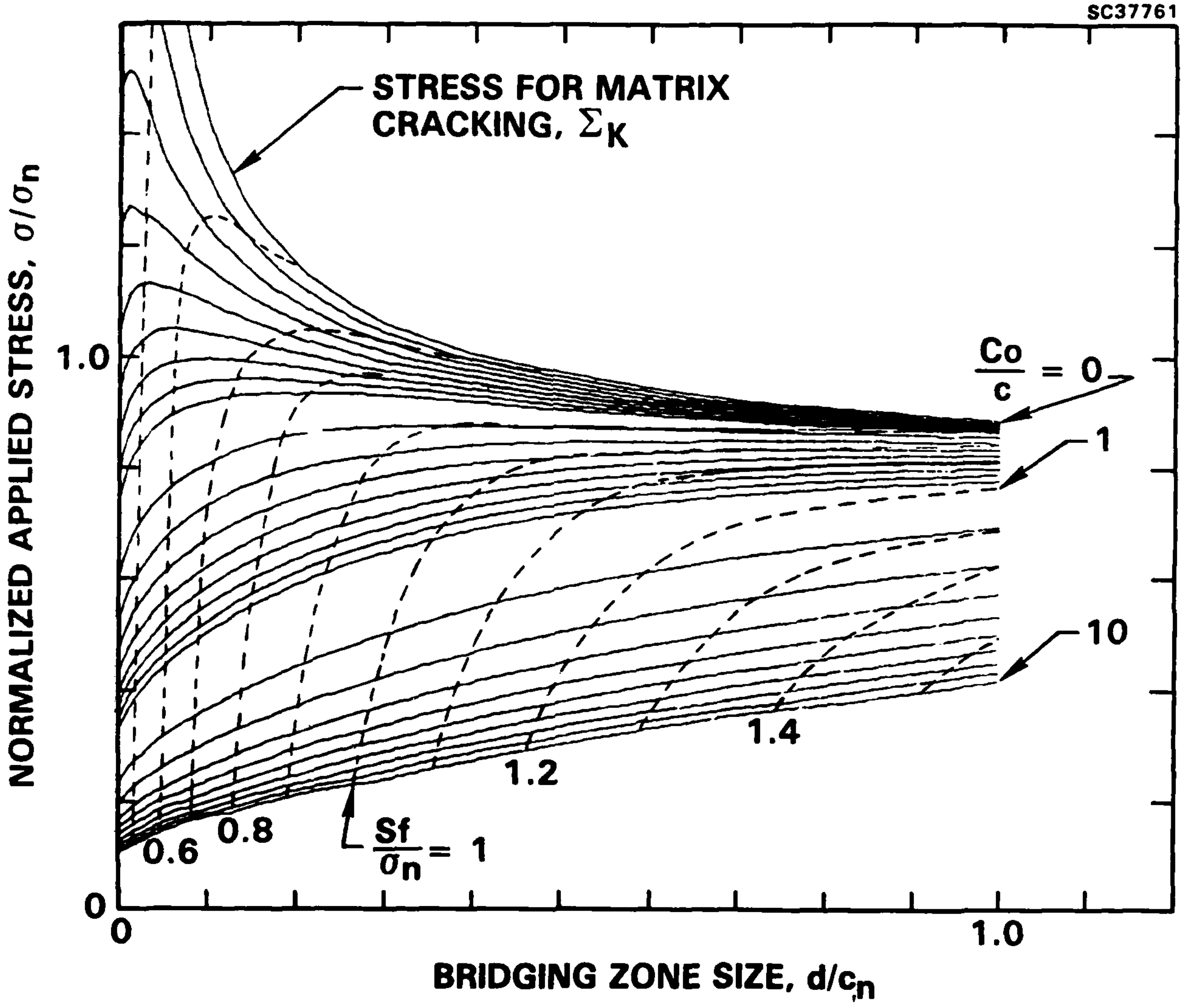
SC37761
STRESS FOR MATRIX CRACKING, Σ_K
$\frac{Co}{c} = 0$
1
10
1.4
1.2
0.6
0.8
$\frac{Sf}{\sigma_n} = 1$
NORMALIZED APPLIED STRESS, σ/σ_n
1.0
0
0
1.0
BRIDGING ZONE SIZE, d/c_n

Figure 7

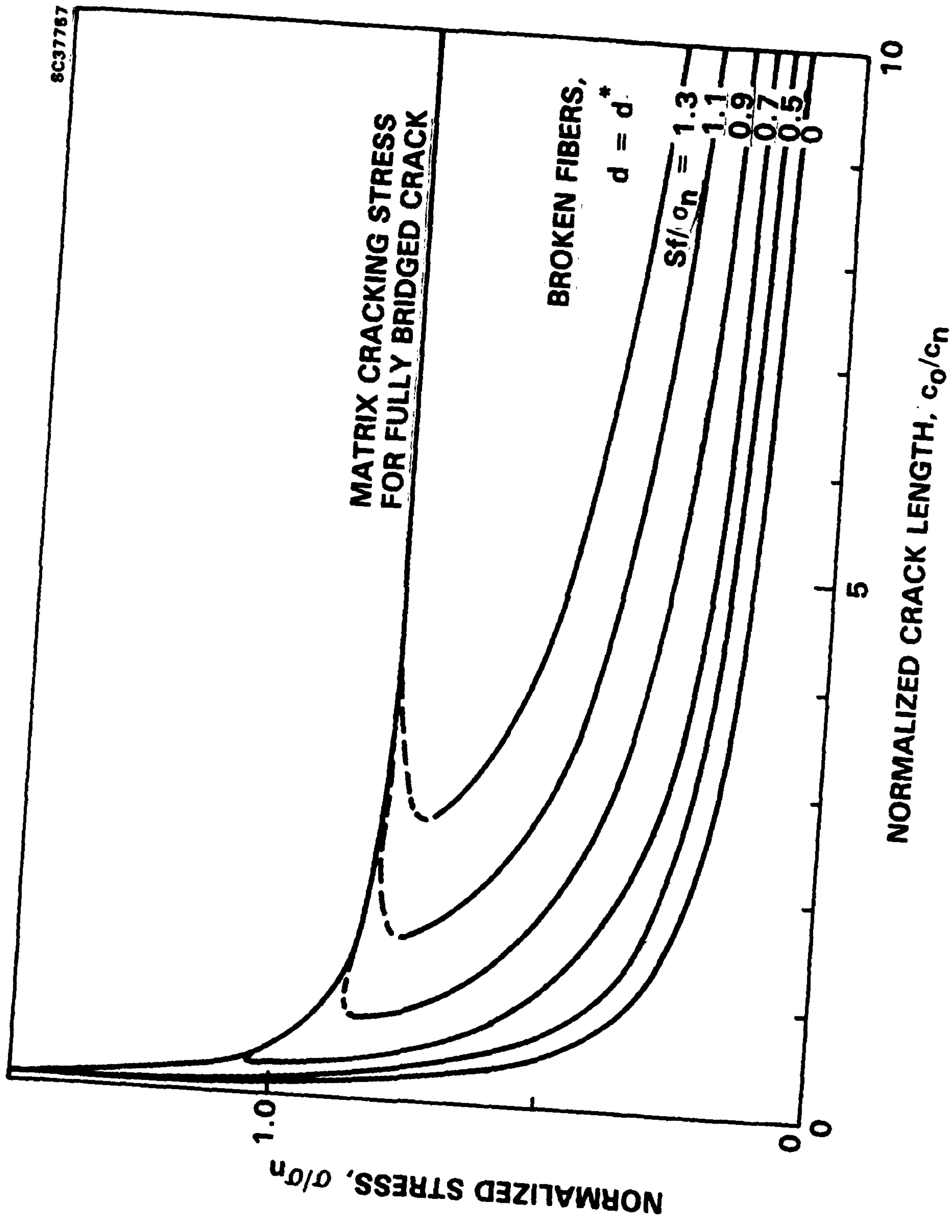
SC37767
MATRIX CRACKING STRESS FOR FULLY BRIDGED CRACK
BROKEN FIBERS, d = d*
Sf/σn = 1.3
1.1
0.9
0.7
0.5
0
NORMALIZED STRESS, σ/σn
1.0
0
NORMALIZED CRACK LENGTH, co/cn
0
5
10

Figure 8

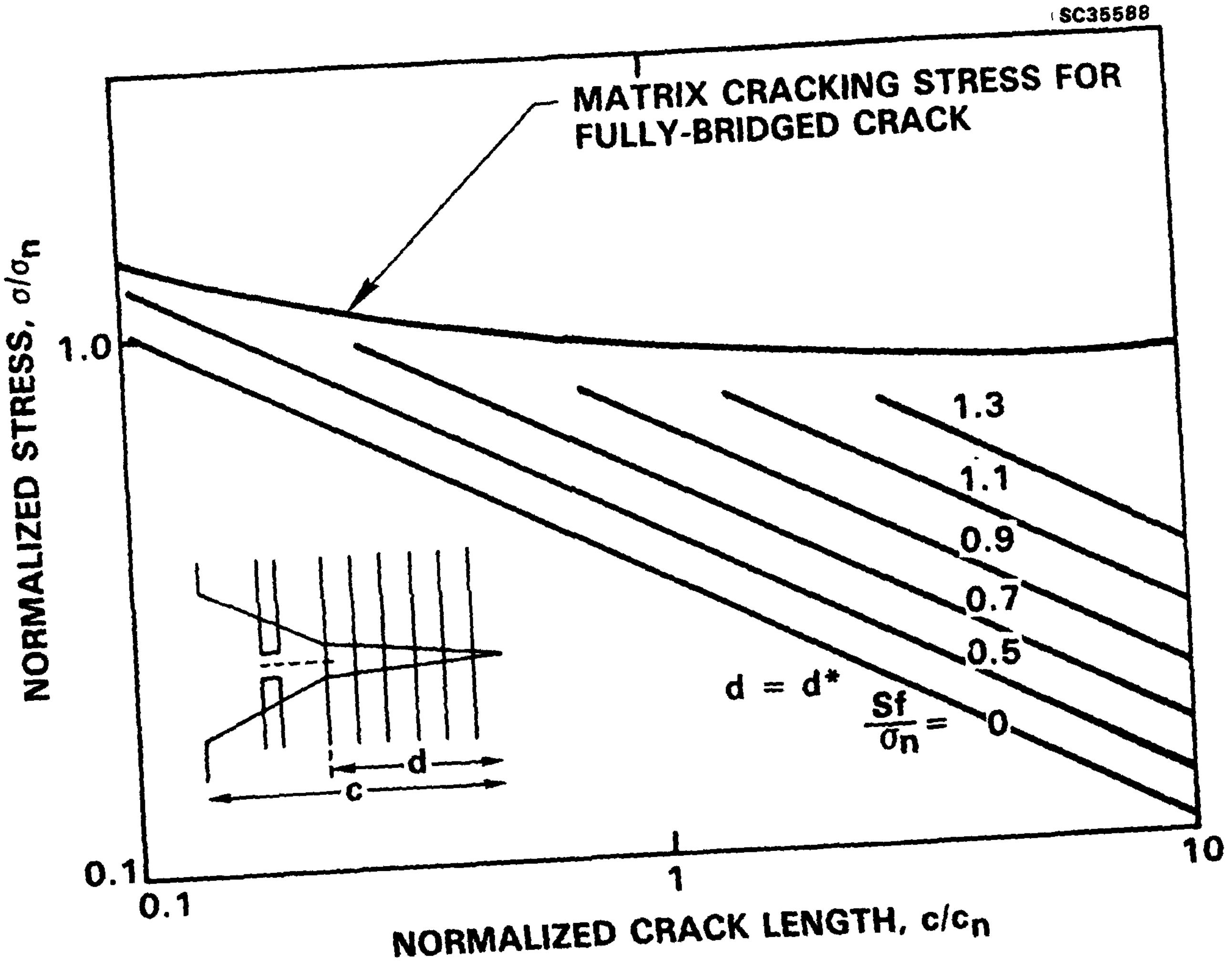
SC35588
MATRIX CRACKING STRESS FOR FULLY-BRIDGED CRACK
NORMALIZED STRESS, σ/σ_n
1.0
0.1
NORMALIZED CRACK LENGTH, c/c_n
0.1
1
10
1.3
1.1
0.9
0.7
0.5
0
$d = d^*$
$\frac{S_f}{\sigma_n} =$
d
c

Figure 9

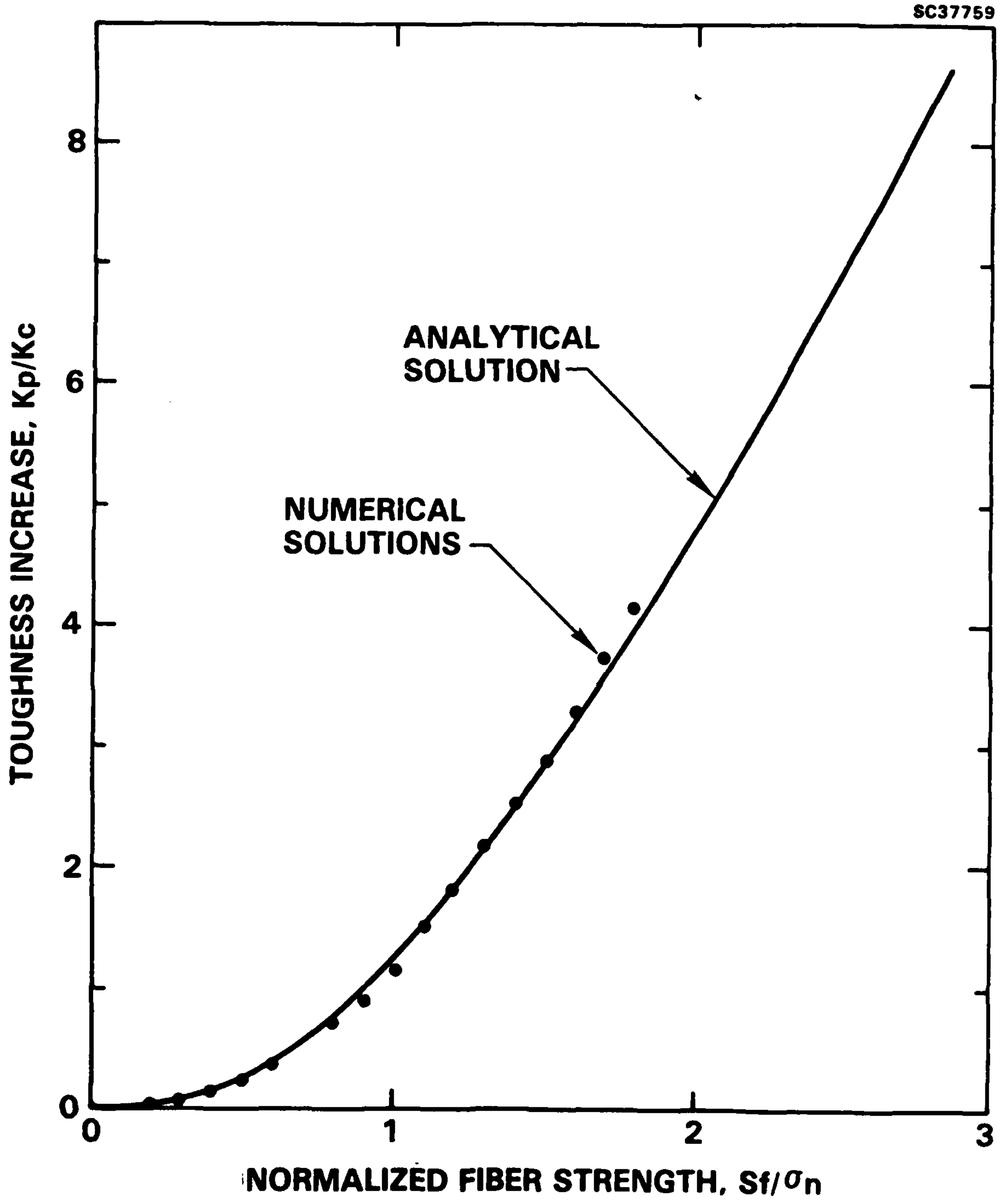
SC37759
TOUGHNESS INCREASE, Kp/Kc
NORMALIZED FIBER STRENGTH, Sf/σn
ANALYTICAL SOLUTION
NUMERICAL SOLUTIONS
0
2
4
6
8
0
1
2
3

Figure 10

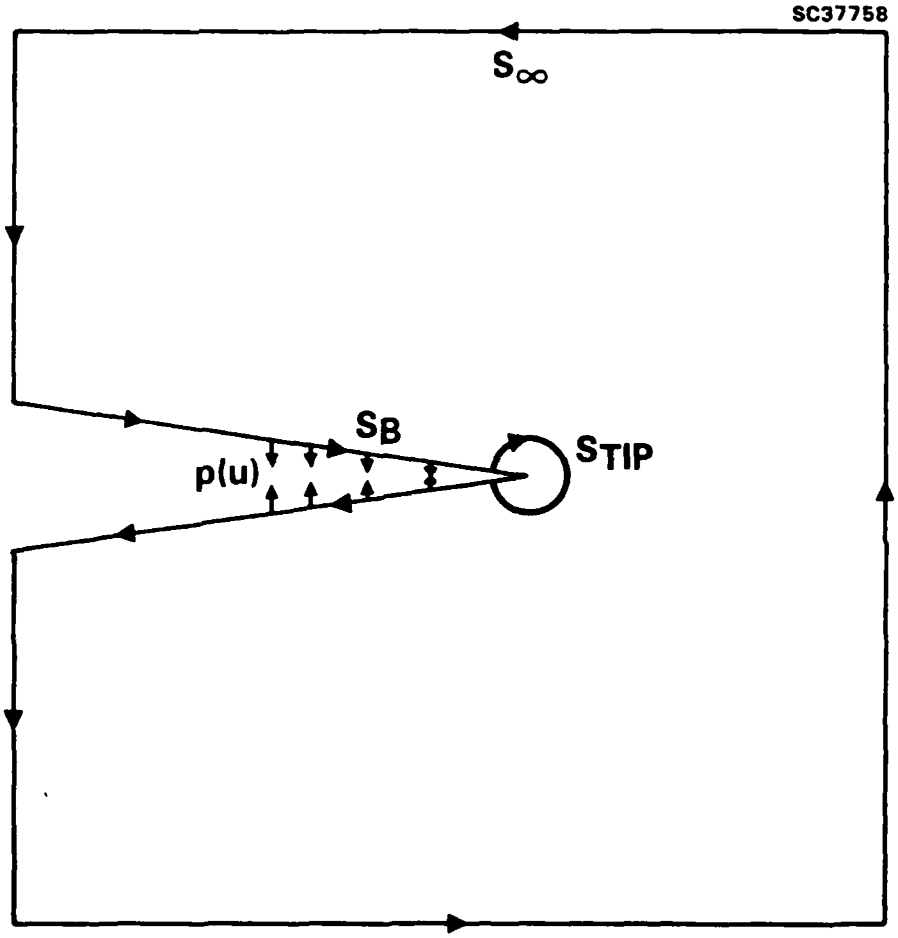

Figure 11

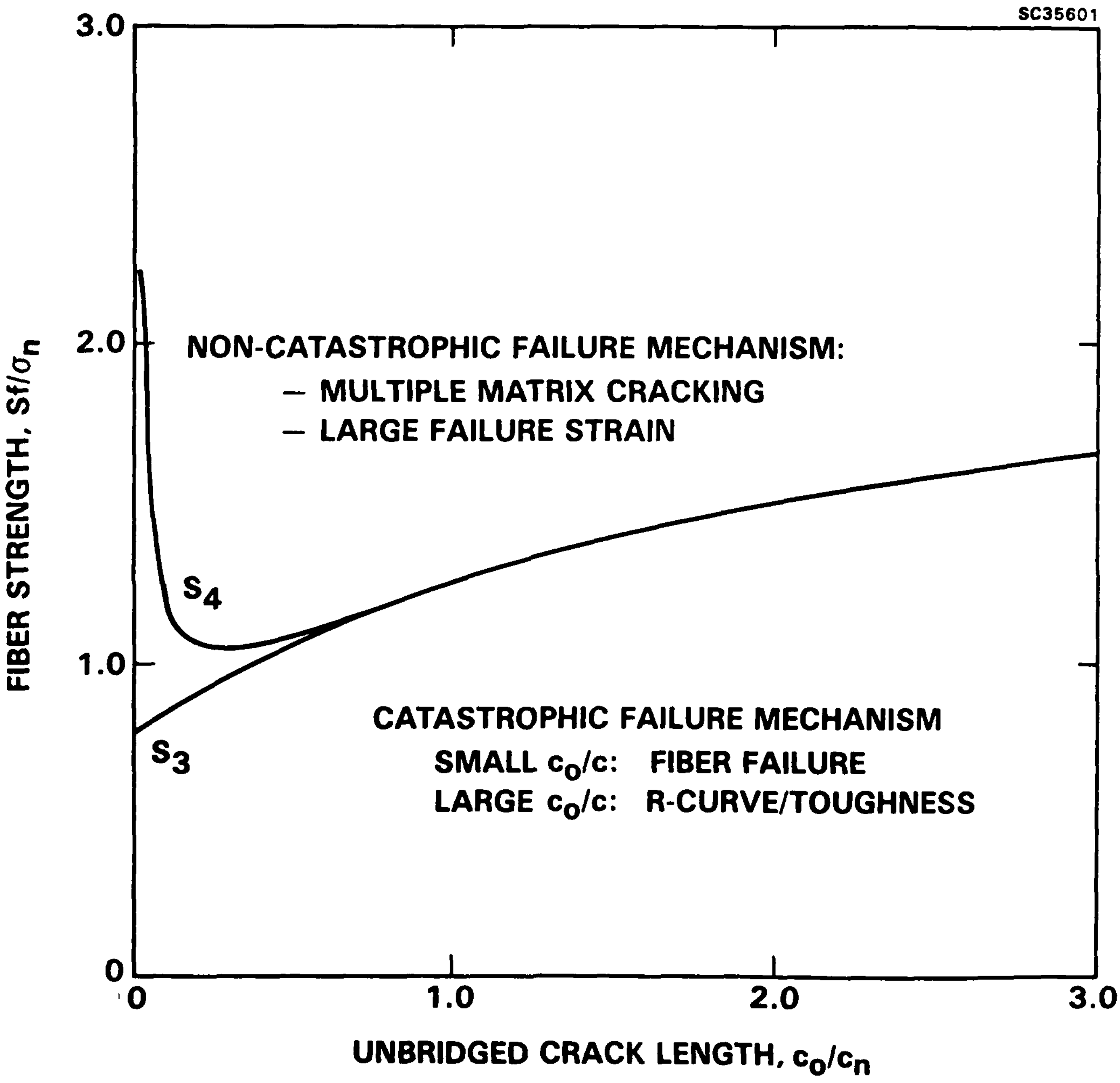
SC35601
3.0
2.0
1.0
0
0
1.0
2.0
3.0
FIBER STRENGTH, S_f/σ_n
UNBRIDGED CRACK LENGTH, c_o/c_n
NON-CATASTROPHIC FAILURE MECHANISM:
— MULTIPLE MATRIX CRACKING
— LARGE FAILURE STRAIN
S_4
S_3
CATASTROPHIC FAILURE MECHANISM
SMALL c_o/c: FIBER FAILURE
LARGE c_o/c: R-CURVE/TOUGHNESS

Figure 12

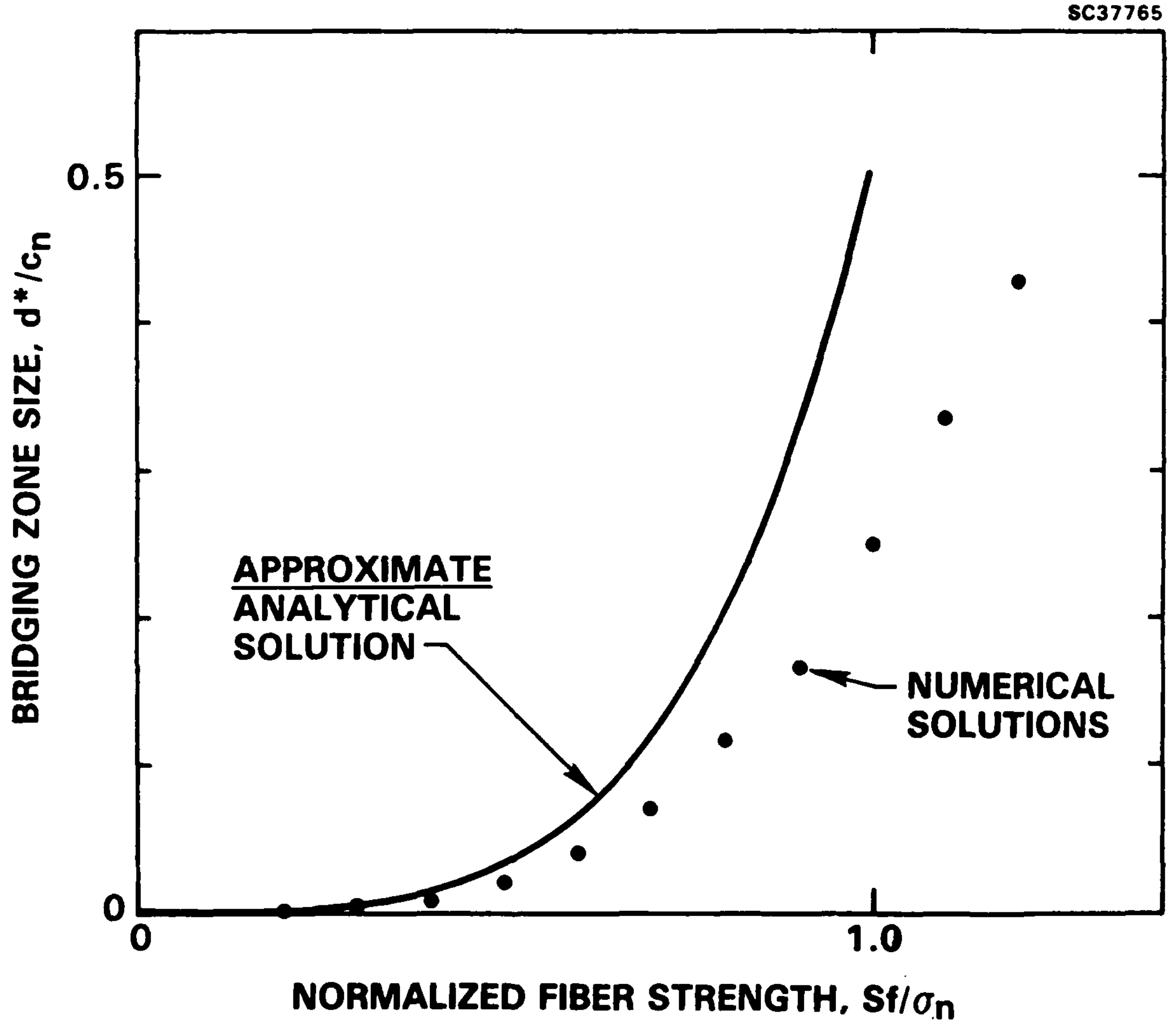
SC37765
BRIDGING ZONE SIZE, d^*/c_n
0.5
0
0
1.0
NORMALIZED FIBER STRENGTH, S_f/σ_n
APPROXIMATE ANALYTICAL SOLUTION
NUMERICAL SOLUTIONS

Figure 13

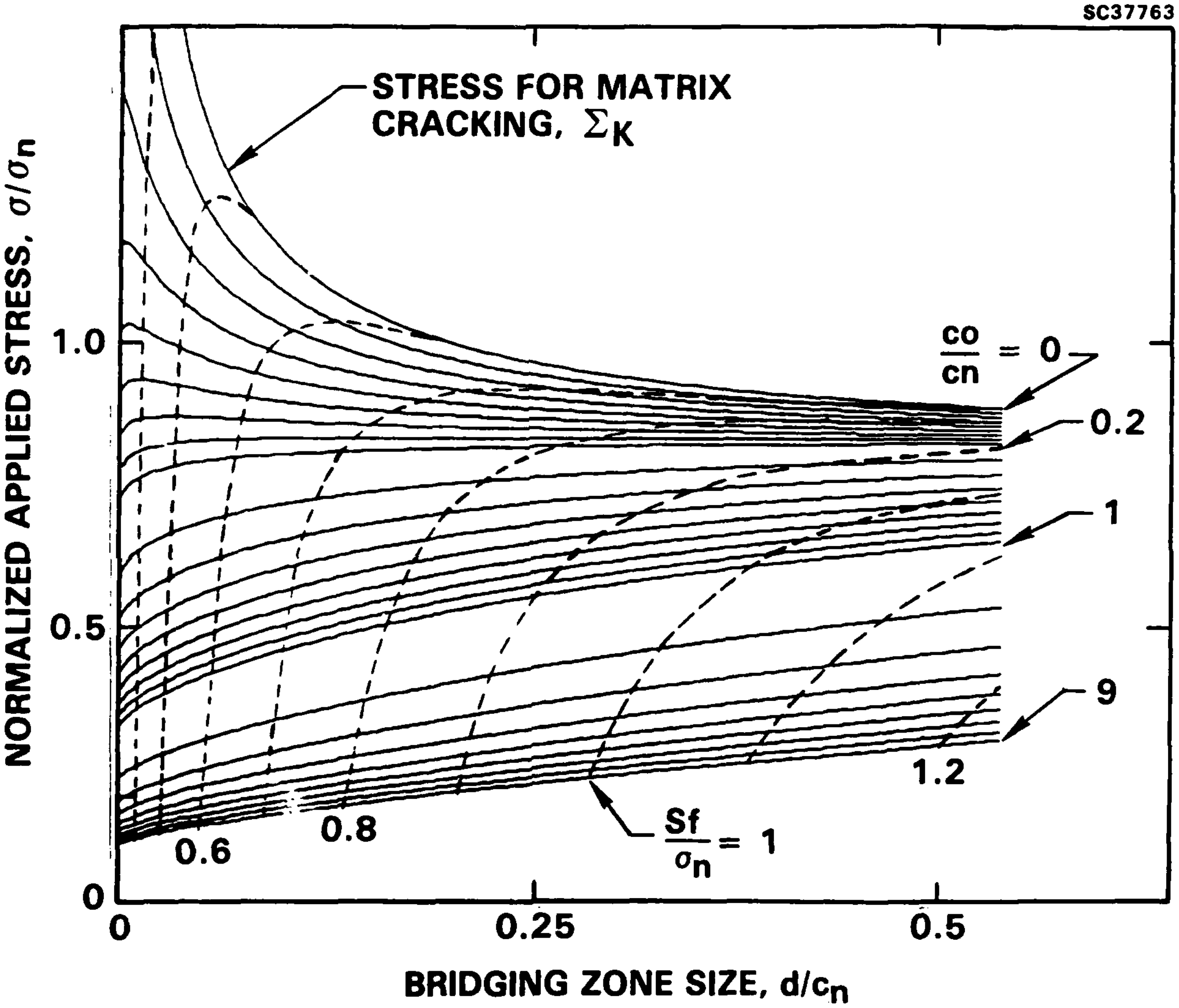
SC37763
STRESS FOR MATRIX CRACKING, Σ_K
NORMALIZED APPLIED STRESS, σ/σ_n
BRIDGING ZONE SIZE, d/c_n
$\frac{co}{cn} = 0$
0.2
1
9
0.6
0.8
1.2
$\frac{Sf}{\sigma_n} = 1$
0
0.5
1.0
0
0.25
0.5

Figure A1

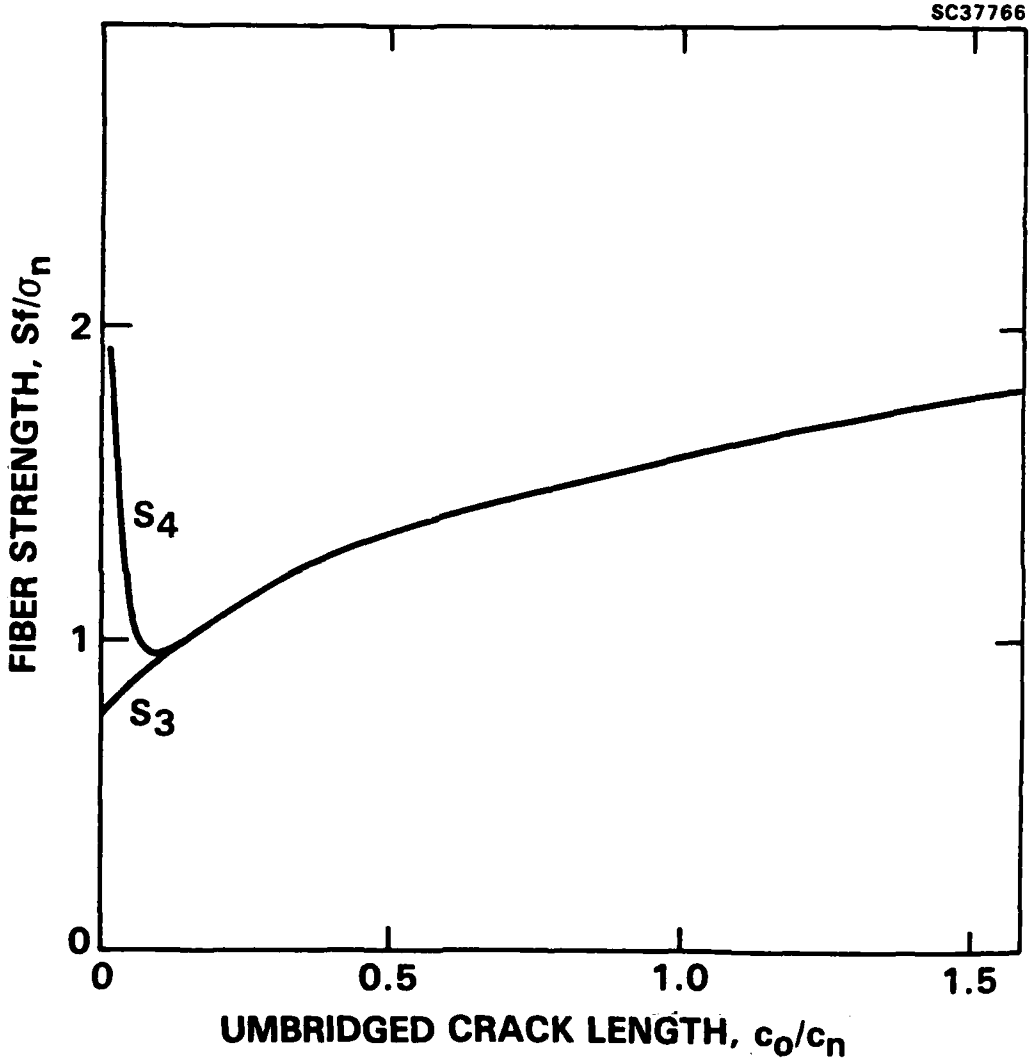
SC37766
FIBER STRENGTH, S_f/σ_n
2
1
0
S_4
S_3
0
0.5
1.0
1.5
UMBRIDGED CRACK LENGTH, c_o/c_n

Figure A2

5.0 THE TENSILE STRENGTH OF UNIAXIALLY REINFORCED CERAMIC FIBER COMPOSITES

in Fracture Mechanics of Ceramics, Vol. 7, pp. 1-15, ed. R.C. Bradt, A.G. Evans, D.P.H. Hasselman and F.F. Lange, Plenum, 1986.

From: FRACTURE MECHANICS OF CERAMICS, Vol. 7
Edited by R.C. Bradt, A.G. Evans, D.P.H. Hasselman
and F.F. Lange
(Plenum Publishing Corporation, 1986)

THE TENSILE STRENGTH OF UNIAXIALLY REINFORCED CERAMIC FIBER COMPOSITES

D.B. Marshall
Rockwell International Science Center
Thousand Oaks, CA 91360

A.G. Evans
Department of Materials Science
University of California
Santa Barbara, CA 93106

ABSTRACT

Recent developments in understanding failure mechanisms and in applying fracture mechanics to ceramic fiber composites are reviewed. Direct observations of failure mechanisms in a uniaxially reinforced SiC/glass-ceramic composite are first summarized, thereby establishing a basis for a fracture mechanics analysis. The key observation is that frictional forces exerted by the fibers on the matrix oppose the opening of matrix cracks. The fracture mechanics analysis defines transitions between several failure mechanisms, provides strength/crack-size relations for each mechanism, and relates strength and/or toughness to microstructural properties of the composite. Implications of the results for designing composites with optimum properties are discussed.

1.0 INTRODUCTION

The resistance of brittle materials to tensile failure can be enhanced considerably by reinforcing with high strength fibers. The most dramatic improvements in properties have been achieved in composites that contain continuous unbonded fibers aligned parallel to the tensile axis. This class of composites includes glasses and glass-ceramics reinforced by carbon[1-4] and SiC fibers.[5-7]

Mechanisms of failure in these composites and in monolithic ceramics can differ substantially. Monolithic ceramics generally fail by the growth of a single crack on a plane normal to the maximum principal stress. Fiber composites, on the other hand, can fail by a variety of mechanisms, dependent upon the applied stress state and the geometry and microstructural characteristics of the composite.[8] Moreover, mechanisms that do not involve failure by growth of a single crack have been observed.[8] In that case fracture toughness cannot be defined in the usual sense.

Despite these complications, fracture mechanics can be applied to analyze failure of fiber composites, provided that the detailed mechanisms of failure are identified for each combination of composite and stress state. Such analyses provide insight into failure processes and allow definition of alternative material properties which characterize the mechanical response. Furthermore, by relating these properties to microstructural parameters, the fracture mechanics analyses provide a means of designing optimum microstructures and anticipating microstructural changes that lead to changes in failure mechanisms.[1,9,10]

The purpose of the present paper is to review recent progress[8-11] in understanding failure mechanisms and in applying fracture mechanics to ceramic composites. Specifically, direct observations of the failure process in a composite material* consisting of approximately 50% uniaxially aligned SiC fibers in a lithium-alumino-silicate (LAS) glass-ceramic matrix are first described. These observations are then used as a basis for developing a fracture mechanics analysis which provides further insight into the mechanics of failure as well as relating strength, toughness, and changes in failure mechanism to microstructural properties.

2.0 FAILURE MECHANISMS

The general features of room-temperature load/deflection curves for flexure or tension tests in the SiC/LAS composite are shown in Fig. 1.[8] In both cases an initial linear elastic region is followed by nonlinear load increase to a maximum, then a continuous load decrease. The noncatastrophic decrease in load gives these materials the appearance of being very "tough." Similar curves have been reported for flexure tests of a SiC/magnesium-alumino-silicate glass ceramic[7] and carbon-fiber/glass-ceramic composites.[2]

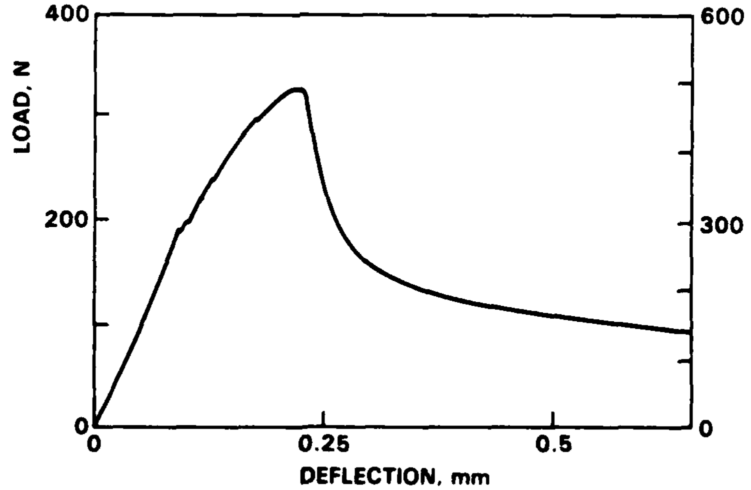

Fig. 1 Load-deflection curve for a SiC/glass ceramic composite.

Direct observation of the tensile surfaces during loading has allowed the damage processes corresponding to each portion of the load/deflection curve to be identified.[8] In both flexure and tension tests

---

*United Technologies Research Center

the onset of nonlinear deflection occurs at a stress of ≈ 300 MPa and coincides with the formation of a single matrix crack. In a tension test this crack passes completely through the central test section, and the applied load is supported entirely by the intact fibers bridging the crack. Further small increase of load causes formation of multiple regularly spaced cracks in the matrix throughout the central test area (Fig. 2). The spacing of the cracks is about 400 μm. Most of the additional deflection after the onset of matrix cracking is due to pull out of the fibers from the matrix and the associated increase in crack opening. The peak load (≈ 500 MPa) is dictated by fiber failure. At deflections beyond the peak, the opening of one of the cracks becomes very large, and final separation involves the pulling of broken fibers through the blocks of matrix formed by multiple cracking.

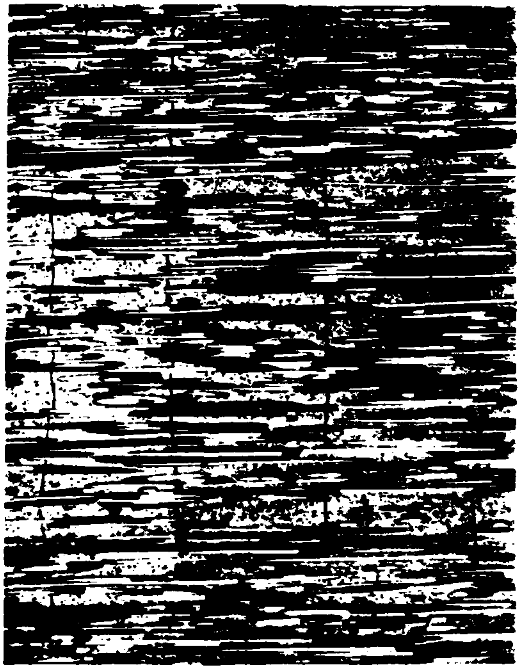

Fig. 2 Tensile surface of a flexure specimen, loaded beyond the linear region of the load-deflection curve. Width of field 1.5 mm. Brightly reflecting regions are polished cross sections of fibers, grey regions are the matrix. After Ref. 8.

In a flexure test the matrix cracks that form at the onset of nonlinear deflection penetrate only to about the midplane of the beam. These cracks destroy the macroscopic uniformity of the beam causing redistribution of stresses. In particular the neutral axis moves towards the compressive surface, resulting in an enhancement of compressive stress. Further loading increases the opening of the cracks. However, the peak load is determined by a kinking instability on the compressive side of the beam. The importance of the stress redistribution was illustrated by a comparison of the compressive strength calculated from beam bending formulae (780 MPa) with the strength indicated by a strain gauge on the compressive surface (1330 MPa).[8] Thus, the peak load-bearing capacity in flexure is dictated by a combination of tensile and compressive failure mechanisms.

At higher temperatures (~ 1000°C) a change in failure mechanism has been observed.[11] Matrix cracking is accompanied by fiber fracture, resulting in catastrophic failure of the composite and loss of the capacity to support high strains to failure. Fracture surface observations indicate that the majority of fibers extend relatively short distances out of the surfaces, thus implying that fiber failure occurs behind the crack tip (fiber failure coincident with, or ahead of the crack tip would yield either no fiber pullout or equal numbers of protruding fibers and holes).

3.0 INFLUENCE OF FIBERS ON MATRIX CRACKING

The tensile stress at which the first matrix crack forms is an important characteristic of the composite. If all of the fibers bridging the matrix crack remain intact, matrix fracture signifies the onset of permanent damage, the loss of protection provided by the matrix against corrosion and oxidation of the fibers, and the likelihood of an enhanced susceptibility to degradation due to cyclic loading. On the other hand, if fiber failure accompanies matrix cracking, catastrophic failure ensues.

Separation of the surfaces of a matrix crack that is bridged by uniaxially aligned reinforcing fibers requires some sliding of the matrix over the fibers. In general, this process entails debonding at the fiber/matrix interface followed by sliding against frictional forces. However, in composites that exhibit the failure mechanisms discussed in the previous section there is no chemical bond between the fibers and matrix.[8] A direct indication of the role of frictional forces in such composites was obtained from observations of matrix cracks during load cycling. Measurements of the crack opening displacements (Fig. 3) indicated that the separations of the crack surfaces were larger during unloading than during loading. These observations imply that the fibers

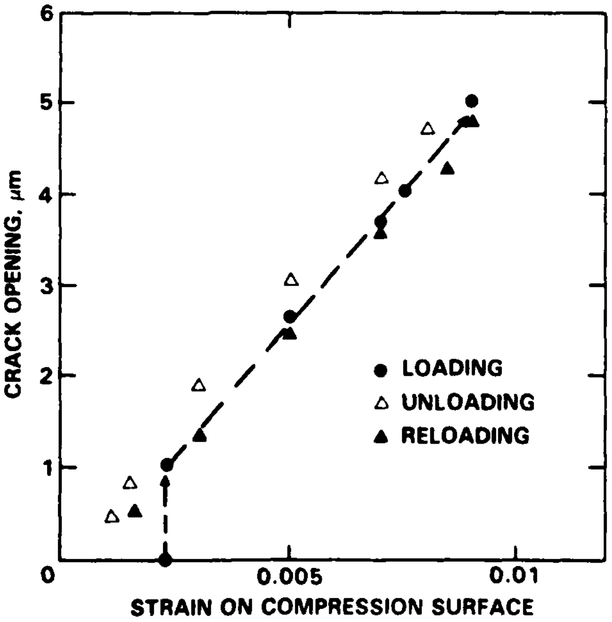

Fig. 3 Plot of separation of crack surfaces in tensile surface of flexure beam during loading, unloading and reloading. After Ref. 8.

exert frictional forces on the matrix, which tend to oppose crack closure during unloading and resist crack opening during loading. Therefore, frictional forces must play an important role in inhibiting the initial extension of the first crack through the matrix.

4.0 FRACTURE MECHANICS ANALYSIS OF MATRIX CRACKING

4.1 Formulation of Problem

The influence of the fibers on the stress for matrix cracking can be evaluated using a stress intensity approach, in which the frictional forces that resist sliding are viewed as crack closure tractions.[9] The influence of these tractions is evaluated by imagining the crack to be formed in two steps. First, all of the bonds across the prospective crack plane (in the fibers as well as the matrix) are cut and stress σ_∞ is applied (Fig. 4a), causing the crack to open. In the second step tractions, T, are applied to the end of each fiber that lies within a distance d of the crack tip. The magnitude of T is chosen so that the fiber ends displace relative to the matrix and allow the fibers to be rejoined (Fig. 4b). In a continuum approximation (c >> fiber spacing), this procedure is equivalent to applying a distribution of closing pressure p(x) to the crack surfaces:

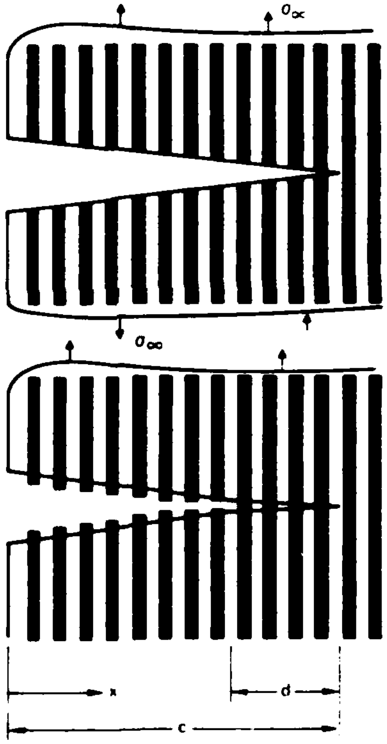

Fig. 4 Hypothetical steps used to evaluate the closure effect of fibers bridging a matrix crack.

$$p(x) = \begin{cases} T(x)\, f & (x > c-d) \\ 0 & (x < c-d) \end{cases} \qquad (1)$$

where x represents the position on the crack surface (Fig. 4b) and f is the volume fraction of fibers. The closure induced by the pressure p(x) opposes the opening due to the applied stress σ_∞. The influence of the applied stress on the crack tip stress intensity can be evaluated by regarding the stresses as a uniform opening pressure, σ_∞, acting at the crack surfaces. Therefore, with the crack surfaces being subject to net pressure $(\sigma_\infty - p(x))$, a composite stress intensity factor can be defined as (for a penny crack* embedded in an infinite medium):

$$K = 2(c/\pi)^{1/2} \int_0^1 \frac{[\sigma_\infty - p(X)]XdX}{\sqrt{1-X^2}} \tag{2}$$

where $X = x/c$.

The stress intensity K characterizes the composite stress and strain fields in the region immediately ahead of the matrix crack. In this region, the matrix and fiber strains are expected to remain compatible, whereupon the stresses exhibit the usual composite relationship

$$\sigma_m/E_m = \sigma_\infty/E \tag{3a}$$

where σ_m is the matrix stress and E is the composite modulus,

$$E = E_m(1-f) + E_f f$$

with E_m and E_f referring to the Young's modulus of the matrix and fibers, respectively. The matrix and composite stress intensities scale with the stresses, so that

$$K = K_m(E/E_m) \tag{3b}$$

where K_m is the stress intensity factor in the matrix. The condition for equilibrium crack growth (in the absence of environmental effects) is given by setting K_m equal to the critical stress intensity factor, K_o, for the matrix. Therefore, the criterion for crack growth can be expressed in terms of K as;

$$K = K_c \equiv K_o(E/E_m) \; . \tag{4}$$

Thus, Eqs. (2) and (4) relate the matrix cracking condition to the applied stress σ_∞.

Evaluation of K in Eq. (2) requires a separate calculation of the pressure distribution p(x). Analysis of fiber pullout from the matrix[9] reveals that the closure pressure is related to the crack opening, u, at a given location by

$$p = 2[u\tau f^2 E_f(1 + \eta)/R]^{1/2} \tag{5}$$

where $\eta = E_f f/E_m(1-f)$, R is the fiber radius, and τ is the sliding frictional stress at the interface. However, the crack opening at a given position is determined by the entire distribution of surface tractions. For a penny crack,[13]

---

*In the analysis for multiple matrix cracking,[9] penny cracks and straight cracks yielded almost identical results. Therefore, for convenience, only penny cracks are considered explicitly in this paper.

$$u(X) = \frac{4(1-\nu^2)c}{\pi E} \int_X^1 \frac{1}{\sqrt{s^2 - X^2}} \int_o^s \frac{[\sigma_\infty - p(t)]tdt}{\sqrt{s^2 - t^2}} ds \qquad (6)$$

where s and t are normalized position coordinates and ν is the Poisson's ratio of the composite. Therefore, analysis of matrix cracking by the stress intensity approach requires solution of Eqs. (5) and (6) to obtain the crack surface tractions, followed by evaluation of the integral in Eq. (2) and combination with the crack growth criterion, Eq. (4).

4.2 Closure Effect of Fibers

Rigorous solutions for u(X) from Eqs. (5) and (6) can only be obtained numerically. However, an analytical solution that closely resembles the exact numerical result[9] can be obtained by assuming an approximate form for the crack profile. This solution has the attraction that the final result can be expressed in simple mathematical form. The approximate crack profile is taken as the solution of Eq. (6) for a crack subject to uniform pressure, with the magnitude of the opening governed by the net stress intensity factor K (Eq. 2);

$$u(x) = 2(1 - \nu^2)K\, c^{1/2}(1 - x^2/c^2)^{1/2}/E\, \pi^{1/2} \quad . \qquad (7)$$

The actual pressure distribution is obtained by combining Eqs. (5) and (7) to give

$$p(x) = [\alpha K\, c^{1/2}(1 - x^2/c^2)^{1/2}]^{1/2} \qquad (x > c - d) \qquad (8a)$$

where

$$\alpha = 8(1 - \nu^2)\tau f^2 E_f(1 + \eta)/E\, R\, \pi^{1/2} \quad . \qquad (8b)$$

With this pressure distribution, the net stress intensity factor (Eq. (2)) is given by

$$K = K_\infty - K_p \qquad (9a)$$

where

$$K_\infty = \Omega\sigma_\infty c^{1/2} \qquad (9b)$$

$$K_p = (16\alpha/9\pi)^{1/2}\, K^{1/2}\, d^{3/4}(2 - d/c)^{3/4} \qquad (9c)$$

and $\Omega = 2/\sqrt{\pi}$. The terms K_∞ and K_p represent the contributions to the crack tip stress intensity due to the applied load and the fiber closure tractions, respectively.

4.3 Multiple Matrix Cracking

If all of the fibers that intersect the crack plane remain intact the traction-induced stress intensity (Eq. (9c)) becomes

$$K_p = (16\alpha/9\pi)^{1/2} K^{1/2}\, c^{3/4} \qquad (10)$$

Thus, the closure effect of the fibers increases indefinitely with crack length. The mechanics of crack growth is most conveniently investigated by combining Eqs. (9) and (10), setting $K = K_c$, and solving for σ_∞ to obtain an equilibrium-stress/crack-size function;

$$\sigma_c = K_c/\Omega c^{1/2} + [16\alpha K_c/9\pi\Omega^2]^{1/2}\, c^{1/4} \qquad (11)$$

This function can be expressed conveniently in normalized form,

$$\sigma_c/\sigma_m = (1/3)(c/c_m)^{-1/2} + (2/3)(c/c_m)^{1/4} \quad (c < c_o) \quad , \tag{12}$$

where

$$c_m = (9\pi K_c/4\alpha)^{2/3} \tag{13a}$$

and

$$\sigma_m = (3/Q)(4\alpha K_c^2/9\pi)^{1/3} \tag{13b}$$

Equation (12) provides a relation between normalized stress and crack length parameters, σ_c/σ_m and c/c_m, without explicit reference to material and microstructural properties (these properties enter only in their influence on the normalizing factors c_m and σ_m). Thus, the mechanics of crack growth may be examined independently of the specific composite system.

Further progress requires that large and small cracks be distinguished. Large cracks must experience a crack opening which asymptotically approaches (but cannot exceed) the equilibrium separation of the completely failed matrix (i.e., two half planes connected by fibers). However, the crack opening expressed by Eq. (7) is unbounded at large c. Therefore, the preceding analysis is used only for cracks smaller than a transition crack length, c_o, defined by setting $p = \sigma_\infty$ at $X = 0$ in Eq. (8a):

$$c_o = (\sigma_\infty^2/\alpha K_c)^2 \quad . \tag{14}$$

For larger cracks, the net force on the fibers that bridge the crack in the region of asymptotic opening (i.e., $X < c-c_o$) must balance the applied load. Consequently, the crack-tip stress concentration is induced exclusively over the length c_o and the stress required to extend the crack must be independent of the total crack length. The resultant steady-state stress, given by Eq. (11) with $c = c_o$, is equal to σ_m.

The complete equilibrium-stress/crack-size function is plotted in Fig. 5. Also plotted for comparison is a solution obtained by numerical integration.[9] It is noted that the stress required to propagate a matrix crack is almost independent of crack length for cracks larger than ~ $c_m/3$. This defines the range of crack sizes over which steady-state conditions apply. The crack response in this region contrasts with the behavior of cracks in unreinforced brittle materials, for which the strength decreases with $c^{-1/2}$.

4.4 Fiber Failure Behind Crack Tip

When fibers fail behind the crack tip,[10] rigorous evaluation of K_p would involve consideration of the statistical nature of fiber strengths. However, in the present analysis, a single-valued fiber strength, S, is assumed.* Then the position within the crack at which fiber failure

---

*A single-valued fiber strength implies that fiber failure occurs between the crack surfaces, so that broken fibers do not exert closure forces on the crack. On the other hand, a statistical distribution of fiber strengths would allow fiber failure within the matrix and continued closure effect until the broken fiber pulls out of the matrix. Therefore, the present calculations yield lower bound values of composite strengths.

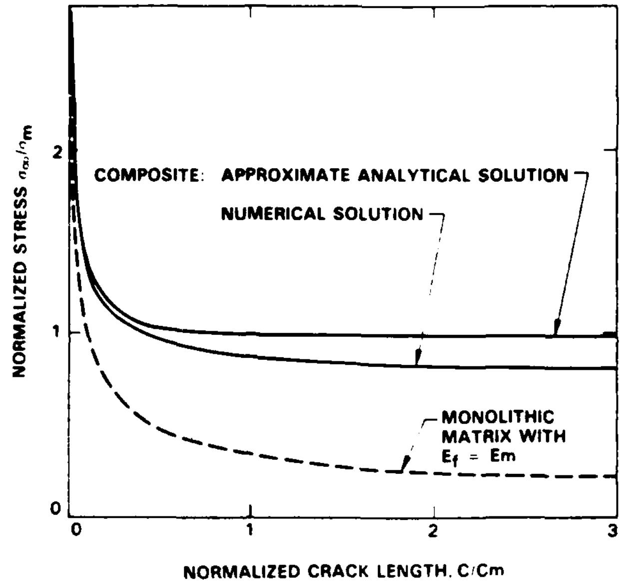

Fig. 5 Equilibrium-stress/crack-size functions for penny-shaped matrix cracks in a composite containing high strength fibers and in a monolithic material. After Ref. 9.

occurs is defined by Eq. (8a), with p(x) = Sf at x = c - d*;

$$d^*(2 - \frac{d^*}{c}) = (Sf)^4/(\alpha K_c)^2 \tag{15}$$

where K has been equated to K_c. Substitution of Eq. (15) into Eq. (9c) then yields

$$K_p = (4/3\sqrt{\pi})\,(Sf)^3/\alpha K_c \quad . \tag{16}$$

In this case, the closure effect of the fibers is manifest as a constant decrease in stress intensity factor (independent of crack length), so that the effect of the fibers is to increase the fracture toughness by $\Delta K_c = K_p$.

Strength/crack-size relations pertinent to this crack configuration can be conveniently compared with the results for the case where fibers do not fail behind the crack tip by normalizing the stresses and crack lengths with the parameters σ_m and c_m defined in the previous section. The relative toughness increase becomes

$$\Delta K_c/K_c = 2(Sf/\sigma_m)^3 \tag{17}$$

and the strength/crack-size relation becomes (Eqs. (9) and (7))

$$(\sigma/\sigma_m) = [1 + 2(Sf/\sigma_m)^3]/3(c/c_m)^{1/2} \tag{18}$$

Equation (18) is plotted in Fig. 6a for several values of the parameter Sf/σ_m. The result from Section 4.3 for multiple matrix cracking (i.e., a fully bridged crack) is also shown. It is noted that, in these normalized coordinates, the crack response is determined by the parameter Sf/σ_m, i.e., the relative magnitudes of the fiber strength and the steady-state matrix cracking stress.

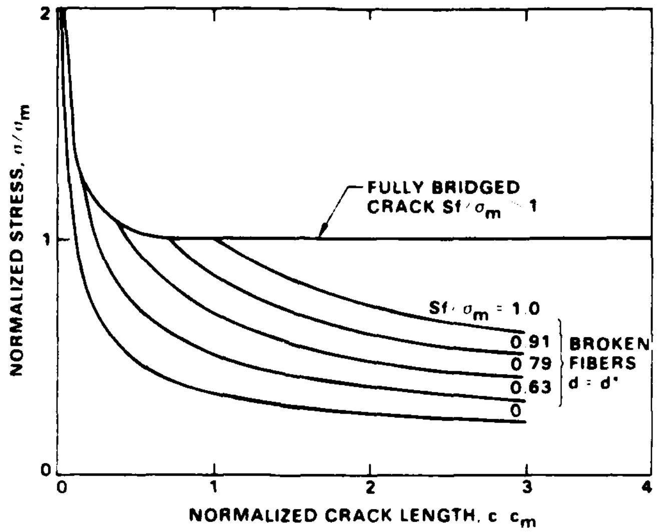

Fig. 6a Strength/crack-size relations for cracks fully bridged by fibers (Eq. 12) and cracks with fiber failure occurring behind the crack tips (Eq. 18).

4.5 Influence of Initial Crack Configuration on Strength

The stength/crack-size relation defined by Eq. (18) for composites with Sf < σ_m corresponds to a special crack configuration in which the trailing edge of the bridging zone is specified by fiber failure. More generally, the crack configuration at instability depends on both the size of the pre-existing matrix crack and the initial fiber bridging state associated with the crack. Insight into the influence of initial crack state on the strength can be obtained by considering two extreme configurations: an initially fully-bridged crack and a crack that initially has no bridging zone.

4.5.1 Initially Fully Bridged Crack

Matrix cracks that are initially fully bridged by fibers show three regions of behavior, depending on the size of the crack. For small cracks (i.e. c < d*) the crack opening is insufficient to cause fiber failure before the matrix crack becomes unstable at an applied stress given by Eq. (12). As the crack extends fiber failure occurs in the wake so that Eq. (12) also defines the strength of the composite. For intermediate sized cracks, the opening at the crack mouth exceeds that required for fiber failure before the matrix crack extends. Then the equilibrium bridging zone (i.e., d = d* defined by Eq. (15)) develops, and the strength of the composite is given by Eq. (18). The crack lengths at which this transition first occurs are given by setting c = d* in Eq. (15);

$$c/c_m = (Sf/\sigma_m)^4 \quad . \qquad (19)$$

The transition crack lengths are also defined in Fig. 6a by the intersections of the strength curve for fully bridged cracks with the set of curves for cracks with broken fibers. For large cracks, the crack opening approaches an asymptotic value (as discussed in Section 4.3) which is smaller than the opening defined by the approximate crack profile that underlies Eq. (18). In this case the net force on the fibers in the asymptotic region balances the applied stress. Therefore, the crack remains fully bridged until the applied stress exceeds Sf, whereupon fiber failure is followed by catastropic failure of the composite. The transition to this long crack limit occurs when the stress defined by Eq. (18) is $<$ Sf. Strength/crack-size relations for these three regions of behavior for initially fully-bridged cracks are shown in Fig. 6b.

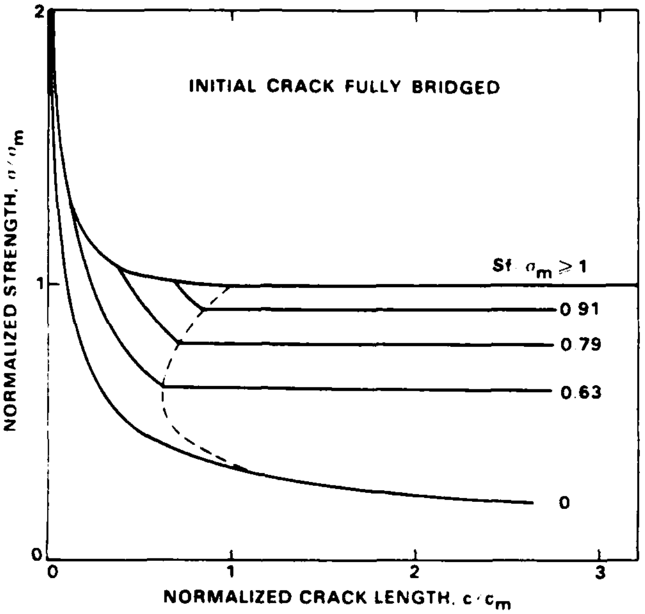

Fig. 6b Strength/crack-size relations for cracks that are initially fully bridged.

4.5.2 Initially Unbridged Crack

Matrix cracks that exist initially with a fiber bridging zone that is smaller than d* can extend stably with increasing applied stress prior to failure. This response is revealed by analyzing the growth of an initially unbridged crack of length c_o which extends so that a fiber bridging zone of length d develops and the total crack length becomes $c_o + d$ (Fig. 7). The equilibrium-stress/crack-size function for this crack is obtained from Eqs. (9) and (13) with $K = K_c$;

$$\sigma_\infty/\sigma_m = (1/3)\ (c_m/c)^{1/2}\ \{1 + 2(d/c_m)^{3/4}\ [2 - (d/c_m)/(c/c_m)]^{3/4}\} \qquad (20)$$

where $c = c_o + d$. The equilibrium stress is plotted as a function of the normalized crack extension, d/c_m, for various values of c_o/c_m in Fig. 7 (solid curves). The broken curves in Fig. 7 indicate the critical zone sizes d* for each value of c_o/c_m and Sf/σ_m, obtained by solving the normalized form of Eq. (15);

$$(d^*/c_m)\ [2 - (d^*/c_m)/(c/c_m)] = (Sf/\sigma_m)^4 \quad . \qquad (21)$$

The curves in Fig. 7 indicate that crack growth is always stable with increasing applied stress for $c_o/c_m \gtrsim 0.15$ and $d < d^*$; stable crack growth occurs until $d = d^*$, whereupon fiber failure accompanies further matrix

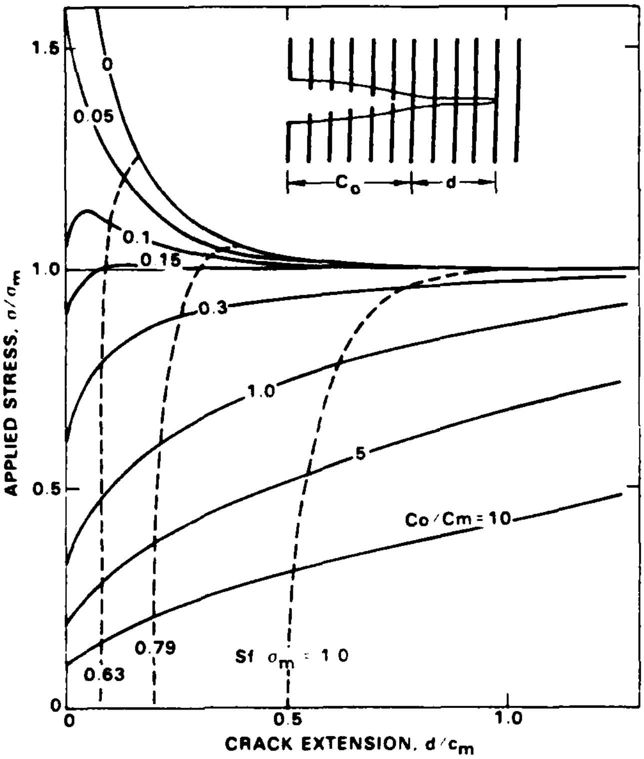

Fig. 7 Variation of equilibrium stress with extension of a partly-bridged crack (solid curves), for several values of the initial unbridged crack length c_o. Broken curves represent loci of the critical zone size, d*, for the onset of fiber failure at the end of the bridging zone.

crack extension, and failure is catastropic. The failure stress (defined by the intersection of the appropriate solid and broken curves in Fig. 7) is given by Eq. (18) with $c = c_o + d^*$. For small initial cracks ($c_o/c_m \lesssim 0.15$) instability of the matrix crack can occur at $d < d^*$. In this case the strength of the composite exceeds the value given by Eq. (18).

The fracture response depicted in Fig. 7 can be characterized alternatively in terms of a crack-growth-resistance that increases with crack extension (R-curve).[10] The R-curve is defined by Eq. (9) with $K_R = K_\infty$ at $K = K_c$, and can be expressed in the normalized form

$$K_R/K_c = 1 + 2\,(d/c_m)^{3/4}\,[2 - (d/c_m)(c_o/c_m + d/c_m)^{-1}]^{3/4} \qquad (22)$$

The R-curves for various values of c_o/c_m are plotted in Fig. 8. Also plotted are the limiting toughnesses, obtained from Eq. (17), for several values of Sf/σ_m. The intersections of these two sets of curves define the critical bridging zone size d*, for each combination of c_o/c_m and Sf/σ_m.

The condition for failure (i.e., unstable crack growth) is defined by $K_\infty = K_R$ and $dK_\infty/dc = dK_R/dc$. Thus, the crack stability depends on the slope of the R-curve, which in turn is dictated by the initial unbridged crack length, c_o. For large cracks, stable growth occurs until $d = d^*$ and K_R equals the limiting toughness. For smaller initial cracks,

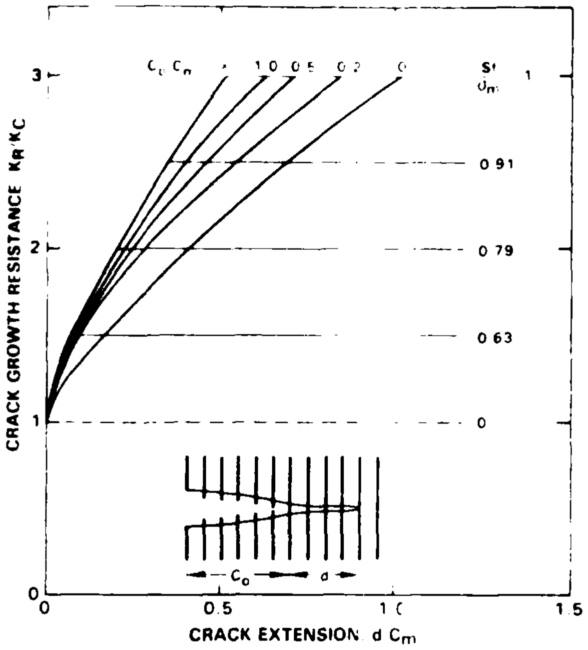

Fig. 8 Crack growth resistance curves for partly-bridged cracks. Horizontal lines represent the limiting toughnesses (i.e., the onset of fiber failure at the end of the bridging zone). After Ref. 10.

instability may be achieved at d < d*. Fully bridged matrix cracks exhibit instability without precursor stable growth.

5.0 DISCUSSION

5.1 Failure Mechanism in Frictionally Bonded Composites

The use of normalized strengths and crack lengths in the fracture mechanics analysis of Section 4.0 has enabled the mechanics and mechanisms of crack growth to be examined independently of the specific material and microstructural properties. The results of the analysis, summarized in Fig. 6, specify strength/crack-size relations for several failure mechanisms, as well as defining conditions for transitions between the mechanisms.

In composites containing fibers with sufficient strength to remain intact after a crack extends completely through the matrix (i.e., Sf > σ_m), the formation of periodic matrix cracks precedes failure of the composite. Then, the tensile strength of the composite can substantially exceed the matrix-cracking stress and large strains-to-failure can be achieved (Fig. 1). Moreover, the stress for matrix cracking is independent of pre-existing crack-size for cracks longer than a characteristic length. Under this condition the matrix cracking stress is an intrinsic property of the composite and is, therefore, both damage tolerant and independent of specimen size. Furthermore, it is noted that a fracture toughness cannot be defined with reference to either the matrix cracking event or the ultimate failure.

If the relative strength of the fibers is smaller (i.e., $Sf < \sigma_m$), failure of the composite coincides with matrix fracture and the strength of the composite becomes sensitive to pre-existing cracks. The failure response is dependent on both the size of the pre-existing matrix crack and the fiber bridging state associated with the crack. The response of cracks that are initially fully bridged by fibers is characterized by a fracture toughness which is enhanced by the reinforcing fibers. On the other hand, a crack that is initially unbridged (e.g., a notch) encounters an increasing resistance (R-curve) as the crack extends in the matrix and develops a bridging zone.

The reinforcing effect of the fibers can be inferred directly from Fig. 6. The lowest curve (i.e., Eq. (18) with $S = 0$) represents the product of the strength of the unreinforced matrix and the modulus ratio E_c/E_m. The differences between this curve and the other solutions represent the reinforcing effects of the fibers for composites with equal fiber and matrix moduli ($E_f = E_m$). For typical composites, the fiber modulus is the larger, and the matrix-cracking stress of the composite is always higher than the strength of the unreinforced matrix for a given crack length. For composites with $E_f < E_m$, the matrix cracking stress is higher than the unreinforced strength within certain ranges of crack lengths and fiber strengths. Thus, it is evident that in general it is not necessary for the fiber modulus to be higher than that of the matrix in order to obtain reinforcement.

5.2 Microstructural Influences

The influence of microstructural properties on strength, toughness and transitions between failure mechanisms can be readily assessed by evaluating the normalizing parameters σ_m and c_m (Eqs. 8 and 13):

$$\sigma_m = [12(1 - \nu^2)K_o^2 \tau E_f f^2(1 - f)(1 + \eta)^2/E_m R]^{1/3} \tag{23}$$

$$c_m = [(9\pi^{3/2}/32)\ K_o E_m(1 - f)^2(1 + \eta)\ R/\tau f^2 E_f(1 - \nu^2)]^{2/3} \tag{24}$$

For $Sf > \sigma_m$ multiple matrix cracking occurs at the steady-state stress $\sigma_o \sim 0.8\ \sigma_m$, provided the pre-existing flaws are larger than about $c_m/3$. For the SiC/glass-ceramic composite, $K_o = 2$ MPa $m^{1/2}$, $E_f = 200$ GPa, $E_m = 85$ GPa, $f = 0.5$, $R = 8$ μm, and $\tau = 2$ MPa. Substitution of these values into Eqs. (23) and (24) yields $c_m = 313$ μm and $\sigma_o = 265$ MPa. Thus, $c_m/3$ represents several fiber spacings. Since the sizes of inherent flaws in ceramics are usually about the same as microstructural dimensions, this result implies that the condition for steady-state matrix-cracking will be generally satisfied for this composite. Moreover, the predicted stress, σ_o, is consistent with measured values of 290 ± 20 MPa.[8] More importantly, Eq. (23) provides a basis for design of optimum microstructures. The critical stress increases with the toughness of the matrix, the modulus and volume fraction of fibers, the frictional stress at the fiber/matrix interface, and decreasing fiber diameter.

The transition to the failure mechanism involving simultaneous fiber failure and matrix cracking is dictated by the relative values of Sf and σ_m. If steady-state matrix cracking is desired, an increase in the volume fraction of fibers aligned in the principal stress axis beneficially influences all of the parameters that determine optimum steady-state properties (i.e., c_m decreases, while both σ_m and Sf increase). However, the allowable increases in other parameters are limited. Increasing τ increases σ_m and decreases c_m, but the maximum increase in σ_m is limited by the fiber-failure stress. Increasing K_o increases σ_m but also has the detrimental effect of increasing c_m. Thus, the maximum acceptable K_o

could be dictated either by the fiber-failure stress or by the requirement that c_m be less than a pre-existing flaw size. These restrictions account for the brittle response observed in a number of fiber or whisker-reinforced brittle systems, and place important bounds on the design of optimum microstructures.

For the failure mechanisms that involve simultaneous fiber failure and matrix cracking the limiting fracture toughness increase is

$$\Delta K_c = S^3 f E_m R / 6 E_f \tau K_o (1 + \eta)(1 - \nu^2) \qquad (25)$$

and the range of crack lengths for which the limiting toughness applies (i.e., $c > d^*$) is defined by Eq. (21)

$$c > (\pi/8) \, [S^2 E_m R/(1 - \nu^2) K_o \tau E_f (1 + \eta)]^2 \quad . \qquad (26)$$

It is interesting to note that the influences of all material parameters on ΔK_c are opposite to their influence on the stress for steady-state multiple matrix cracking (i.e., σ_m). This arises because, for a given fiber strength (which does not influence σ_m), the ratio Sf/σ_m decreases with increasing σ_m thus leading to a smaller fiber-bridging zone (Eq. 21) and a decreased toughness increment (Eq. 17).

ACKNOWLEDGEMENT

Funding for this work was supplied by the U.S. Office of Naval Research, Contract numbers N00014-85-C-0416 and N00014-79-C-0159.

REFERENCES

1. J. Aveston, G.A. Cooper, and A. Kelly, pp. 15-26 in the Properties of Fiber Composites, Conf. Proc. Nat. Physical Lab., IPC Science and Technology Pres Ltd., Surrey, England, 1971.
2. R.A.J. Sambell, A. Briggs, D.C. Phillips, and D.H. Bowen, J. Mater. Sci. 7[6], 676-681 (1972).
3. D.C. Phillips, J. Mater. Sci. 9[11], 1847-54 (1974).
4. D.C. Phillips, J. Mater. Sci. 7[10] 1175-91 (1972).
5. K.M. Prewo and J.J. Brennan, J. Mater. Sci. 15[2] 463-8 (1980).
6 K.M. Prewo and J.J. Brennan, J. Mater. Sci. 17[4] 1201-6 (1982).
7. J.J. Brennan and K.M. Prewo, J. Mater. Sci. 17[8] 2371-83 (1982).
8. D.B. Marshall and A.G. Evans, J. Amer. Ceram. Soc. 68[5] 225-31 (1985).
9. D.B. Marshall, B.N. Cox and A.G. Evans, Acta. Met., in press.
10. D.B. Marshall and A.G. Evans, in proceedings of the Fifth International Conference on Composite Materials.
11. A.G. Evans, M.D. Thouless, D.B. Johnson-Walls, E. Luh, and D.B. Marshall, in proceedings of Fifth International Conference on Composite Materials.
12. G.C. Sih, Handbook of Stress Intensity Factors, Lehigh University, Bethlehem, Pennsylvania, 1973.
13. I.N. Sneddon and M. Lowengrub, "Crack Problems in the Classical Theory of Elasticity," Wiley, New York, 1969.

END

12-86

DTIC